ISBN 4-901329-11-8

Proceedings of the Tenth International Conference on

Information

March 6 – 7, 2021
Hosei University, Tokyo, Japan

Edited by Lei Li, Ryuichi Ashino, Chih-Cheng Hung

Published by International Information Institute
www.information-iii.org

The Tenth International Conference on Information

March 6 - 7, 2021, Hosei University, Tokyo, Japan

Hosted by International Information Institute

Suraiya Parveen - *Hamdard University, India*

Biswas Ranjit - *Jamia Hamdard University, India*

Wen-Pei Sung - *National Chin-Yi University of Technology, Taiwan*

Motofumi Suzuki - *The Open University of Japan, Japan*

Eiji Uchino - *Yamaguchi University, Japan*

Jinfang Wang - *Yokohama City University, Japan*

Xiulun Wang - *Mie University, Japan*

Hongwei Zhao - *Hosei University, Japan*

PROGRAM COMMITTEE

Anna Antonyova - *University of Presov in Presov, Slovak Republic*

Elsayed Atlam - *Taibah University, KSA*

Innocentius Bernarto - *Universitas Pelita Harapan, Indonesia*

Guoyue Chen - *Akita Prefectural University, Japan*

Myung-Sun Chung - *Joongbu University, Korea*

Guangzhe Dong - *J.F. Oberlin University, Japan*

Jiaoman Du - *The University of Tokyo, Japan*

Kensuke Fujinoki - *Tokai University, Japan*

Chenqiang Gao - *Chongqing University of Posts and Telecommunications, China*

Yu-Teng Jacky Jang - *Tunghai University, Taiwan*

Sreenivasan Jayashree - *Multimedia University, Malaysia*

Chisato Kitazawa - *Yamaguchi University, Japan*

Chang Yi Kong - *Shizuoka University, Japan*

Katsumi Kurita - *Tokyo Metropolitan College of Industrial Technology, Japan*

Chaoqian Li - *Yunnan University, China*

Ke Li - *Nihon University, Japan*

Mingcheng Liao - *National Chin-Yi University of Technology, Taiwan*

Huiming Liu - *Hohai University, China*

Novel Lyndon - *Universiti Kebangsaan Malaysia, Malaysia*

Robert C. Meurant - *The Institute of Traditional Studies, Korea*

Tomoyuki Nagase - *Hirosaki University, Japan*

Hong Shen - *Tohoku Bunka Gakuen University, Japan*

Kwan-Yong Sim - *Swinburne University of Technology, Malaysia*

Sheng Wang - *Xi'an Jiaotong University, China*

Jongsoo Yoon - *Kangnam University, Korea*

Xiao-Yu Zhang - *Beijing Forestry University, China*

Tiejun Zhao - *Niigata Agro-Food University, Japan*

CONTENTS

ISBN 4-901329-11-8

Graph Embedding from Theory to Applications

Prof. Irwin King
President of International Neural Network Society,
Professor of the Chinese, University of Hong Kong
irwinking@gmail.com

Abstract

Graph embedding refers to the problem of projecting the elements in a graph, including nodes, edges, substructures, or the whole graph, to a low-dimensional space while preserving the graph's structural information. Graph embedding is an essential technique for analyzing various types of large-scale networks such as social networks, traffic networks, semantic networks, etc. To cope with the growing scale and diversifying structure of modern networks, researchers have proposed novel methods for graph embedding for feature engineering. In this talk, we present the recent advances and future directions in the theoretical development graph embedding and introduce some common applications for social network analysis, such as node classification, link prediction, community detection, and social recommendation.

Bio

Prof. King's research interests include machine learning, social computing, web intelligence, data mining, and multimedia information processing. In these research areas, he has over 210 technical publications in journals and conferences. In addition, he has contributed over 30 book chapters and edited volumes. Moreover, Prof. King has over 30 research and applied grants. One notable patented system he has developed is the VeriGuide System, previously known as the CUPIDE system, which detects similar sentences and performs readability analysis of text-based documents in both English and in Chinese to promote academic integrity and honesty. Prof. King is the Book Series Editor for "Social Media and Social Computing" with Taylor and Francis. He is also an Associate Editor of the ACM Transactions on Knowledge Discovery from Data and a

former Associate Editor of the IEEE Transactions on Neural Networks and IEEE Computational Intelligence Magazine. He is a member of the Editorial Board of the Open Information Systems Journal, Journal of Nonlinear Analysis and Applied Mathematics, and Neural Information Processing-Letters and Reviews Journal. He has also served as Special Issue Guest Editor for Neurocomputing, International Journal of Intelligent Computing and Cybernetics, Journal of Intelligent Information Systems, and International Journal of Computational Intelligent Research. He is a IEEE Fellow and a senior member of ACM. Currently, he is serving the Neural Network Technical Committee and the Data Mining Technical Committee under the IEEE Computational Intelligence Society. He also serves International Neural Network Society as the President. Moreover, he is the General Co-Chair of the WebConf2020, ICONIP2020 and in various capacities in a number of top conferences such as WWW, NIPS, ICML, IJCAI, AAAI, etc. Prof. King is Professor at the Department of Computer Science and Engineering, and a former Associate Dean (Education), Faculty of Engineering at The Chinese University of Hong Kong. He had worked at the AT&T Labs Research, San Francisco and was also teaching Social Computing and Data Mining as a Visiting Professor at UC Berkeley in early 2010s. He received his B.Sc. degree in Engineering and Applied Science from California Institute of Technology, Pasadena and his M.Sc. and Ph.D. degree in Computer Science from the University of Southern California, Los Angeles.

Proceedings of the Tenth International
Conference on Information (Information'2021)
ISBN 4-901329-11-8

Research Trend on Developing Smart Remote Patient Monitoring Systems for the COVID-19 Era and Beyond

Prof. Sabah Mohammed

Editor in Chief of the IGI Global International Journal of Extreme Automation and Connectivity in Healthcare, Professor of Lakehead University
Email: sabah.mohammed@lakeheadu.ca

Abstract

As information technology continues to dramatically evolve, many researchers and strategy decision making believe the Internet of Things (IoT) could play a pivotal role in reshaping industry all together. It is the domino effect wind of change that we need to understand and plan for. This particularly important in the COVID-19 era and beyond where we need to create a robust connected healthcare ecosystem. In healthcare, IoT may just redefine how apps, devices and people interact and connect with one another to deliver healthcare solutions. The benefits are more than obvious. It could help reduce costs, improve outcomes and disease management, and enhance patient experiences. This invited talk will shed light on the current and future trends taking place in the patient monitoring field and the key market drivers that design engineers need to consider.

Biography

Dr. Sabah Mohammed research interest is in intelligent systems that have to operate in large, nondeterministic, cooperative, highly connected, survivable, adaptive or partially known domains. His continuous research is inspired by his PhD work back in 1981 from Brunel University (UK) on the employment of the Brain Activity Structures for decision making (planning and learning) that enable processes (e.g. agents, mobile objects) and collaborative processes to act intelligently in their environments to timely achieve the required goals. Having trained in medicine with a computer science PhD in Artificial Intelligence (AI), Dr. Mohammed is full Professor at the department of Computer Science at Lakehead University (Ontario Canada) since 2002 and core professor at the BioTechnology program at Lakehead. Dr. Mohammed efforts in establishing healthcare related programs at Lakehead are notable like the specialization Health informatics, BioTechnology and the Bioinformatics programs at Lakehead. With a research background in industry and academia, he has a strong international research

reputation for his work on clinical decision support systems supporting remote areas, ubiquitous and extreme environments. Prior to his work at Lakehead University, Dr. Mohammed was the chair of three computer science departments at HCT, Philadelphia and Applied Science Universities. Dr. Mohammed is the Editor in Chief of the of the IGI Global International Journal of Extreme Automation and Connectivity in Healthcare (IJEACH), Associate Editor of the IEEE Access and the founding EiC of the Int. J. of Emerging Technologies of Web Intelligence (JETWI) . He is currently the supervisor of the Smart Health FabLab at Lakehead University. Dr. Mohammed chair the special interest group on Smart and Connected Health with the IEEE ComSoc eHealth TC. Dr. Mohammed is currently working on the development of IoT and mobility technologies that have impact on remote patient monitoring in Rural Areas . Dr. Mohammed is also a Professional Engineer of Ontario, Information Processing Professional with CIPS and Senior Member of IEEE with research supported by major granting organizations like NSERC, MITACS, ONCAT and CFI. More information on Dr. Mohammed can be found on his institution website http://flash.lakeheadu.ca/~mohammed.

Proceedings of the Tenth International
Conference on Information (Information'2021)
ISBN 4-901329-11-8

Time Series Forecasting with Artificial Neural Networks

Prof. Lean Yu
Beijing University of Chemical Technology, Elsevier Most Cited Chinese Researchers

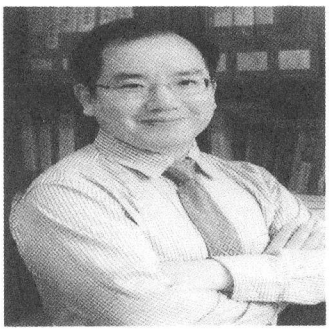

Abstract

In this talk, artificial neural networks (ANNs) are used as an important prediction tool for time series forecasting. The four main forms using ANNs to predict time series are introduced. In particular, some important issues about data preparation in ANN forecasting are involved in this talk. Finally, some related research progress on ANNs in time series forecasting done by presenters are briefly given.

Short Bio

Prof. Lean Yu received his Ph.D. degree in Management Sciences and Engineering from Academy of Mathematics and Systems Science, Chinese Academy of Sciences (CAS) in 2005. He is currently a professor and PhD supervisor of School of Economics and Management, Beijing University of Chemical Technology. He is a winner of National Science Fund for Distinguished Young Scholars, National Program for Support of Top-Notch Young Professionals and "Hundred Talents Program" of Chinese Academy of Sciences. He is acted as a guest editor, managing editor, associate editor and editorial members of many international journals including Computers & Operations Research and Journal of Computer Science. So far, he has published five monographs (two monographs have been published by Springer-Verlag) and over 100 SCI/SSCI articles in some top journals including IEEE Transactions on Evolutionary Computation and IEEE Transactions on Knowledge and Data Engineering. At the same time, he received many awards and honors, such as "Elsevier Most Cited Chinese Researchers" from Elsevier, "China Youth Science and Technology Award" from the Organization Department of the Central Committee of the CPC, "The 100 National Best PhD Theses Award" from Academic Degrees Committee of State Council and Ministry of Education of China, "First Class Prize for Beijing Science and Technology Award" from the Beijing Municipal Government, First Class Prize for Natural Science Award of Ministry of Education (MOE), Beijing Mao Yisheng Youth Science and Technology Award, and "Lu Jia-xi Young Talent Award" of Chinese Academy of Sciences. His research interests include business intelligence, big data mining, economic forecasting and intelligent financial management.

Proceedings of the Tenth International
Conference on Information (Information'2021)

ISBN 4-901329-11-8

An estimation of a scale parameter based on the Fourier-Mellin transform

Akira Morimoto
Faculty of Education, Osaka Kyoiku University, Osaka 582-8582, Japan
morimoto@cc.osaka-kyoiku.ac.jp

Abstract

The Mellin transform is well known as a scale invariant transform. The Fourier-Mellin transform is not only scale invariant but also time shift invariant. Based on the Fourier-Mellin transform, an algorithm, which checks whether two speech signals $f(t)$ and $g(t)$ have a relation $g(t) = \beta f(\alpha t - \gamma)$ and estimates α and β, is proposed. Several experiments have shown the usefulness of the algorithm.

Keywords : the Mellin transform, the Fourier-Mellin transform, scale invariant, time shift invariant, speech signal

1 Introduction

The Mellin transform [1, 2, 3] is well known as a scale invariant transform. For speech signal $f(t)$ and its scale transform $f_\alpha(t) = f(\alpha t)$, we can estimate $\alpha > 0$ by the Mellin transform (See §2). From $f(t)$ and its scale-shift transform $f_{\alpha,\gamma}(t) = f(\alpha t - \gamma)$, we cannot estimate the scale α.

The absolute value of the Fourier transform is time shift invariant. If we apply the Mellin transform to the absolute value of the Fourier transform, then we can estimate α from $f(t)$ and $f_{\alpha,\gamma}(t)$. This method is called the Fourier-Mellin transform (see §3). The Fourier-Mellin transform are widely applied in various fields, for example, mammalian hearing [4], rhythm description [5], gray-Level image description [6], etc.

In §4, we propose Algorithm 9 which checks whether two speech signals $f(t)$ and $g(t)$ have a relation $g(t) = \beta f(\alpha t - \gamma)$. If the relation exists, we can estimate α and β by the algorithm. Several experiments have shown the usefulness of the algorithm.

2 The Mellin transform

We Define the Mellin transform according to [1].

Definition 1. For $\omega > 0$, the Mellin transform of a function f is

$$\mathcal{M}f(\omega) = \int_0^{+\infty} f(t)\, t^\omega \, dt.$$

The inverse Mellin transform is

$$f(t) = \frac{1}{2\pi i} \int_{c-i\infty}^{c+i\infty} \{\mathcal{M}f(\omega)\}\ t^{-\omega-1}\, d\omega,$$

where $c \in \mathbb{R}$ and $i = \sqrt{-1}$.

Property 2. *For a scale $\alpha > 0$, the Mellin transform of $f_\alpha(t) = f(\alpha t)$ is*

$$\mathcal{M}f_\alpha(\omega) = \alpha^{(\omega+1)}\, \mathcal{M}f(\omega).$$

Hence, the scale parameter α is

$$\alpha = \left(\frac{\mathcal{M}f_\alpha(\omega)}{\mathcal{M}f(\omega)} \right)^{1/(\omega+1)}. \tag{1}$$

Example 3. Define $f(t)$ by

$$f(t) = \begin{cases} \sin(2\pi t), & 0 \le t \le 2, \\ 0, & \text{otherwise}, \end{cases}$$

we set $g(t) = f(t-2)$ and $g_\alpha(t) = g(\alpha t)$ with $\alpha = 0.7$. In the upper left of Figure 1, the blue real line corresponds to $g(t)$ and the red broken line corresponds to $g_{0.7}(t)$. Using the equation (1), we make a graph of α against ω illustrated in the upper right of Figure 1. The graph is like a constant function, because the range of fluctuation is about 0.5% of 0.7. Then we estimate the scale α at 0.7. We set $h(t) = f_{0.7}(t-2)$. In the lower left of Figure 1, the blue real line and the red broken line correspond to $g(t)$ and $h(t)$, respectively. We make a graph of α against ω illustrated in the lower right of Figure 1. We cannot estimate α from the graph. The time shift interferes with an estimation of α.

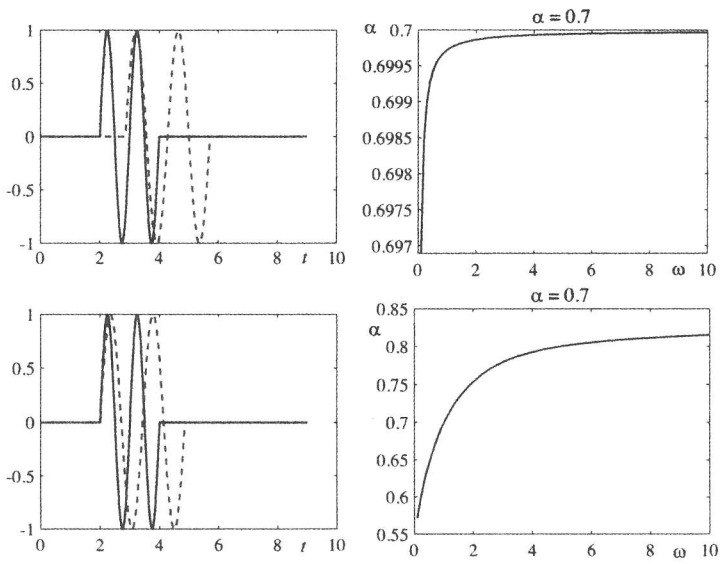

Figure 1: Upper left: $g(t) = f(t-2)$ (blue real line) and $g_{0.7}(t)$ (red broken line). Upper right: α against ω. Estimate α at 0.7. Lower left: $g(t)$ (blue real line) and $h(t) = f_{0.7}(t-2)$(red broken line). Lower right: α against ω.

3 The Fourier-Mellin transform

Definition 4. The Fourier transform of a function f is

$$\mathcal{F}f(\xi) = \widehat{f}(\xi) = \int_{-\infty}^{+\infty} f(t)\, e^{-i\xi t}\, dt.$$

Property 5. *The Fourier transform of* $f_\alpha(t) = f(\alpha t)$ *is*

$$\widehat{f_\alpha}(\xi) = \frac{1}{\alpha}\, \widehat{f}\left(\frac{\xi}{\alpha}\right).$$

Property 6. *The Fourier transform of a time shift* $f(t-\gamma)$ *is*

$$\mathcal{F}[f(\cdot - \gamma)](\xi) = e^{-i\gamma\xi}\, \mathcal{F}f(\xi).$$

Therefore, $|F[f(\cdot - \gamma)](\xi)| = |\mathcal{F}f(\xi)|$.

Definition 7. The Fourier-Mellin transform of a function f is

$$\mathcal{FM}[f](p,\omega) = \int_0^{+\infty} \left|\widehat{f}(\xi)\right|^p \xi^\omega d\xi,$$

where $p \geq 1$ is a constant.

Property 8. *For a scale $\alpha > 0$, the Fourier-Mellin transform of $f_{\alpha,\beta,\gamma}(t) = \beta f(\alpha t - \gamma)$ is*

$$\mathcal{FM}[f_{\alpha,\beta,\gamma}](p,\omega) = \alpha^{(\omega+1-p)}\, \beta^p\, \mathcal{FM}[f](p,\omega). \tag{2}$$

Algorithm 9. For $f(t)$ and $g(t)$, we decide whether $g(t) = f_{\alpha,\beta,\gamma}(t)$, and estimate α and β in the following steps:

1. Take the natural logarithm of the equation (2), we have

$$\begin{aligned} R(p,\omega) &= \log\left(\mathcal{FM}[f_{\alpha,\beta,\gamma}](p,\omega)\right) - \log\left(\mathcal{FM}[f](p,\omega)\right) \\ &= (\omega + 1 - p)\log\alpha + p\log\beta. \end{aligned}$$

2. Fix $p = 4$. For several ω, we estimate $\log\alpha$ and $\log\beta$ by the least square method.

3. Using the estimation of β, plot a graph of

$$\alpha = \left(\frac{\mathcal{FM}[f_\alpha](p,\omega)}{\beta^p\, \mathcal{FM}[f](p,\omega)}\right)^{1/(\omega+1-p)} \tag{3}$$

   against ω.

4. If the graph of α is like a constant function, we decide $g(t) = f_{\alpha,\beta,\gamma}(t)$, and estimate α by the step 2.

Example 10. We apply Algorithm 9 to speech signals. We play the same speech signal with different sampling rates which are 12000 Hz and 16000 Hz, and record them. The upper left of Figure 2 is graphs of two speech signals. The upper right of Figure 2 is graphs of the absolute values of the Fourier transforms. We make a graph of $R(p,\omega)$, $p = 4$ against ω (See the middle left of Figure 2). Using the least square method, we estimate $\alpha = 1.3338$ and $\beta = 1.5016$. We plot a graph of α against ω. the middle right of Figure 2 is like a constant function, because the range of fluctuation is about 2% of $\alpha = 1.3338$. Then we decide the second speech is just a time-shifted of the first speech with the scale α.

In the case of different speeches, the lower left of Figure 2 is the graphs of two different speech signals. We plot a graph of α against ω. We decide two speeches have no relation, because the lower right of Figure 2 is not like a constant function.

Acknowledgements

This work was partially supported by JSPS KAKENHI Grant Numbers 20K03653.

References

[1] R. Godement, Analysis III, "Analytic and Differential Functions, Manifolds and Riemann Surfaces", Springer, 2015.

[2] L. Cohen, "The scale representation". in IEEE Transactions on Signal Processing, **41**, 3275–3292, 1993, doi: 10.1109/78.258073.

[3] A. De Sena and D. Rocchesso, "A Fast Mellin and Scale Transform", EURASIP J. Adv. Signal Process. 2007, 089170 (2007), doi: 10.1155/2007/89170.

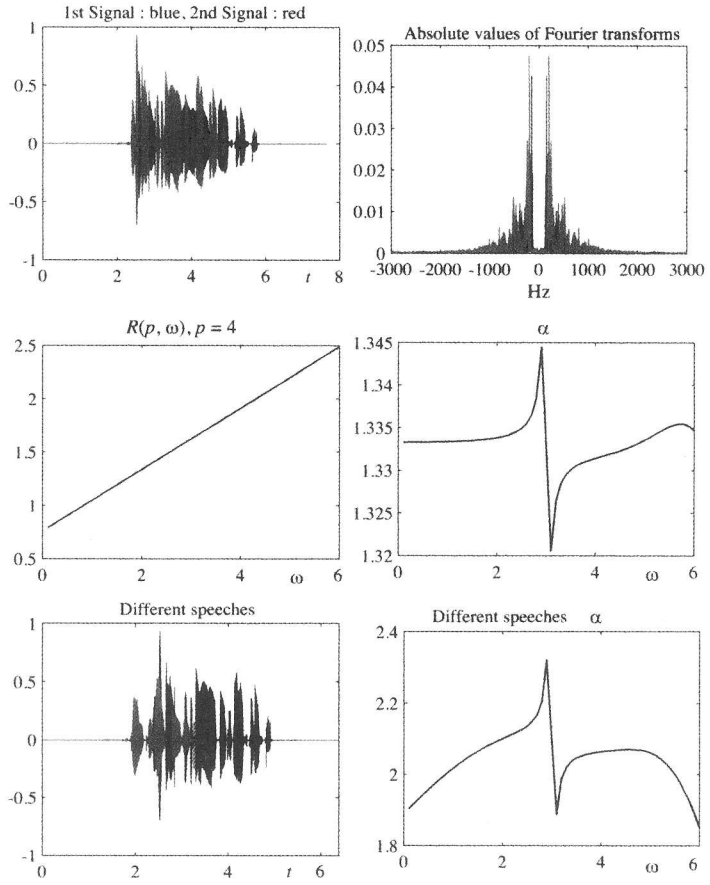

Figure 2: Upper left: the first speech (blue), the second speech (red). Upper right: the absolute values of the Fourier transforms. Middle left: $R(p,\omega)$, $p = 4$. Middle right: the graph of α against ω. The range of fluctuation is about 2% of $\alpha = 1.3338$. We decide the second speech is some scale transform of the first speech. Lower left: different speeches. Lower right: the graph of α against ω. The graph is not like a constant function.

[4] R A Altes, "The Fourier-Mellin transform and mammalian hearing", J Acoust Soc Am. 1978 Jan;63(1):174-83. doi: 10.1121/1.381708.

[5] U. Marchand and G. Peeters, "Scale and shift invariant time/frequency representation using auditory statistics: Application to rhythm description", 2016 IEEE 26th International Workshop on Machine Learning for Signal Processing (MLSP), 1–6, 2016, doi: 10.1109/MLSP.2016.7738904.

[6] S. Derrode and F. Ghorbel, "Robust and Efficient Fourier-Mellin Transform Approximations for Gray-Level Image Reconstruction and Complete Invariant Description", Computer Vision and Image Understanding, **83**, 57–78, 2001, doi: 10.1006/cviu.2001.0922.

Proceedings of the Tenth International
Conference on Information (Information'2021)
ISBN 4-901329-11-8

Uncertainty Principles Related to Fractional Fourier Transform

Mawardi Bahri[a] and Ryuichi Ashino[b]

[a] Department of Mathematics, Hasanuddin University, Makassar 90245, Indonesia
e-mail: mawardibahri@gmail.com
[b] Mathematics and Informatics, Osaka Kyoiku University, Osaka 582-8582, Japan
e-mail: ashino@cc.osaka-kyoiku.ac.jp

Abstract

A direct relation between the Fourier transform and the fractional Fourier transform is studied. Some properties of the fractional Fourier transform are investigated using this relation. Several versions of uncertainty principles involving the fractional Fourier transform are presented.

Keywords: fractional Fourier transform, Donoho-Stark uncertainty principle, fractional wavelet transform

AMS Subject Classification: 11R52, 42A38, 15A66, 83A05, 35L05

1 Fractional Fourier Transform (FRFT)

The inner product of $L^2(\mathbb{R})$ and Fourier transform of $f \in L^2(\mathbb{R})$ are defined by

$$\langle f, g\rangle_{L^2(\mathbb{R})} = \int_{\mathbb{R}} f(t)\overline{g(t)}\,dt, \quad \mathcal{F}\{f\}(\xi) = \frac{1}{\sqrt{2\pi}}\int_{\mathbb{R}} f(t)e^{-it\xi}\,dt.$$

The fractional Fourier transform of $f \in L^1(\mathbb{R})$ is defined by $\mathcal{F}^\theta\{f\}(\xi) = \displaystyle\int_{\mathbb{R}} f(t)K^\theta(t,\xi)\,dt$, where

$$K^\theta(\xi,t) = \begin{cases} C^\theta e^{i(t^2+\xi^2)\frac{\cot\theta}{2} - it\xi\csc\theta}, & \theta \neq n\pi \\ \frac{1}{\sqrt{2\pi}}e^{-it\xi}, & \theta = \frac{\pi}{2} \\ \delta(t-\xi), & \theta = 2n\pi \\ \delta(t+\xi), & \theta = (2n+1)\pi, n \in \mathbb{Z}. \end{cases} \tag{1}$$

Here, δ is the Dirac delta function and

$$C^\theta = \frac{e^{i(\frac{\theta}{2}-\frac{\pi}{4})}}{\sqrt{2\pi\sin\theta}} = \sqrt{\frac{1-i\cot\theta}{2\pi}}. \tag{2}$$

Note that

$$\begin{aligned} \mathcal{F}^\theta\{f\}(\xi) &= C^\theta \int_{\mathbb{R}} f(t)e^{i(t^2+\xi^2)\frac{\cot\theta}{2} - it\xi\csc\theta}\,dt \\ &= C^\theta e^{i\xi^2\frac{\cot\theta}{2}} \int_{\mathbb{R}} f(t)e^{it^2\frac{\cot\theta}{2} - it\xi\csc\theta}\,dt \\ &= C^\theta e^{i\xi^2\frac{\cot\theta}{2}} \sqrt{2\pi}\mathcal{F}\{e^{it^2\frac{\cot\theta}{2}} f(t)\}(\xi\csc\theta). \end{aligned} \tag{3}$$

Denote

$$f_\theta(t) = e^{it^2 \frac{\cot\theta}{2}} f(t), \tag{4}$$

then we have

$$\frac{e^{-i\xi^2 \frac{\cot\theta}{2}}}{\sqrt{1 - i\cot\theta}} \mathcal{F}^\theta\{f\}(\xi) = \mathcal{F}\{f_\theta\}(\xi \csc\theta), \qquad \frac{e^{-i\xi^2 \frac{\cot\theta}{2}}}{\sqrt{1 - i\cot\theta}} \mathcal{F}^\theta\{e^{it^2 \frac{\cot\theta}{2}} f\}(\xi) = \mathcal{F}\{f\}(\xi \csc\theta). \tag{5}$$

Now we provide the different proof of Parseval formula for the FRFT using the direct relation between the FT and FRFT.

Lemma 1.1 (FRFT Parseval). *For all $f, g \in L^2(\mathbb{R})$, the following relation holds:*

$$\langle f, g\rangle_{L^2(\mathbb{R})} = \langle \mathcal{F}^\theta\{f\}, \mathcal{F}^\theta\{g\}\rangle_{L^2(\mathbb{R})}, \tag{6}$$

and

$$\|f\|^2_{L^2(\mathbb{R})} = \|\mathcal{F}^\theta\{f\}\|^2_{L^2(\mathbb{R})}. \tag{7}$$

2 Uncertainty Principles for FRFT

Our interest is to derive two uncertainty principles involving the FRFT. They are generalized forms of the uncertainty principles related to the conventional Fourier transform.

Theorem 2.1 (FRFT uncertainty principle). *Let f be in $L^2(\mathbb{R})$. If $\mathcal{F}^\theta\{f\} \in L^2(\mathbb{R})$, then the following inequality holds:*

$$\int_{\mathbb{R}} |t|^2 |f(t)|^2 \, dt \int_{\mathbb{R}} |\xi|^2 |\mathcal{F}^\theta\{f\}(\xi)|^2 \, d\xi \geq \frac{|\sin\theta|^2}{4} \left(\int_{\mathbb{R}} |f(t)|^2 \, dt \right)^2. \tag{8}$$

Extension of the above theorem is showed by the following result.

Theorem 2.2. *Under the same conditions as in Theorem 2.1 we have*

$$\int_{\mathbb{R}} |t|^s |f(t)|^s \, dt \int_{\mathbb{R}} |\xi|^s |\mathcal{F}^\theta\{f\}(\xi)|^s \, d\xi \geq \frac{|\sin\theta|^{\frac{s}{2}+1}}{2^s} \left(\int_{\mathbb{R}} |f(t)|^s \, dt \right)^s \tag{9}$$

for $1 \leq s \leq 2$.

We state the following result, which describes the sharp Hausdorff-Young inequality related to the FRFT .

Theorem 2.3 (FRFT Hausdorff-Young). *For any $1 \leq r \leq 2$ such that $\frac{1}{r} + \frac{1}{s} = 1$. Then for every function f in $L^r(\mathbb{R})$, it holds*

$$\left(\int_{\mathbb{R}} |\mathcal{F}^\theta\{f\}(\xi)|^s \, d\xi \right)^{1/s} \leq |\sin\theta|^{\frac{1}{s} - \frac{1}{2}} r^{1/2r} s^{-1/2s} \left(\int_{\mathbb{R}} |f(t)|^r \, dt \right)^{1/r}. \tag{10}$$

Proof. Applying the sharp Hausdorff-Young inequality related to the conventional Fourier transform results in

$$\left(\int_{\mathbb{R}} |\mathcal{F}\{f\}(\xi)|^s \, d\xi \right)^{1/s} \leq r^{1/2r} s^{-1/2s} \left(\int_{\mathbb{R}} |f(t)|^r \, dt \right)^{1/r}. \tag{11}$$

Including f_θ defined by (4) into both sides of (11) yields

$$\left(\int_{\mathbb{R}} |\mathcal{F}\{f_\theta\}(\xi)|^s \, d\xi\right)^{1/s} \leq r^{1/2r} s^{-1/2s} \left(\int_{\mathbb{R}} |f_\theta(t)|^r \, dt\right)^{1/r}. \tag{12}$$

We further have

$$\left(\int_{\mathbb{R}} |\mathcal{F}\{f_\theta\}(\xi \csc\theta)|^s \, d\xi \csc\theta\right)^{1/s} \leq r^{1/2r} s^{-1/2s} \left(\int_{\mathbb{R}} |f_\theta(t)|^r \, dt\right)^{1/r}. \tag{13}$$

Using (5) we write the above identity as

$$\left(\int_{\mathbb{R}} \left|\frac{e^{-i\xi^2 \frac{\cot\theta}{2}}}{\sqrt{1-i\cot\theta}} \mathcal{F}^\theta\{f\}(\xi)\right|^s d\xi \csc\theta\right)^{1/s} \leq r^{1/2r} s^{-1/2s} \left(\int_{\mathbb{R}} |e^{it^2 \frac{\cot\theta}{2}} f(t)|^r \, dt\right)^{1/r}. \tag{14}$$

Thus

$$\left(|\sin\theta|^{\frac{s}{2}-1} \int_{\mathbb{R}} |\mathcal{F}^\theta\{f\}(\xi)|^s \, d\xi\right)^{1/s} \leq r^{1/2r} s^{-1/2s} \left(\int_{\mathbb{R}} |f(t)|^r \, dt\right)^{1/r}. \tag{15}$$

Or, equivalently,

$$\left(\int_{\mathbb{R}} |\mathcal{F}^\theta\{f\}(\xi)|^s \, d\xi\right)^{1/s} \leq |\sin\theta|^{\frac{1}{s}-\frac{1}{2}} r^{1/2r} s^{-1/2s} \left(\int_{\mathbb{R}} |f(t)|^r \, dt\right)^{1/r}, \tag{16}$$

which finishes the proof of the theorem. □

Theorem 2.4 (FRFT Donoho-Strak'uncertainty Principle). *Suppose that E and T are measurable subsets of $\mathbb{R}$. Suppose that $f \in L^1(\mathbb{R}) \cap L^s(\mathbb{R})$ with $1 \leq s \leq 2$ such that $\frac{1}{s} + \frac{1}{r} = 1$. Then for any f is ϵ_E-concentrated to E in $L^1(\mathbb{R})$-norm and $\mathcal{F}^\theta\{f\}$ is ϵ_T-concentrated to T in $L^r(\mathbb{R})$-norm we have*

$$\|\mathcal{F}^\theta\{f\}\|_{L^r(\mathbb{R})} \leq \frac{|C^\theta||E|^{1/r}|T|^{1/r}\|f\|_{L^s(\mathbb{R})}}{(1-\epsilon_E)(1-\epsilon_T)}. \tag{17}$$

In particular, for $s = 2$, equation (17) becomes

$$(1-\epsilon_E)(1-\epsilon_T) \leq |C^\theta|\sqrt{|E||T|}. \tag{18}$$

Theorem 2.5. *Let E and T be measurable subsets of $\mathbb{R}$ and let $f \in L^r(\mathbb{R})$ with $1 \leq r \leq 2$ such that $\frac{1}{r} + \frac{1}{s} = 1$. If f is ϵ_E-bandlimited to E in $L^r(\mathbb{R})$-norm, then the following inequality holds:*

$$\|P_E f\|_{L^r(\mathbb{R})} \leq \left(|E|^{\frac{1}{r}}|T|^{\frac{1}{r}}|C^\theta||\sin\theta|^{\frac{1}{s}-\frac{1}{2}} r^{1/2r} s^{-1/2s}(1+\epsilon_T) + \epsilon_T\right)\|f\|_{L^r(\mathbb{R})}. \tag{19}$$

Theorem 2.6. *Assume the same conditions as in Theorem 2.5. Under the additional condition that the function f is ϵ_E-concentrated to E in $L^r(\mathbb{R})$-norm, then one has*

$$\frac{1-\epsilon_E-\epsilon_T}{1+\epsilon_T} \leq |E|^{\frac{1}{r}}|T|^{\frac{1}{r}}|C^\theta||\sin\theta|^{\frac{1}{s}-\frac{1}{2}} r^{1/2r} s^{-1/2s}. \tag{20}$$

Acknowledgments.

The first author is partially supported by grant from Ministry of Research, Technology and Higher Education, Indonesia under PDUPT scheme. The second author is partially supported by JSPS KAKENHI Grant Number 20K03653.

References

[1] L. B. Almeida, The fractional Fourier transform and time-frequency representations, IEEE Trans.Signal Process., **42**(11), 3084–3091, 1994.

[2] X. Guanlei, W. Xiaotong, and X. Xiaogang, The logarithmic, Heisenberg's and short-time uncertainty principles associated with fractional Fourier transform, Signal Processing, **89**(3), 339–343, 2009.

[3] V. Namias, The fractional order Fourier transform and its application to quantum mechanics, IMA J. Appl. Math., **25**(3), 241–265, 1980.

[4] J. Shi, N. Zhang and X. Liu, A novel fractional wavelet transform and its applications, Sci. China Inf. Sci, **55**(6), 1270–1279, 2012.

[5] A. Prasad, S. Manna, A. Mahato, and V. K. Singh, Generalized continuous wavelet transform associated with the fractional Fourier transform, J. Comput. Appli. Math., **259**, 660–671, 2014.

[6] H. M. Ozaktas, Z. Zalevsky, and M. A. Kutay, The Fractional Fourier Transform with Application in Optics and Signal Processing, John Wiley & Sons, Chichester, England, 2001.

[7] J. Shi, X. Liu, and N. Zhang, On uncertainty principle for signal concentrations with fractional Fourier transform, Signal Processing, **92**(12), 2830–2836, 2012.

[8] Z. I. Zayed, On the relationship between the Fourier and fractional Fourier transforms, IEEE Signal Processing Letters, **3**(12), 310–311, 1996.

[9] Z. I. Zayed, A convolution and product theorem for the fractional Fourier transform, IEEE Signal Processing Letters, **5**(4), 101–103, 1998.

[10] S. K. Singh, The fractional S-transform on space of type S, Journal of Mathematics, **vol. 2013**, Article ID 105848, 2013, 9 pages, https://doi.org/10.1155/2013/105848.

[11] H. Dai, Z. Hibao, W. Wang, A new fractional wavelet transform, Communications in Nonlinear Science and Numerical Simulation, **44**, 19–36, 2017.

[12] M. Bahri and R. Ashino, Logarithmic uncertainty principle, convolution theorem related to continuous fractional wavelet transform and its properties on a generalized Sobolev space, International Journal of Wavelets, Multiresolution and Information Processing, **15** (5), 2017.

[13] R. Roopkumar, Quaternionic one-dimensional fractional Fourier Transform, Optik, **127** (4), 2016, 11657–11661.

[14] D. I. Donoho and P. B. Stark, Uncertainty principles and signal recovery, SIAM J. Appl. Math. **49**(3), 1989, 90–931.

Proceedings of the Tenth International
Conference on Information (Information'2021)
ISBN 4-901329-11-8

A REMARK ON WEIGHTED ESTIMATES FOR MULTILINEAR FOURIER MULTIPLIERS WITH MIXED NORM

MAI FUJITA AND YOSHIROH MACHIGASHIRA

Weighted estimates for multilinear Fourier multipliers satisfying Sobolev regularity with mixed norm are discussed. Our result can be understood as a generalization of [4] by using the L^r-based Sobolev space, $1 < r \leq 2$ with mixed norm.

1. Introduction

In this talk, we consider the boundedness of Fourier multiplier operators. Roughly speaking, the purpose of this study is to investigate "smoothness and integrable index" of multipliers which are measured by the Sobolev spaces defined in several ways. In this section, we give a prototype of main result, that is to say, $n = N = 1$ in Theorem 2.1.

Let $N = 1$. This means we consider the linear setting. For $m \in L^\infty(\mathbb{R}_\xi)$, the linear Fourier multiplier operator T_m is defined by

$$T_m(f)(x) = \mathcal{F}^{-1}[m(\xi)\widehat{f}(\xi)] = \left\{\mathcal{F}^{-1}[m] * f\right\}(x) = \frac{1}{2\pi}\int_{\mathbb{R}} e^{ix\cdot\xi} m(\xi)\widehat{f}(\xi)\, d\xi$$

for $f \in \mathcal{S}(\mathbb{R})$, where $x, \xi \in \mathbb{R}$ (see Section 3 for the definitions of function spaces). As an example of this operators, namely, **systems**, we recall the Hilbert transform, that is, **the Analytic Signals**. The multiplier m of the Hilbert transform on $\mathbb{R}$ is given by $m(\xi) = -i\mathrm{sgn}(\xi)$. Next, we recall the cut-off function, **scalling** and **localization**. Let $\Psi \in \mathcal{S}(\mathbb{R})$ be such that

$$\mathrm{supp}\,\Psi \subset \{\xi \in \mathbb{R} : 1/2 \leq |\xi| \leq 2\}, \quad \sum_{k\in\mathbb{Z}} \Psi(\xi/2^k) = 1, \quad \xi \in \mathbb{R}\setminus\{0\}.$$

We set

$$m_j(\xi) = m(2^j\xi)\Psi(\xi), \quad j \in \mathbb{Z}.$$

Our aim is to assure the boundedness of T_m, that is, **stability of this system** under the condition $m_j \in H^s_2$, where H^s_2 is the L^2-based Sobolev space.

In the next section, we give the notation and main result in the general setting.

2. The Result

For $m \in L^\infty(\mathbb{R}^{Nn})$, the N-linear Fourier multiplier operator T_m is defined by

$$T_m(f_1,\dots,f_N)(x) = \frac{1}{(2\pi)^{Nn}}\int_{(\mathbb{R}^n)^N} e^{ix\cdot(\xi_1+\cdots+\xi_N)} m(\xi)\widehat{f_1}(\xi_1)\dots\widehat{f_N}(\xi_N)\, d\xi$$

for $f_1,\dots,f_N \in \mathcal{S}(\mathbb{R}^n)$, where $x \in \mathbb{R}^n$, $\xi = (\xi_1,\dots,\xi_N) \in (\mathbb{R}^n)^N$ and $d\xi = d\xi_1\dots d\xi_N$. Let $\Psi \in \mathcal{S}(\mathbb{R}^{Nn})$ be such that

$$\mathrm{supp}\,\Psi \subset \left\{\xi \in \mathbb{R}^{Nn} : 1/2 \leq |\xi| \leq 2\right\}, \quad \sum_{k\in\mathbb{Z}} \Psi(\xi/2^k) = 1, \quad \xi \in \mathbb{R}^{Nn}\setminus\{0\},$$

and set

$$m_j(\xi_1,\dots,\xi_N) = m(2^j\xi_1,\dots,2^j\xi_N)\Psi(\xi_1,\dots,\xi_N), \quad j\in\mathbb{Z}.$$

We denote by $\|T_m\|_{L^{p_1}(w_1)\times\cdots\times L^{p_N}(w_N)\to L^p(w)}$ the smallest constant C satisfying

$$\|T_m(f_1,\dots,f_N)\|_{L^p(w)} \le C\prod_{i=1}^N \|f_i\|_{L^{p_i}(w_i)}, \quad f_1,\dots,f_N\in\mathcal{S}(\mathbb{R}^n)$$

(see Section 3 for the definition of function spaces).

In the unweighted case, Tomita [13] proved a Hörmander type multiplier theorem for multilinear operators, namely, if $s > Nn/2$ then

$$\|T_m\|_{L^{p_1}(\mathbb{R}^n)\times\cdots\times L^{p_N}(\mathbb{R}^n)\to L^p(\mathbb{R}^n)} \lesssim \sup_{j\in\mathbb{Z}} \|m_j\|_{H_2^s(\mathbb{R}^{Nn})}$$

for $1 < p_1,\dots,p_N,p < \infty$ satisfying $1/p_1+\cdots+1/p_N = 1/p$, where $H_2^s(\mathbb{R}^{Nn})$ is the L^2-based Sobolev space of usual type. Grafakos-Si [6] extended this result to the case $p \le 1$ by using the L^r-based Sobolev space, $1 < r \le 2$. For further results in this direction, see [5, 9, 10]. Let $1 < p_1,\dots,p_N < \infty$ and $1/p_1+\cdots+1/p_N = 1/p$. In the weighted case, Fujita-Tomita [4] proved that if $n/2 < s_i \le n$, $p_i > n/s_i$ and $w_i \in A_{p_is_i/n}$ for $i = 1,\dots,N$, then

$$\|T_m\|_{L^{p_1}(w_1)\times\cdots\times L^{p_N}(w_N)\to L^p(w)} \lesssim \sup_{j\in\mathbb{Z}} \|m_j\|_{H_2^{\vec{s}}((\mathbb{R}^n)^N)}, \tag{1}$$

where $w = w_1^{p/p_1}\dots w_N^{p/p_N}$ and $H_2^{\vec{s}}((\mathbb{R}^n)^N)$ is the Sobolev space of product type. This result can also be obtained from another approach of [7]. See [8, 1] for the endpoint cases.

The following is our main result which can be understood as a generalization of [4]. Taking $r_i = 2, i = 1,\dots,N$ in (2), we have (1). Si [12] obtained some weighted estimates for multilinear Fourier multipliers with the L^r-based Sobolev regularity, $1 < r \le 2$.

Theorem 2.1. *Let $1 < p_1,\dots,p_N < \infty$, $1/p_1+\cdots+1/p_N = 1/p$, $\vec{r} = (r_1,\dots,r_N) \in (1,2]^N$, $r_N \le r_{N-1} \le \cdots \le r_2 \le r_1$, $\vec{s} = (s_1,\dots,s_N) \in \mathbb{R}^N$ and $n/r_i < s_i \le n$ for $i = 1,\dots,N$. Assume*

$$p_i > n/s_i \quad \text{and} \quad w_i \in A_{p_is_i/n} \quad \text{for} \quad i = 1,\dots,N.$$

Then

$$\|T_m\|_{L^{p_1}(w_1)\times\cdots\times L^{p_N}(w_N)\to L^p(w)} \lesssim \sup_{j\in\mathbb{Z}} \|m_j\|_{H_{\vec{r}}^{\vec{s}}((\mathbb{R}^n)^N)}, \tag{2}$$

where $w = w_1^{p/p_1}\cdots w_N^{p/p_N}$ and $H_{\vec{r}}^{\vec{s}}((\mathbb{R}^n)^N)$ is the Sobolev space of product type with mixed norm

3. Preliminaries

Let $n \in \mathbb{N}$ be the dimension of the Euclidean space. The Lebesgue measure in $\mathbb{R}^n$ is denoted by dx (See, for example, [11, Chapter 1, 2]). Let N be a natural number, $N \ge 2$. An operator T acting on N-tuples of functions defined on $\mathbb{R}^n$ is called the N-linear operator. For two non-negative quantities A and B, the notation $A \lesssim B$ means that $A \le CB$ for some unspecified constant $C > 0$ independent of A and B, and the notation $A \approx B$ means that $A \lesssim B$ and $B \lesssim A$. Let $\mathcal{S}(\mathbb{R}^n)$

and $\mathcal{S}'(\mathbb{R}^n)$ be the Schwartz spaces of all rapidly decreasing smooth functions and tempered distributions, respectively. We define the Fourier transform $\mathcal{F}f$ and the inverse Fourier transform $\mathcal{F}^{-1}f$ of $f \in \mathcal{S}(\mathbb{R}^n)$ by

$$\mathcal{F}f(\xi) = \widehat{f}(\xi) = \int_{\mathbb{R}^n} e^{-ix\cdot\xi} f(x)\,dx \quad \text{and} \quad \mathcal{F}^{-1}f(x) = \frac{1}{(2\pi)^n}\int_{\mathbb{R}^n} e^{ix\cdot\xi} f(\xi)\,d\xi$$

(See, for example, [3, Chapter 1]). Let $0 < p < \infty$ and $w \geq 0$. The weighted Lebesgue space $L^p(w)$ consists of all measurable functions f on $\mathbb{R}^n$ such that

$$\|f\|_{L^p(w)} = \left(\int_{\mathbb{R}^n} |f(x)|^p w(x)\,dx\right)^{1/p} < \infty.$$

Let $1 < p < \infty$. We say that a weight w belongs to the Muckenhoupt class A_p if

$$\sup_B \left(\frac{1}{|B|}\int_B w(x)\,dx\right)\left(\frac{1}{|B|}\int_B w(x)^{1-p'}\,dx\right)^{p-1} < \infty,$$

where the supremum is taken over all balls B in $\mathbb{R}^n$, $|B|$ is the Lebesgue measure of B and p' is the conjugate exponent of p, that is, $1/p + 1/p' = 1$. It is well known that the Hardy-Littlewood maximal operator M is bounded on $L^p(w)$ if and only if $w \in A_p$([3, Theorem 7.3]).

For $s \in \mathbb{R}$, the Sobolev space $H_2^s(\mathbb{R}^n)$ consists of all $f \in \mathcal{S}'(\mathbb{R}^n)$ such that

$$\|f\|_{H_2^s(\mathbb{R}^n)} = \left(\int_{\mathbb{R}^n} \left|(1+|\xi|^2)^{s/2}\widehat{f}(\xi)\right|^2 d\xi\right)^{1/2} < \infty.$$

The norm of the Sobolev space of product type $H_2^{\vec{s}}((\mathbb{R}^n)^N)$, $\vec{s} = (s_1, \ldots, s_N) \in \mathbb{R}^N$, for $F \in \mathcal{S}'((\mathbb{R}^n)^N)$ is also defined by

$$\|F\|_{H_2^{\vec{s}}((\mathbb{R}^n)^N)} = \left(\int_{(\mathbb{R}^n)^N} \left|(1+|\xi_1|^2)^{s_1/2}\ldots(1+|\xi_N|^2)^{s_N/2}\widehat{F}(\xi)\right|^2 d\xi\right)^{1/2},$$

where $\xi = (\xi_1, \ldots, \xi_N) \in (\mathbb{R}^n)^N$.

We recall the definition of L^p-spaces with mixed norm ([2]). Let $\vec{p} = (p_1, \ldots, p_N) \in (0,\infty)^N$. The Lebesgue spaces with mixed norm $L^{\vec{p}}((\mathbb{R}^n)^N)$ consists of all measurable functions F on $(\mathbb{R}^n)^N$ such that

$$\|F\|_{L^{\vec{p}}((\mathbb{R}^n)^N)} = \Big\|\|F(x_1, \ldots, x_N)\|_{L^{p_1}(\mathbb{R}^n, dx_1)}\cdots\Big\|_{L^{p_N}(\mathbb{R}^n, dx_N)} < \infty,$$

where $(x_1, \cdots, x_N) \in (\mathbb{R}^n)^N$ and dx_i is the Lebesgue measure with respect to the variable $x_i, i = 1, \ldots, N$. The norm of the Sobolev space of product type with mixed norm $H_{\vec{r}}^{\vec{s}}((\mathbb{R}^n)^N)$, $\vec{s} = (s_1, \ldots, s_N) \in \mathbb{R}^N$ and $\vec{r} = (r_1, \ldots, r_N) \in (1,\infty)^N$, for $F \in \mathcal{S}'((\mathbb{R}^n)^N)$ is also defined by

$$\|F\|_{H_{\vec{r}}^{\vec{s}}((\mathbb{R}^n)^N)} = \left\|\mathcal{F}^{-1}\left[\langle\xi_1\rangle^{s_1}\cdots\langle\xi_N\rangle^{s_N}|\widehat{F}(\xi)|\right]\right\|_{L^{\vec{r}}((\mathbb{R}^n)^N)},$$

where $\xi = (\xi_1, \ldots, \xi_N) \in (\mathbb{R}^n)^N$ and $\langle\xi_i\rangle = (1+|\xi_i|^2)^{1/2}, i = 1, \ldots, N$.

The following lemmas will be used in the proof of Theorem 2.1.

Lemma 3.1 ([2, Young's inequality for mixed norms]). *Let* $\vec{p} = (p_1, \cdots, p_N) \in [1,\infty]^N$, *then*

$$\|f * g\|_{L^{\vec{p}}((\mathbb{R}^n)^N)} \leq \|f\|_{L^{\vec{p}}((\mathbb{R}^n)^N)}\,\|g\|_{L^{(1,\cdots,1)}((\mathbb{R}^n)^N)}.$$

Lemma 3.2 ([2, Hausdorff-Young's inequality for mixed norms]). *Let* $\vec{p} = (p_1, \cdots, p_N) \in [1,2]^N$ *and* $p_N \le p_{N-1} \le \cdots \le p_1$, *then*

$$\|\mathcal{F}[f]\|_{L^{\vec{q}}((\mathbb{R}^n)^N)} \le \|f\|_{L^{\vec{p}}((\mathbb{R}^n)^N)}$$

where $\vec{q} = (p_1', \cdots, p_N')$ *and* p_i' *is the conjugate exponent of* $p_i, i = 1, \ldots, N$.

4. Key Lemma

The following lemma is a key lemma in the proof of Theorem 2.1.

Lemma 4.1. *Let* $r > 0$, $\vec{r} = (r_1, \ldots, r_N)$, $r_N \le r_{N-1} \le \cdots \le r_2 \le r_1$, $\vec{s} = (s_1, \ldots, s_N)$, $n/r_i < s_i \le n$ *and* $n/s_i < q_i < r_i$, $i = 1, \ldots, N$. *Then, the estimate*

$$\left|T_{m(\cdot/2^j)}(f_1, \ldots, f_N)(x)\right| \lesssim \|m\|_{H^{\vec{s}}_{\vec{r}}((\mathbb{R}^n)^N)} \prod_{i=1}^{N} M(|f_i|^{q_i})(x)^{1/q_i}$$

holds for all $x \in \mathbb{R}^n$, $j \in \mathbb{Z}$ *and* $m \in H^{\vec{s}}_{\vec{r}}((\mathbb{R}^n)^N)$ *with* $\operatorname{supp} m \subset \{\xi = (\xi_1, \ldots, \xi_N) \in (\mathbb{R}^n)^N : |\xi| \le r\}$.

References

[1] M. Asano, On boundedness of multilinear Fourier multiplier operators on weighted Hardy spaces (Japanese), Reports of harmonic analysis seminar 2016, Vol. 32, 75–76.

[2] A. Benedek and R. Panzone, The spaces L^p, with mixed norm, Duke Math. J. 28 (1961), 301–324.

[3] J. Duoandikoetxea, Fourier Analysis, Graduate Studies in Mathematics 29, Amer. Math. Soc., Providence, RI, 2001.

[4] M. Fujita and N. Tomita, Weighted norm inequalities for multilinear Fourier multipliers, Trans. Amer. Math. Soc. 364 (2012), 6335–6353.

[5] L. Grafakos, A. Miyachi and N. Tomita, On multilinear Fourier multipliers of limited smoothness, Canad. J. Math. 65 (2013), 299–330.

[6] L. Grafakos and Z. Si, The Hörmander multiplier theorem for multilinear operators, J. Reine Angew. Math. 668 (2012), 133–147.

[7] G. Hu and C-C. Lin, Weighted norm inequalities for multilinear singular integral operators and applications, Anal. Appl. (Singap.) 12 (2014), 269–291.

[8] W. Li, Q. Xue and K. Yabuta, Weighted version of Carleson measure and multilinear Fourier multiplier, Forum Math. 27 (2015), 787–805.

[9] A. Miyachi and N. Tomita, Minimal smoothness conditions for bilinear Fourier multipliers, Rev. Mat. Iberoam. 29 (2013), 495–530.

[10] A. Miyachi and N. Tomita, Boundedness criterion for bilinear Fourier multiplier operators, Tohoku Math. J. 66 (2014), 55–76.

[11] W. Rudin, Real and Complex Analysis, Third edition. McGraw-Hill Book Co., New York, 1987.

[12] Z. Si, Some weighted estimates for multilinear Fourier multiplier operators, Abstr. Appl. Anal. 2013, Art. ID 987205, 10pp.

[13] N. Tomita, A Hörmander type multiplier theorem for multilinear operator, J. Funct. Anal. 259 (2010), 2028–2044.

Mai Fujita,
Email address: fujita-m89@ex.osaka-kyoiku.ac.jp

Yoshiroh Machigashira, Division of Math, Sciences, and Information Technology in Education, Osaka Kyoiku University, Kashiwara, Osaka 582-8582, Japan
Email address: machi@cc.osaka-kyoiku.ac.jp

Proceedings of the Tenth International
Conference on Information (Information'2021)
ISBN 4-901329-11-8

Big Data and Machine Learning: Algorithms for Analysis - with Case Studies

Yousuo Zou*, Leah Luo**, and Anne Zou***

*Computer Science Program, University of Guam, 303 University Drive, Mangilao, GU 96923, USA

**Department of Electrical Engineering and Computer Science, Syracuse University, Syracuse, NY 13244, USA

*** Department of Computer Science, Vanderbilt University, 2301 Vanderbilt Place, Nashville, TN 37235, USA

Abstract

In this paper the authors try to introduce 3 categories of algorithms recently used in big data and machine leaning analysis: a. Statistical and probability methods, b. Neutral networks algorithms methods, and c. the Optimized function analysis based on analytic mathematics and numerical methods (e.g. the Stenger Methods or the SINC Methods), which the author are using to train students at University of Guam. The paper also gives examples of case studies to show how to employ SINC Methods to do analysis and to solve linear regression, and particularly nonlinear regression problems.

Key Words Algorithms, Big Data Analysis, Optimized analysis methods, SINC Methods, Case studies

1.Introduction

In the study of data analysis and machine learning, in order to reduce the error of analysis and make accurate prediction for future performance, we need to select right analysis algorithms for the patterns of selected data. The recently used algorithms for data analysis and machine learning we teach our students can be classified into three categories. The 1ts category is to search the highest probability to make decision [1]; the 2nd category of methods is using electronic circuits to simulate human's brain nerve systems to reach the best physical status to make decision. This is the traditional computer science methods which have been very complicatedly developed with hundreds of layers of neural networks [2]. The 3rd category of methods combines mathematical and computer sciences, called optimized analytic function methods or newly developed SINC Methods, which have been initiated and developed by one of the authors' former PhD Adviser of 1990s, Professor Frank Stenger and his research team (especially his postdocs, PhDs and Master students). Therefore, we call these methods the Stenger Methods [3]. The above three analysis categories are different approaches, but the result is the same: the smartest decision-making.

In the above mentioned 3 categories of algorithms, the 1st and 2nd categories have been well introduced in publications, especially in various textbooks taught in colleges and universities worldwide [4, 5], we will not repeat them to discuss here. In the following we will concentrate on the 3rd category of algorithms, the Stenger Methods or SINC Methods. We will start from a group of PDEs (partial differential equations generated by the equation of the Least Squared Error Expression. Then we discuss the methods to solve the group of PDEs in case studies according to different patterns of the experimental data to find the optimized function, $Y(X)$, which can best describe the selected experimental data. We will tell how the SINC Methods work and how to use them to solve real world problems in data analysis and machine learning. We will also give a case study using a set of the real-world tourism industrial data and the optimized analytic function methods to show the accuracy of analysis of the methods.

2. Optimized Function Algorithms Based on the Least Squared Error Methods

Now, assume we have a group of experimental data from which we want to discover the laws (or regularities) of nature that are hiding in these experimental data (excluding instrument errors and computational errors of algorithms).

$$\begin{array}{lllll} x_i: & x_1, & x_2, & x_3, \quad \ldots, & x_n \\ y_i: & y_1, & y_2, & y_3, \quad \ldots, & y_n \end{array} \qquad (1)$$

Let's use the principle of Least Square method to find the unknown law expressed in mathematical format (or formula), $Y(X)$, *where* $X = (x_1, x_2, \cdots, x_n)$,

$$Q(X) = \sum_{i=1}^{n} [Y_i(X) - y_i]^2 = min. \qquad (2)$$

According to Expression *(2)*, we can have [making use of data set *(1)*]:

$$\begin{aligned} \frac{\partial Q}{\partial a_1} &= \sum_{i+1}^{n} 2(Y_i(X) - y_i) \frac{\partial Y}{\partial a_1} = 0 \\ \frac{\partial Q}{\partial a_2} &= \sum_{i=1}^{n} 2(Y_i(X) - y_i) \frac{\partial Y}{\partial a_2} = 0 \\ &\vdots \\ \frac{\partial Q}{\partial a_m} &= \sum_{i=1}^{n} 2(Y_i - y_i) \frac{\partial Y}{\partial a_m} = 0 \end{aligned} \qquad (3)$$

In the following we will discuss how to solve the Equations *(3)* above to find the optimized function, $Y(X)$, to do data analysis and machine learning.

3. Case Studies

3.1. Case 1: Linear Data Patterns

If the selected dataset *(1)* above is a linear pattern, Equations *(3)* can be easily solved in the regular linear regression methods either by traditional statistical regression method or by the optimized analytic function method, which needs to solve a group of linear algebraic equations using linear algebraic knowledge. The detailed computational procedures can be seen in regular mathematics or computer science textbooks.

3.2. Case 2: Nonlinear Data Patterns

If the selected datasets *(1)* above are nonlinear patterns, the method to solve Equations *(3)* will be complicated. For a weak nonlinear case, we can use some mathematical transformations to turn it into a group of linear algebraic equations to find their nonlinear analytic regression solutions, or, use a weak nonlinear approximation method to obtain an approximate analytic regression solution [6]. However, if the selected datasets *(1)* above appear as a strong nonlinear case, we wouldn't have the usual set of analytic solutions. But we can use computers to get numeric approximate solutions based on different computational algorithms, such as Newton-Gaussian iteration method or by SINC methods. The detailed steps and procedures for nonlinear regression using optimized analytic and numeric functions can be seen in textbooks and research papers published by Professor Frank Stenger [7].

The widely used new computational methods, the Stenger Methods (or SINC Methods) are mainly developed by Professor Frank Stenger and his graduate students at University of Utah and at various universities in the US and other countries. SINC methods are based on linear algebra, complex analytical

functions, Fourier transformation, Newton iteration and etc. SINC methods are highly efficient, more accurate high-performance computational algorithms compared to currently existing computational methods. SINC methods can re-write the whole sets of existing computational algorithms and make a revolution in future computational engineering and computational science. No other method of computation accomplishes such breadth of applicability, Due to their efficiency, these methods make possible the accurate solution of frequently occurring computational problems which were hitherto extremely difficult, or impossible to carry out. Parallel computation, e.g., the solution of multidimensional problems falls out very simply and efficiently for algorithms based on *SINC* methods. In the following we give an example as a real-world case study using a set of tourism industrial data, which is very important to the economy development for the island of Guam, to show the accuracy of the optimized analytic function methods applying into data analysis and machine learning.

3.3. Case 3: Data Analysis of Japanese Tourists Visited Guam in 2004 – 2017

The number of Japanese arrivals to Guam annually from 2004 to 2017 are listed in Table 1.

Table 1. Japanese Tourist Arrivals to Guam Annually during 2004 – 2017

Year	x_i	Number of Arrivals (y_i)	Number of Predicted (Y_i)
2004	0	894035	895275
2005	1	936219	937874
2006	2	959779	950826
2007	3	929618	934132
2008	4	882782	887792
2009	5	815262	811805
2010	6	884801	479888
2011	7	819256	819253
2012	8	907765	908574
2013	9	912093	911278
2014	10	826830	827096
2015	11	779405	790282
2016	12	752757	741870
2017	13	674343	677964

The data pattern can be visualized in Figure 1 below. It shows the selected data is a highly nonlinear pattern. Traditionally, we can use the classical Newton-Gaussian iteration method to solve the group of nonlinear algebraic equations generated from Equations *(3)*. The nature of the Newton-Gaussian iteration method is to use infinite linear functions with extremely short time-interval to simulate the nonlinear curve step by step. But this classical method causes huge computer's CPU computational efforts and consumes a lot of computer's memory. Therefore, it is not a high-performance computing method. In this study we have developed a new type of high-performance algorithm, use a set of finite simplest nonlinear analytic functions to replace the classical linear functions to approximate the selected nonlinear data curve. The detailed algorithms and computational procedures can be seen in [6, 7, 8].

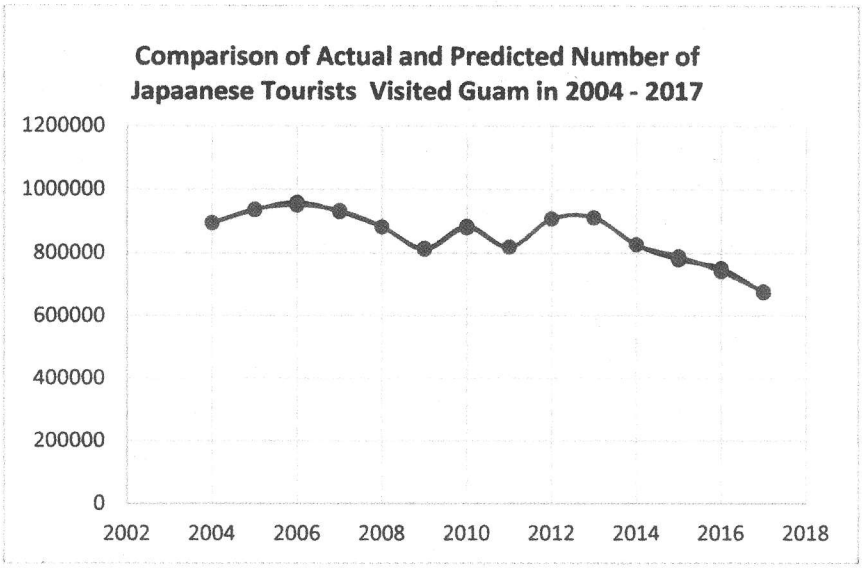

Fig. 1. Comparison of original data (Japanese arrivals annual to Guam, blue curve) and the optimized analytic function predicted data (red curve)

4. Accuracy and Error Analysis of the Nonlinear Regression Using the Optimized Function Algorithms

The computational results of the error analysis are listed in the following Table 2 using the standard total deviation and Pearson correlation coefficient methods.

Table 2. Statistical analysis of errors and Pearson correlation coefficient

Error type	Error formula	Error value
Total least square error	$Q(X) = \sum_1^{14}(y_i - Y(x_i))^2$	393182929.8
Mean value of original data	$\bar{y} = \frac{1}{14}\sum_1^{14} y_i$	855353.2143
Total difference of original data and mean value	$\sum_1^{14}(y_i - \bar{y})$	3872.47
Total variance	$\delta_{14}^2 = \frac{1}{14}\sum_1^{14}(y_i - \bar{y})^2$	6012994643
Standard total deviation	δ_{14}	77543.50161
Pearson correlation coefficient	$\frac{\sum_1^{14}(x_i - \bar{x})(y_i - \bar{y})}{\sqrt{\sum_1^{14}(x_i - \bar{x})^2}\sqrt{\sum_1^{14}(y_i - \bar{y})^2}}$	**0.997687109**

The accuracy and error analysis are used to compare the accuracy and errors generated by different analysis methods (or algorithms), therefore we can decide which method should be selected for high-performance computing in data analysis and machine learning research. From the Table 2, we can see the correlation coefficient of the selected nonlinear regression method is very high, 0.9977, almost 100%. The errors between function predicted and original data are among the least of other traditional statistical regression methods.

5. Conclusion

In the above, we have introduced the three categories of algorithms of analysis being used in big data analysis and machine learning research: neural network methods, statistical and probability methods, and optimized analytic function methods, among which, the authors emphasized on the category of the Stenger Methods or SINC Methods starting from a group of PDEs or partial differentials Equations *(3)* from the Least Squared Error Method to simulate and predict selected datasets. For the different data patterns, the paper made case studies on both linear and nonlinear cases to solve Equations (3) using the optimized analytic function methods. The paper also includes a special case study with real-world data of Japanese tourists visited Guam in 2004 – 2017 to show the accuracy and effectiveness of the optimized analytic function methods in big data analysis and machine learning research.

References

[1] James, G., Witten, D., Hastie, T., and Tibshirani R An Introduction to Statistical Learning: with Applications in R (Springer Texts in Statistics) 1st ed. 2013, Corr. 7th printing Edition, @Springer (2017), ISBN-13: 978-1461471370, ISBN-10: 1461471370.

[2] Aggarwal, C. C., Neural Networks and Deep Learning, A Textbook, @Springer International Publishing AG, part of Springer Nature (2018). ISBN 978-3-319-94462-3, ISBN 978-3-319-94463-0.

[3] Stenger, F., Numerical Methods Based on SINC and Analytic Functions, @Springer, New York (1993).

[4] Wang, L., and Wang, X. D., Introduction to Algorithms of Machine Learning, pp.388 (in Chinese), @Tsinghua University Press, Beijing (2019). (In Chinese: 王磊，王晓东: 机器学习导论，388 页， @清华大学出版社，北京， 2019). ISBN 978-7-302-52456-6.

[5] Ben, K, Mao, X., Zhang, Y., Zheng, D., Cai, D., Artificial Intelligence: Theory and Practice, pp 331 (in Chinese), @China Machine Press, Beijing (2016). (In Chinese: 贲可荣，毛新军，张彦铎，郑笛，蔡敦波，人工智能实践教程，331， @机械工业出版社， 北京，2016），ISBN 978-7-111-53869-1.

[6] Zou, Y., Chen, Z., and Xu, J., Binding Visualization Method and Numeric Method Together to Analyze Large Data – with A Case Study, Journal of advances in Mathematics and Computer Science, 15 (4), (2016), 1 -10,

[7] Stenger, F., Handbook of SINC Numerical Methods, @CRC Press, 2011, republished in (2017), pp 482, ISBN 9781138116177.

[8] Jarng, S.- S., Swanson, C., Lee, F., and Zou, Y., 64 Bands Hybrid Noise Reduction and Feedback Cancellation Algorithm for Hearing Aid, International Journal of Control and Automation, 7 (1), (2014), 427 – 436.

Corresponding Author **Yousuo Zou**, PhD,
Division of Mathematical and Computer Sciences
College of Natural and Applied Sciences
University of Guam
303 University Drive
Mangilao, GU 96923, USA
Email: yjzou@triton.uog.edu

Proceedings of the Tenth International
Conference on Information (Information'2021)
ISBN 4-901329-11-8

A New 2.5D Schema of the Regular and Semi-regular Polyhedra and Tilings: Classes II and IV

Robert C. Meurant

Director Emeritus, Institute of Traditional Studies; Adjunct Professor, Seoul National University College of Engineering PG Dept.; Exec. Director, Research & Education, Harrisco Enco • 4/1108 Shin-Seung Apt, ShinGok-Dong 685 Bungi, Uijeongbu-Si, Gyeonggi-Do, Republic of Korea 480-070 • Email: rmeurant@gmail.com

1. Abstract/Introduction

Inspired by Critchlow [1], I previously advanced a new order in space to account for the regularities and relationships of the regular and semi-regular polyhedra, in three classes I–III of {2,3,3}, {2,3,4}, and {2,3,5} symmetry, and its extension to the regular and semi-regular tilings of the plane, of two classes IV & V of {2,3,6} and {2,4,4} symmetry [2]. Each class consisted of 7 polytopes, together with a further enantiomorphic 8th snub polytope, which functioned as a transition polytope. Within each class, 3D polyhedra (2D polygonal arrays) were presented in inverted "T" form, consisting of a horizontal base truncation sequence between positive (+ve) polar and negative (–ve) polar polytope: PL^{+}– TP^{+}– QR – TP^{-}– PL^{-}; and a vertical transcendent sequence: 1° QR – (1.5° SnbQR) – 2° SR – 3° GR (with SnbQR in either enantiomorph form). In this work, I assume that the reader is familiar with that earlier research, which PDF is downloadable from my homepage [2]. The recognition of the regular polyhedra of +ve & –ve tetrahedra, octahedron & cube, and icosahedron & dodecahedron as extreme polar forms, mediated by the perfect forms of the Class I–III quasi-regular polyhedra of the respective 'tetratetrahedron' (2-colored octahedron), 'octahexahedron' (cuboctahedron), and icosidodecahedron (and corresponding Class IV & V quasi-regular 2D polygonal tri–hex and square–square arrays), was a relevant critical insight informing another of my papers [3].

In this present paper, I advance a cubic 2.5-dimensional schema to better describe the morphological structure of each class, by firstly positing a null polytope VP; then transforming the structural order of each class from the inverted T form of two sequences, into a cubic schema of two expansion sequence clusters, whereby in either, a seed polytope expands in either of two ways into two kinds of intermediary polytope, then in the other way, to a fully developed polytope. I describe this in relation to the most important Class II of {2,3,4} symmetry, as it corresponds to the polyhedra that constitute all 16 (10 distinct) of the Class III honeycombs. To confirm the validity of the order, I also describe Class IV of {2,3,6} symmetry of the regular and semi-regular tilings of the plane, which like Class II & III, is asymmetric: polar opposites are not the same though recolored polytopes, but different polytopes. The diverse correspondences of the order across classes are rigorous. In a longer development of this paper, I anticipate describing all five classes of the revised new order in space, characterizing the polytopes and their expansion sequences and clusters thereof.

Keywords: all-space-filling, polyhedra, honeycomb, tiling, structural morphology, semi-regular, order.
Supplementary Information: Colored figures and downloads http://www.rmeurant.com/its/si-21.html
A New Order in Space [2]: available at **PDF 06** at http://www.rmeurant.com/its/papers/polygon-1.html
(NB. To save space, the cubic 2.5D schema in shown throughout in vertically compressed cuboid form).

Nomenclature

+ve, positive; –ve, negative; C, class; CB, Cube; CO, Cuboctahedron; DD, Dodecagon (12-gon); E, Edge; E^0, Neutral Edge; F: Face; GR, Great Rhombic; GRCO, Great Rhombic Cuboctahedron; HX, Hexagon; NS, Neutral Square; ntrl, Neutral; OG, Octagon; OH, Octahedron; P/PL, Pole/Polar; $PL^{+/-}$, +/–ve Polar; QR, Quasi-regular; RS, Rotated (tRuncated) Square; RT, Rotated (tRuncated) Triangle; RX, Rotated Hexagon; Snb, Snub; SnbCO, Snub Cuboctahedron; SnbQR, Snub Quasi-regular; SQ, Square; SR, Small Rhombic; SRCO, Small Rhombic Cuboctahedron; T, Tetrahedron; Tr, Truncated; TC, Truncated Cube; TH, Tri–Hex (array); TO, Truncated Octahedron; TP, Truncated Polar; $TrP^{+/-}$, Truncated +/–ve Polar; TR, Triangle; $V^{+/-}$, +/–ve Vertex; V^0, Neutral Vertex; VP_C, Verticial Polytope.

2. Honeycomb/Tiling Investigations

Inspired by Grünbaum and Shephard [4], I later investigated the structural morphology of the all-space-filling polyhedral honeycombs of Class I–III of {2,3,3|2,3,3}, {2,3,3|2,3,4}, and {2,3,4|2,3,4} symmetry, and the corresponding polygonal tilings of the plane of Classes IV & V of {2,3,6} & {2,4,4} symmetry [5–7]. I gained significant insight into the honeycomb order when I posited for each class C the null quasi-regular polytope, as the vertex of zero dimension, with zero extension, but with +ve and –ve polar vertices V^+ and V^-, and neutral (ntrl) vertices V^0, all coincident in the **verticial polytope** $\mathbf{VP_C} = V^+ + V^0 + V^-$, while allowing spatial extension in the expansion sequences. This insight was first in relation to the various 3D honeycombs, especially the polyhedral honeycomb Class III of {2,3,4|2,3,4} symmetry, and later extended to the 2D honeycomb Class IV & V of {2,3,6} & {2,4,4} symmetry [5–7].

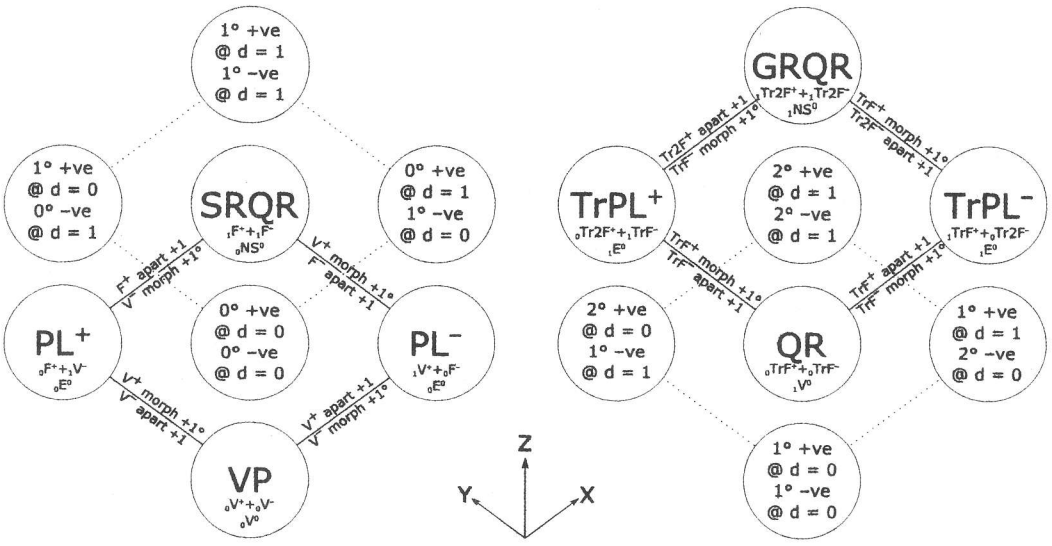

Fig. 1. Archetypal expansion sequence diamond clusters at lower (left) and upper (right). Texts of upper left and lower right diamonds refer to the faces of their lower and upper polytopes, respectively. 0° face is V, 1° face is PF (left); 1° face is TrPF, 2° is twice truncated = double frequency face (right). Seed polytope expands in 2 ways, as one pole morphs while other separates by +1, and *vice versa*; then morphed pole separates by +1 while separated pole morphs, and *vice versa*, to common rhombic QR.

Further progress was made through the organizing principle of the common formal structure of an expansion sequence cluster, of contracted seed honeycomb that in the first stage, expands in either of two ways to two intermediary honeycombs; and in the second stage,

expands further in the other of the two ways, respectively, to the fully expanded honeycomb [5–7]. A common pattern to all 16 Class III {2,3,4|2,3,4} honeycombs (of 10 distinct forms) [6: fig. 2] then became evident. The schema was also seen in the Class IV & V honeycomb 2D tiling arrays, allowing its recognition in the Class IV & V polytope arrays, and abstraction to the Class I–III polytopes. This revised order and 2.5D schema of the polyhedra enabled deep insight into the structural morphology of the regular & semi-regular polytopes (Fig. 1).

3. The revised order of the Class II polytopes and their 2.5D schema

The initial step of introducing the null polytope, in this Class II, the null CO VP_{II}, is to locate it on the central transcendent vertical axis, below the QR CO, in effect a 0° element. But this does not provide adequate relation to the other polyhedra. The appropriate formal structure then becomes two overlapping diamonds separated vertically (omitting SnbCO), recognizing two groups of 4 of the now 8 elements, in which each element of one group has a unique pair in the other group, logically pairing the lower form with its upper truncated form (Figs. 2, 3).

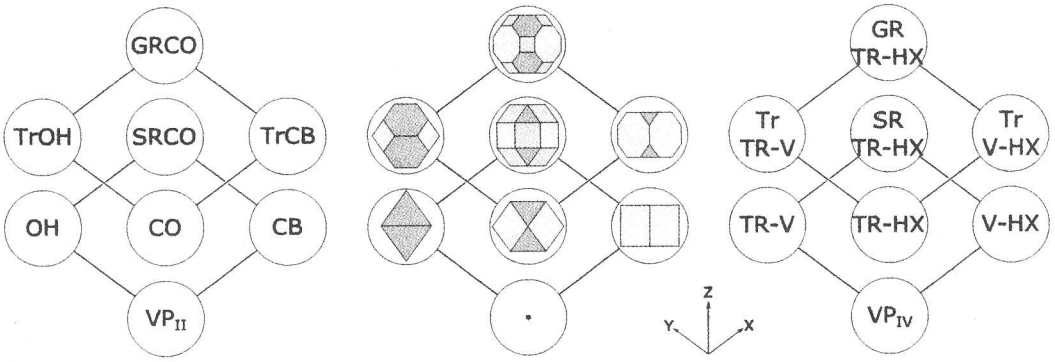

Fig. 2. Overlapping diamonds of the schema: Class II (left) & on neutral axis (center), Class IV (right).

This suggested investigating the corresponding transformations on each of the x, y, and z axes of the figure, where the two overlapping diamonds could now be recognized as the lower and upper faces of a cube in projection, in which those x, y, z axes could be examined (Fig. 3).

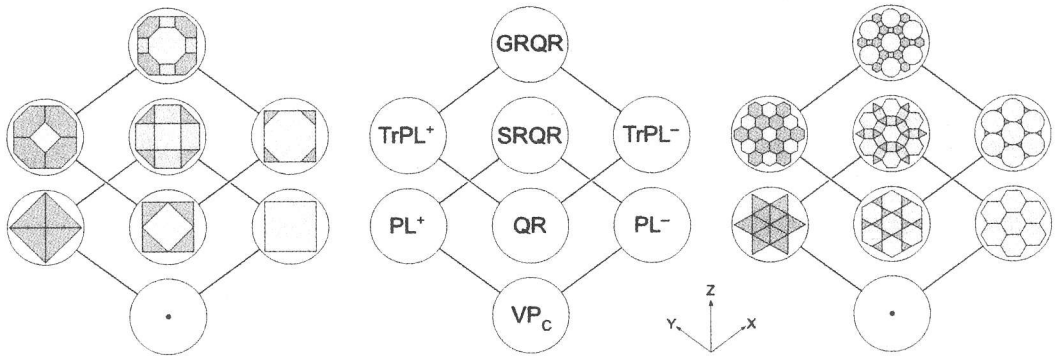

Fig. 3. Class II {2,3,4} (left), general 2.5D schema (center), Class IV {2,3,6} (right), on negative axis.

This schema shows a high degree of regularity. As previously mentioned, the vertical axis transformations correspond to truncations, hence the null polytope VP_{II} can be deduced to be a truncation of the QR CO; V^+, V^0, & V^- coincide in the verticial VP_{II}: $VP = V^+ + V^0 + V^-$.

In the lower diamond sequence cluster, the seed form of the null VP_{II} expands on the x-axis to the PL^- CB, and y-axis to the PL^+ OH: $^{OH}\nwarrow_{NV}\nearrow^{CB}$; then on the x-axis the OH, and on the y-axis the CB, expand to the common neutral SRCO: $_{OH}\nearrow^{SRCO}\nwarrow_{CB}$.

In the upper diamond sequence cluster, the seed form of the neutral QR CO expands on the x-axis to the TP^- TC, and y-axis to the TP^+ TO: $^{TO}\nwarrow_{CO}\nearrow^{TC}$; then on the x-axis the TC, and on the y-axis the TO, expand to the common neutral GRCO: $_{TO}\nearrow^{GRCO}\nwarrow_{TC}$, correspondingly.

Polyhedra axes are common to all polyhedra in a class, but vary class-to-class. Class II –ve, ntrl, & +ve axes are defined as the normal axes of the (100), (110), & (111) planes, respectively. OH vertices and CB faces are –ve, the edges of both in two orientations are ntrl, while OH TR faces and CB vertices are +ve. The QR CO is composed of –ve RSs and +ve RTs. Transformations of the constituent polytopes (faces/edges/vertices) of the 8 polyhedra or polygonal arrays in a class can then be characterized by axis of the 2.5D schema. For Class II:
On the z-axis (↑), –ve elements increase 1°: ($V_0^- \uparrow RS_0^-$, $SQ_0^- \uparrow OG_0^-$, $V_1^- \uparrow RS_1^-$, $SQ_1^- \uparrow OG_1^-$); ntrl elements separate, so adjoining vertices become unit distance apart: ($V_0^0 \uparrow V_1^0$, $2\times(E_0^0 \uparrow E_1^0)$, $NS_0^0 \uparrow NS_1^0$), the $2\times(E_0^0 \uparrow E_1^0)$, being in 2 sets of different orientations; and +ve elements increase 1°: ($V_0^+ \uparrow RT_0^+$, $TR_0^+ \uparrow HX_0^+$, $V_1^+ \uparrow RT_1^+$, $TR_1^+ \uparrow HX_1^+$).
On the x-axis (↗), –ve elements increase 1°: ($V_0^- \nearrow SQ_0^-$, $RS_0^- \nearrow OG_0^-$, $V_1^- \nearrow SQ_1^-$, $RS/_1^- \nearrow OG_1^-$); N elements increase 1°: $2\times(V^0 \nearrow E^0$, $E^0 \nearrow NS)$; and +ve elements separate, so adjoining vertices become unit distance apart: ($V_0^+ \nearrow V_1^+$, $TR_0^+ \nearrow TR_1^+$, $RT_0^+ \nearrow RT_1^+$, $HX_0^+ \nearrow HX_1^+$).
On the y-axis (↖), *reading steps right to left (R2L)*, –ve elements separate, so adjoining vertices become unit distance apart: ($V_1^- \nwarrow V_0^-$, $SQ_1^- \nwarrow SQ_0^-$, $RS_1^- \nwarrow RS_0^-$, $OG_1^- \nwarrow OG_0^-$); ntrl elements increase 1°: ($E_0^0 \nwarrow V_0^0$, $NS_0^0 \nwarrow E_0^0$, $E_1^0 \nwarrow V_1^0$, $NS_1^0 \nwarrow E_1^0$); and +ve elements increase 1°: $TR_0^+ \nwarrow V_0^+$, $HX_0^+ \nwarrow RT_0^+$, $TR_1^+ \nwarrow V_1^+$, $HX_1^+ \nwarrow RT_1^+$) (refer Figs. 1–3).

The Class IV –ve axes are defined as the normal axes of the mid-faces of the triangles of the PL TR array, the ntrl axes in two sets of orientations as the normal axes of the mid-edges of the PL TR and PL HX arrays, respectively, and the +ve axes as the normal axes of the mid-faces of the hexagons of the PL HX array, respectively. Hence the PL^+ TR array V^- and PL^- HX array HX are –ve, the edges of both polar arrays in two sets are ntrl, while the PL^+ TR array TR and PL^- HX array V^- are +ve. The QR TR–HX (TH) array is composed of –ve RXs and +ve RTs. Transformations of the constituent polytopes (faces/edges/vertices) of the 8 Class IV polygonal arrays can then be characterized by axis of the 2.5D schema:
On the z-axis (↑), –ve elements increase by 1°: ($V_0^- \uparrow RX_0^-$, $HX_0^- \uparrow DD_0^-$, $V_1^- \uparrow RX_1^-$, $HX_1^- \uparrow DD_1^-$); ntrl elements separate, so that adjoining vertices became unit distance apart: ($V_0^0 \uparrow V_1^0$, $2\times(E_0^0 \uparrow E_1^0)$, $NS_0^0 \uparrow NS_1^0$), the $2\times(E_0^0 \uparrow E_1^0)$ being in 2 sets of different orientations; while +ve elements increase by 1°: ($V_0^+ \uparrow RT_0^+$, $TR_0^+ \uparrow RX_0^+$, $V_1^+ \uparrow RT_1^+$, $TR_1^+ \uparrow RX_1^+$).
On the x-axis (↗), –ve elements increase by 1°: ($V_0^- \nearrow HX_0^-$, $RX_0^- \nearrow DD_0^-$, $V_1^- \nearrow HX_1^-$, $RX_1^- \nearrow DD_1^-$); ntrl elements increase by 1°: ($V_0^0 \nearrow E_0^0$, $E_0^0 \nearrow NS_0^0$, $V_1^0 \nearrow E_1^0$, $E_1^0 \nearrow NS_1^0$); and +ve elements separate, so that adjoining vertices become unit distance apart: ($V_0^+ \nearrow V_1^+$, $TR_0^+ \nearrow TR_1^+$, $RT_0^+ \nearrow RT_1^+$, $RX_0^+ \nearrow RX_1^+$).
On the y-axis (↖), *reading steps R2L*, –ve elements separate, so adjoining vertices become unit distance apart: ($V_1^- \nwarrow V_0^-$, $HX_1^- \nwarrow HX_0^-$, $RX_1^- \nwarrow RX_0^-$, $DD_1^- \nwarrow DD_0^-$), ntrl elements increase by 1°: ($E_0^0 \nwarrow V_0^0$, $NS_0^0 \nwarrow E_0^0$, $E_1^0 \nwarrow V_1^0$, $NS_1^0 \nwarrow E_1^0$); and +ve elements increase 1°: ($TR_0^+ \nwarrow V_0^+$, $RX_0^+ \nwarrow RT_0^+$, $TR_1^+ \nwarrow V_1^+$, $RX_1^+ \nwarrow RT_1^+$). (*NB*. All 2D polytope arrays (Figs. 2 & 3) repeat to infinity).

The snub form is clearly a transitional form, as evidenced in the jitterbug sequences I recognized in my early research [2] for each polytope Class I–V contraction SRQR → SnbQR → QR; in Class II, SRCO → SnbCO → CO; and in Class IV, SRTH → SnbTH → TH. The Snub polytope in either or both of its enantiomorphs thus sits at the center of the schematic 2.5D cube its class, mediating the lower and higher diamonds. Class II SnbCO or Class IV SnbTH is, as before, between the 1° QR CO or TH and the 2° SRCO or SRTH, respectively.

The original linear horizontal truncation polytope sequence of $PL^{+} - TP^{+} - QR - TP^{-} - PL^{-}$ is devolved in the 2.5D schema to a revised 'M'-shaped sequence; while the original neutral linear vertical transcendent sequence now extends to include the null verticial polytope VP.

4. Commentary

In this paper, there are several key threads. The notion of sequence cluster of elements is abstracted from Class III of the polyhedral periodic arrays (honeycombs), recognized in Classes IV & V of the 2D polygonal periodic arrays (tilings); seen to therefore characterize the 2D Classes IV & V of the regular & semiregular polytopes (2D polygonal arrays), which have the same geometric form; then here generalized to all five classes of the regular & semiregular polytopes, as in the exemplary Class II of {2,3,4} symmetry. The sequence cluster (or sequence pair) can be seen as a diamond arrangement of two × two-step sequences, from the inferior fully contracted central compound, in the first step expanding left & right to intermediary polar +ve & –ve compounds, respectively; then in the second step expanding further to right & left, respectively, to converge in the common superior fully expanded compound. At each step, in either sequence, +ve faces either expand to the next higher rank in their hierarchy, or separate by unit distance (edge length), from adjoining to adjacent. Meanwhile, –ve faces show the converse: they either separate by unit distance, or expand to higher level, respectively. The facial elements that separate in the first step, expand in the second, and *vice versa*. This beautiful pattern of formal evolution seems to be fundamental to the polytopes (as individual compounds), as well as the honeycombs & tilings (the periodic regular & semi-regular repetitions of compounds to fill all 3D & 2D space, respectively). The 2.5D schema shows lower & upper diamonds; in the lower, the +ve & –ve verticial faces develop from the seed VP_C to expand left & right to +ve & –ve polar-faced $PL^{+/-}$ compounds; these +ve & –ve faces separate right & left to recombine in the SR—which then jitterbugs, contracting through the central snub to the QR in the upper diamond—from which the truncated +ve & –ve faces separate left & right to their truncated polar compounds; then expand right & left to their double-frequency faces to recombine, culminating in the GR.

In earlier research, I organized the regular & semi-regular 2D & 3D polytopes by symmetry into five parallel classes, characterized by an inverted "T" pattern of horizontal truncation sequence & vertical transcendence sequence of 7 compounds (8 including the transitional snub form, in either enantiomorph). That provided a useful schema to appreciate the relationships between these polytopes. In this paper, I integrate the null polytope of zero dimension for each class that I later recognized in the 3D honeycombs and then 2D tilings, to present a cubic (here shown cuboid) 2.5D schema that better accounts for the intrinsic order within each polytope class. While the relations between class are unaltered, the class-to-class correspondences remain rigorous: within each class, the corresponding polytope stands in

formally equivalent relationship to its neighbors. In each class there are now 8 compounds (9 counting the transitional snub compound, in either enantiomorph). The virtual null polytopes can be imagined as the QR compound of their class, but of zero extent, so all +ve, ntrl, & –ve vertices of the QR coexist in the same verticial point. There are thus 5 such null polytopes, one for each class; while by analogy, the real QR represents the truncated form of the null VP.

In this paper I concentrate on Class II of the polyhedra of {2,3,4} symmetry, as they are the most important and characterize the major Class III honeycombs of {2,3,4|2,3,4} symmetry; and also refer to Class IV of the polygons of {2,3,6} symmetry to validate the 2.5D cubic schema extended to the 2D case. Classes II & IV (& III) are non-symmetric, in that their polar forms are not the same (c.f. the Class I or V reoriented $T^{+/-}$ or recolored $SQ^{+/-}$).

5. Conclusion

This novel 2.5D schema of the regular and semi-regular 3D polyhedra & 2D polygonal arrays proves vital towards characterizing their structural morphology, and is applicable across classes; the behavior in one class is perfectly reflected in the other classes, as in the exemplar jitterbug sequences. In addition, the schema recognizes for each class a null polytope VP_C, whose virtual properties are deducible from the schema. The schema exploits the same motif of diamond expansion sequence cluster derived from the Class III all-space-filling polyhedral honeycombs and Class IV & V polygonal tiling patterns of the plane, so appears archetypal.

In future research, I anticipate developing this paper to include all five classes I–V of the regular and semi-regular 3D polyhedra and 2D polygonal tilings to present a completely revised new order in space; then in later work, reapply the schema and component diamonds to the five classes I–V of the all-space-filling honeycombs and tilings, in order to gain further insight into their structural morphology, with potential applications to lattice structure, bone scaffolding, polymer composites, kinetic space structures, and in general, to appreciate and appropriately utilize the inherent subtle and profound harmonic structure of empirical space.

6. References

1. K. Critchlow, Order in Space. Thames and Hudson, London, 1969.
2. R. C. Meurant, A New Order in Space – Aspects of a Three-fold Ordering of the Fundamental Symmetries of Empirical Space, as evidenced in the Platonic and Archimedean Polyhedra – Together with a Two-fold Extension of the Order to include the Regular and Semi-regular Tilings of the Planar Surface. *International Journal of Space Structures*, Vol.6 No.1, University of Surrey, Essex, 1991, 11–32. Download **PDF 06** at http://www.rmeurant.com/its/papers/polygon-1.html
3. R. C. Meurant, The Myth of Perfection of the Platonic Solids. People and Physical Environment Research PAPER Conference on Myth Architecture History Writing, University of Auckland, New Zealand, July 1991. **PDF 07** at http://www.rmeurant.com/its/papers/polygon-1.html
4. B. Grünbaum and G. C. Shephard, Tilings and Patterns. W. H. Freeman, New York, 1987.
5. R. C. Meurant, Towards a Meta-Order of the All-Space-Filling Polyhedral Honeycombs through the Mating of Primary Polyhedra. *Information Journal*, Vol.19, No. 6(B), June 2016, 2111–2124.
6. R. C. Meurant, Expansion Sequences and their Clusters of the All Space-filling Periodic Polyhedral Honeycombs. *Information Journal*, Vol.20, No.10(A), Oct. 2017, 7345–7362.
7. R. C. Meurant, Towards a New Order of the Polyhedral Honeycombs: Part III: The Developed Metaorder, Form and Counterform. *Information Journal*, Vol.22, No.1, Jan. 2019, 23–45.

Proceedings of the Tenth International
Conference on Information (Information'2021)
ISBN 4-901329-11-8

A Solution for Ride-sharing Route Choice Problem based on Genetic Algorithm

Chaoze Song* and Lei Li**

*Graduate School of Science and Engineering, Hosei University, Koganei, Tokyo 184-8584 Japan
E-mail:jiyu499@gmail.com

** Faculty of Science and Engineering, Hosei University, Koganei, Tokyo 184-8584 Japan
E-mail:lilei@hosei.ac.jp

Abstract

The growth of the amount of vehicles has leads to many problems. To solve these problems, we did a research about ridesharing. Ridesharing is a pattern of transportation in which people with similar itineraries and time schedules utilize spare seats in the vehicle and share the travel cost [2]. In this paper, we came up with a new mathematical model to solve the ride-sharing route choice problem and experimented it in a virtual traffic scene. According to the result, our model performs better than the previous one.

Keywords: ride-sharing, Genetic Algorithm, route choice, optimization problem

1. Introduction

With the development of economic globalization, people's living standard has been improved a lot which contributed to a large growth of the amount of private cars. Because of private cars, people's lives have been much more convenient. However, on the other hand, problems such as traffic congestion, the occupation of city space, air pollution, and the over-consumption of energy have not been solved yet. Furthermore, on account of the increase in the population, the amount of vehicles has grown as well. While there are too many unoccupied seats in the moving vehicles which is a large waste of resources.

So far, most researches in the field of ridesharing are about the fundamental theory of ridesharing such as the current status and tendency of ride-sharing, the organizing pattern of ride-sharing and so on. The researchers have done many qualitative analysis upon many aspects of ride-sharing which have enriched the ride-sharing theory. There are also some researchers who have done some quantitative analysis. However, researches on the ridesharing route choice are almost about mathematical models based on one-to-many organizing patterns. Moreover, the factors and constraint conditions are comparatively simplex. For the calculation of the mathematical models, they mainly utilized heuristic algorithms and greedy algorithm [1]. In Zhou's paper [1], he came up with a mathematical model and applied it in a virtual ride-sharing scene as an experiment. Nevertheless, the scale of the traffic scene is relatively small.

In this paper, we proposed a new mathematical model and tested it in the same map with Zhou, but we enlarged the scale including the amount of vehicles and passengers. Finally, we have got an optimal route which has a better performance.

2. Mathematical Model

The problem consists of a set $D = \{1,2,...,d\}$ of n vehicles, a set $R = \{1,2,...,r\}$ of r passengers, and a set $V = \{1,2,...,v\}$ of v stations. Each vehicle i belongs to set D. Each passenger r belongs to set V. Each station m/n belongs to set V. Each street is regarded as a line linked with two vertices (stations).

2.1 Optimized Objective Function

$$min \sum_{i \in D} \sum_{m,n \in V} C_{m,n}^{i} X_{m,n}^{i,j} \tag{1}$$

$C_{m,n}^{i}$ is the cost that vehicle i pass through the street linked with station m and station n. $X_{m,n}^{i,j}$ is a decision variable. If the passenger j riding vehicle i passed the street linked with station m and station n, $X_{m,n}^{i,j}$ will be 1, otherwise $X_{m,n}^{i,j}$ will be 0. Our optimization objective is to minimize the total cost.

2.2 Constraint Conditions

$$\sum_{m,n \in V} t_{m,n} X_{m,n}^{i,j} \leq T_j \tag{2}$$

$$e_m^i \geq 1 \tag{3}$$

$$\sum_{i \in D} X_{m,n}^{i,j} = 1 \tag{4}$$

$$\sum_{n \in V} X_{m,n}^{i,j} - \sum_{n \in V} X_{n,m}^{i,j} = \begin{cases} 1, & m = O_j \\ -1, & m = D_j \\ 0, & otherwise \end{cases} \tag{5}$$

$$a_{n+1}^{i} - b_n^i \geq t_{n,n+1} \tag{6}$$

$$b_n^i \leq t_n^j \leq a_n^i \tag{7}$$

Where $X_{m,n}^{i} = \begin{cases} 1, & \sum_{j \in R} X_{n,m}^{i,j} > 0 \\ 0, & otherwise \end{cases}$,or $X_{m,n}^{i,0} > 0$.

$t_{m,n}$ is the theoretical time cost when a vehicle passes through the street linked with station m and station n. T_j is the max travel total time of passenger j. Constraint (2) ensures that the theoretical total travel time is shorter than the max travel total time of the passenger j. e_m^i is the amount of unoccupied seats in vehicle i when vehicle i is at the station m. Therefore, constraint

(3) ensures that there is at least one unoccupied seat in the vehicle so that it can contain new passengers. Constraint (4) ensures that all the passengers in this system will be picked up, namely, there will be no one who can not get a car. O_j is the origin of passenger j. O_d is the destination of passenger j. Constraint(5) defines the origin and destination of passenger j. a_n^i is the timing when vehicle i arrives at station m. b_n^i is the timing when vehicle i departs from station m. Constraint (6) ensures the practical time cost longer than the theoretical one. Constraint (7) is the time window constraint.

3. The Proposed Algorithm

In this paper, we use Genetic Algorithm to solve the above-mentioned mathematical model. Genetic Algorithms encode a potential solution to a specific problem on a simple chromosome-like data structure and apply recombination operators to these structures to preserve critical information. Genetic algorithms are often viewed as function optimizers, although the range of problems to which genetic algorithms have been applied are quite broad. An implementation of genetic algorithms begins with a population of (typically random) chromosomes. One then evaluates these structures and allocated reproductive opportunities in such a way that these chromosomes which represent a better solution to the target problem are given more chances to 'reproduce' than those chromosomes which are poorer solutions. The 'goodness' of a solution is typically defined with respect to the current population [3].

4. Experimentation and Results

We used the map of Zhou's paper [1], and enlarged the scale of the experiment.

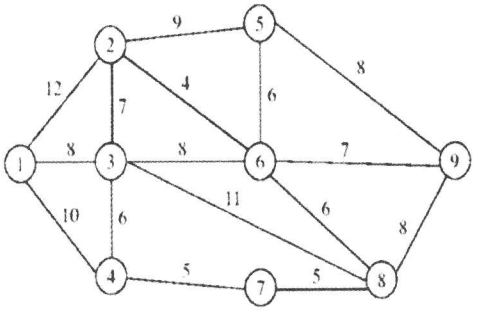

Figure 1 map

O-D pair demand	passenger amount	O-D pair demand	passenger amount
1-6	4	6-4	9
2-8	8	7-3	6
3-9	11	8-7	10
4-5	9	9-2	7
5-1	6		

Table 1 O-D Pair & passenger amount

As shown in the figure, there are 9 stations. In the virtual scene, there are 3 vehicles, each vehicle can contain 4 passengers. There are 9 origin-destination pair travel demands. The amount of passengers of each demand is shown in Table1.

The parameters' settings of the genetic algorithm are: population size = 80, number of generations = 100, crossover probability = 0.4, mutation probability = 0.1, and select probability = 0.8.

The figure2 shows the process that Genetic Algorithm found the optimal solution whose value is 138. The optimal route plan is shown in Table2.

Car	Route	Cost
1	2-6-8	10
2	6-3-4	14
3	3-6-9-6	26
4	5-2-1	21
5	4-3-6-5	20
6	1-2-6	16
7	7-4-3	11
8	8-7	5
9	3-6-9	15

Table 2 Result data

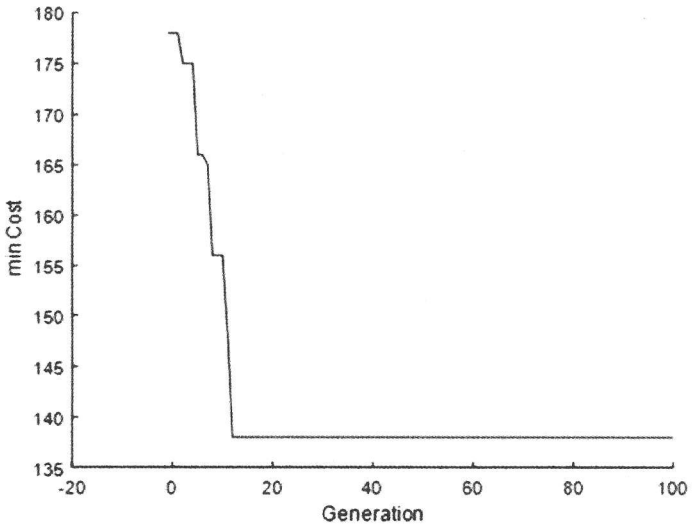

Figure 2 GA process

References

[1] Zhou, He-ping, et al. "The route choice and rate optimization model of taxi-pooling." *Journal of Changsha University of Science and Technology (Natural Science)* 8.4 (2011): 20-24.

[2] Shen, Bilong, Yan Huang, and Ying Zhao. "Dynamic ridesharing." *Sigspatial Special* 7.3 (2016): 3-10.

[3] Houck, Christopher R., Jeff Joines, and Michael G. Kay. "A genetic algorithm for function optimization: a Matlab implementation." *Ncsu-ie tr* 95.09 (1995): 1-10.

[4] Alonso-Mora, Javier, et al. "On-demand high-capacity ride-sharing via dynamic trip-vehicle assignment." *Proceedings of the National Academy of Sciences* 114.3 (2017): 462-467.

[5] Agatz, Niels, et al. "Optimization for dynamic ride-sharing: A review." *European Journal of Operational Research* 223.2 (2012): 295-303.

[6] Davis, Lawrence. "Handbook of genetic algorithms." (1991).

[7] Chan, Nelson D., and Susan A. Shaheen. "Ridesharing in North America: Past, present, and future." *Transport reviews* 32.1 (2012): 93-112.

[8] Furuhata, Masabumi, et al. "Ridesharing: The state-of-the-art and future directions." *Transportation Research Part B: Methodological* 57 (2013): 28-46.

Proceedings of the Tenth International
Conference on Information (Information'2021)
ISBN 4-901329-11-8

Industrial Network and Cluster, Restructuring Production Chain Based on Specialization and Division of Labour after the 2020 Pandemic

LI Ke

College of Economics, Nihon University, Tokyo, Japan
Email: li.ke@nihon-u.ac.jp

Abstract

After the 2020 pandemic, the whole world will look remarkably different with the consideration of global supply chain. This paper develops a general equilibrium model with endogenous industrial cluster and endogenous industrial network of division of labour to formalise and explore the interrelationship and rules of industrial cluster, network of division of labour, the economies of specialization and agglomeration under the new era of post-pandemic global econ0my. The model suggests that institutional efficiency and mutual-trust, and competition among countries and industries will facilitate important circular effects, which propelling and shaping the arrangement and allocation of industrial clusters, the position located at the supply chain, and consequently the status of economic growth. In particular, the improvements in institutional efficiency and mutual-trust over economic and technology systems will expand the demand for transactions and network size, which in turn will determine the development of cluster and network scope, as well as the position at the network.

Keywords: Industrial network, Industrial cluster, Specialization, Division of labour, Infra-marginal analysis, Supply chain

1. Introduction

Even after the 2020 pandemic subsides gradually, the world will be remarkably different with the system of global supply chain. The supply shock that begun in China in February of 2020 and the demand shock followed as the global economy shut down exposed the weaknesses and vulnerabilities in the production strategies and supply chains of firms. Those events, combined with the US-China trade war, have triggered a rise in economic nationalism. As a result, manufacturers worldwide will be under greater political and competitive pressures to increase their domestic production, grow employment in their home countries, reduce or even eliminate their dependence on sources perceived as risky, and rethink their usage of inventory from the global supply chains. All the concern have recalled our attention on the relevant issue of industrial cluster and industrial network [16].

There are enormous studies have been conducted lately on the issues of industrial cluster and industrial network, which reflect substantial concern over economic growth and development through global division of labour and specialization. Among them, Michael Porter [25, 26, 27, 28, 29, 30, 31, 32, 33] has discussed the "industrial cluster" on the foundations of market economies which contains interrelated and dynamic mixtures of cooperative arrangements and competitive relationships. This research stream can be traced back and significantly influenced by Alfred Marshall's notions of "industrial districts" and "industrial atmospheres" [17,18], and also Piore and Sabel's term of "flexible specialization" [24]. Porter defines a cluster as a geographic concentration ("geographical proximity") of competing and cooperating companies, suppliers, service providers, and associated institutions, which is resulted from the relationships among factor conditions, demand conditions, related and supporting industries, corporate strategy, and structure and rivalry [27]. Moreover, industrial clusters have been recently also studied as groupings of interrelated firms that innovate and generate economic growth, such as "collective efficiency" [34], the function and effect of knowledge externalities and spill-overs [3, 5, 7, 8], and the dynamic nature of interactive learning necessary for innovation [2]. Furthermore, Chandler argues that historically, economies of scale and scope have been achieved mainly by large private and public enterprises [6]. Similarly, Lazonick [15] and Florida and Kenny [9] also point out that large and high-end corporations a.re at the Heart of the innovation process and growth since they have, unlike small firms, the ability to combine technology, investment, clearly

defined organizational structures, and the adoption of labour practices of flexible specialization, "just-in-time" production, and outsourcing; and multi-skilled and multi-tasked employees. Regarding the determinants of cluster, Nelson and Winter [20] and Nelson and Sampat [19] point out that location choice by firms is driven by transportation cost minimization and optimal combination of key location-specific inputs for an optimal level of production in order to maximize profit, and how institutional arrangement affects economic performance. The institutions are as standard "social technologies", and economic growth results from the co-evolution of physical and social technologies. According to Storper [36], firms in clusters or industrial districts are aimed at securing competitive advantage. In general, firms in clusters can take advantage of positive externalities and also force them to compete more fiercely with the firms within other clusters which will provide the incentive for the clustered firms to innovate [25]. Hence, cluster can be regarded as increasing various arrangements of networked firms, it can be considered as a broader scale as a foundation for economic growth, specifically at the level of the regional economy where promotion of entrepreneurial networks and clusters can occur [4, 14, 34, 38].

Regarding industrial networks, the literature on networks has historical roots in both the theory of the firm and the literature on "growth poles". In particular, the latter recognises the leading firms' role and potential for positive spill-overs for a number of non-geographically concentrated production and commercial partners, through a "process of polarisation" or "propulsive development" [23]. In Perroux's original formulation, a growth pole referred to the linkages between firms and industries. "Propulsive firms" are those firms that are large relative to other firms and generate induced growth through inter-industry linkages as the industry expands its output [23]. This theory has significant impact in the promotion of "linkage studies" that, rather than being related to the idea of "geographical proximity" [29], it is more valid to develop and discuss the importance of linkages within trans-local firms, subsectors, commodity chains, as well as global supply chains [21]. All these arguments stress the importance of networks and linkages within wider spaces as a way to benefit from abilities and advantages that cannot be reaped in local economies alone. Besides, there are different meanings over networks depending on other theoretical approach adopted, such as theories of transactions costs, resource dependency, strategic management, and social network theory. There are basically three sets of concepts, based on strategy, network management, and social dimensions [39]. Harrison et al. [13] have seen technological learning as one of the dynamic agglomeration outcomes to be derived from combining geographical closeness and formal transactions based or informal relationships. In a context where the agglomeration of firms and institutions is relevant to enhance local competitiveness and make relational activities easier, the explicit interactive dimension of networking provides an indication of the relational thickness of the system as well as its openness with respect to linkages across different localities [1,11, 12]. As for Eisingerich, Andreas, Bell, and Tracey [9], there is a social network to develop regional cluster performance. High performing clusters are underpinned by network strength and network openness, but that the effects of these on the performance of a cluster as a whole are moderated by environmental uncertainty. The networks are instruments that may help firms to voluntarily expand their own competences by means of complementary partners beyond limitations of their own organisation and of the localities where they are settled. In this context, the process of "learning" offers a dynamic perspective on the nature of both networking and clustering [9]. Hence, following the competence view, networking can be beneficial because it may stimulate communication and convey new stimuli towards firms, thus enhancing learning opportunities that may lead to technological upgrading and improved competitiveness.

Although the notions of industrial cluster and industrial network have been widely applied, they still largely remain fuzzy as a concept especially when we consider their own interrelated relationships and their relationships with the factors and variables from the whole economy, such as the institutional arrangements, trading efficiency, the level of specialization and agglomeration, as well as their dynamic evolutionary. The current literatures have addressed many important aspects of cluster and network, yet there is still short of robust frameworks to combine and explore them together under one competitive market. From these perspectives, further studies on overlapping meaning of industrial

clusters and networks need be conducted. In this paper, it will regard industrial clusters and networks as two forms of production organisation, and they may be complementary with each other. This paper introduces a theoretically driven framework to provide structure and process related measures that can be used to explain how cluster and network actually operate and interrelate within an economy. The objective of this paper is to bring together the inter-individual strategic decision making and the network of division of labour in order to explore the conditions underlying the development of different types and level of industrial networks, institutional efficiency and mutual-trust, as well as geographically and non-geographically clustered. In particular, this paper will examine the relationship among institutional arrangement, fixed learning and entry cost, transaction conditions, and the cluster governance structure and process at the corporate level, the cluster level and/or the economy level.

2. A Model and Framework with Industrial Cluster and Industrial Network of Division of Labour

2.1 The basic model

Following Yang [40], let's consider an economy with a continuum of consumer-producers of mass M. This assumption implies that population size is very large. It avoids an integer problem of the numbers of different specialists, which may lead to non-existence of equilibrium with the division of labour [37]. Each consumer-producer has identical, non-satiated, continuous, and rational preference represented by the following utility function:

(1a) $u = f(x^c, y^c)$,

where $x^c \equiv (x + k_x \cdot x^d)$ and $y^c \equiv (y + k_y \cdot y^d)$ are the amounts of the two final goods that are consumed, x and y are the amounts of the two goods that are self-provided, x^d and y^d are the amounts of the two goods that are purchased from the market, and $k_i \in (0,1)$ and $i = x, y$ or z. Fraction 1-k_i of a good sold disappears in transit due to an iceberg transaction cost, or k_i is a trading efficiency coefficient, which represents the conditions governing transactions. Regarding the effect of geographic concentration or Porter's "geographical proximity"[27], we further assume that $k_i = (1 - t_i) \cdot K_i$, and here t_i is the coefficient of relative geographic distance, and K_i relates to the general trading conditions and the institutional environment that affect trading efficiency. $f(.)$ is continuously increasing and quasi-concave. For simplicity without losing the generality, it is assumed that $f(.) = (x^c) \cdot (y^c)$. Each consumer-producer's production functions are:

(1b) $x^p = x + x^s = max\{l_x - F,\ (z + k_z \cdot z^d)^\alpha \cdot (l_x - F),\ (z + k_z \cdot z^d)^\beta \cdot (l_x - F)\}$,
and $k_i = (1 - t_i) \cdot K_i$, and $i = x, y$ or z.
$y^p = y + y^s = l_y - b$ and $b \in (0, 1)$,
$z^p = z + z^s = l_z - b$ and $b \in (0, 1)$,

where x^p and y^p are the amounts of the two final goods produced, z^p is the amount of the intermediate good produced, z^d is the amount of intermediate good z purchased from the market, x^s, y^s and z^s are the amounts of the goods sold. F is the fixed learning and entry cost in producing good x; and b is the fixed learning and entry cost in producing good y and z. F is the parameter representing the elasticity of output of good x with respect to input level of intermediate good z. Moreover, parameter α is the efficiency coefficient and general effect of roundabout production with intermediate goods, which will indicate one feature of economies of specialization and $\alpha \geq 1$ [40]. Besides, β is employed to indicate the degree and level of industrial cluster, which means the efficiency coefficient of industrial cluster, and it can be defined as $\beta = \alpha + e - \theta$. Here, θ represents the level of coordination cost, management cost and exogenous transaction costs of industrial cluster, and $\theta \in (0, 1)$; and e is the institutional efficiency and mutual-trust coefficient to describe external economic and technology systems for specialization and industrial agglomeration, and $e \in (0, 1)$. With the concern of the economies of

agglomeration and the economies of specialization and division of labour, which are the major features of industrial cluster, under certain conditions we can expect $\beta \geq 1$, which means there will be increasing returns in producing the final good x with cluster pattern. However, there will also involve all sorts of internal coordination cost, management cost and endogenous and exogenous transaction costs for manufacturing product x with cluster pattern. If without cluster, the firms will also encounter exogenous and endogenous transaction costs, such as transportation cost, measurement cost of quantity and quality of products, information searching and matching cost, anticipated moral hazard, knowledge block and many marketing related expenses, etc.. Hence, there is a trade-off here for engaged firms to decide whether to organise an industrial cluster or just through the normal market trades, which will be analysed later in this paper.

The endowment constraint for each individual endowed with one unit of working time is given as follows:

(1c) $\quad l_x + l_y + l_z = 1$,

where l_i is the amount of labour allocated to the production of good i. This system of production implies that each individual's labour productivity increases as she narrows down her range of production activities. As shown by Yang [40], the aggregate production schedule for three individuals discontinuously jumps from a low profile to a high profile as each person jumps from producing three goods to a production pattern in which at least one person produces only one good (specialization). The difference between the two aggregate production profiles is considered as positive network effects of division of labour on aggregate productivity. This network effect implies that each person's decision of her level of specialization, or gains from specialization, depends on the number of participants in a large network of division of labour, while this number is determined by all individuals' decisions in choosing their levels of specialization (so-called the Young theorem) [43]. Since economies of specialization is individual specific (learning by doing must be achieved through individual specific practice and cannot be transferred between individuals), labour endowment constraint is specified for each individual, so that increasing returns are localized.

The budget constraint for an individual is,

(1d) $\quad p_x(x^s - x^d) + p_y(y^s - y^d) + p_z(z^s - z^d) = 0$.

Due to the continuum number of individuals and the assumption of localized increasing returns in this large economy, a Walrasian regime prevails in this model. The specification of the model generates trade-offs between economies of division of labour and transaction costs. The decision problem for an individual involves deciding on what and how much to produce for self-consumption, to sell and to buy from the market. In other words, the individual chooses 9 variables, such as x, x^s, x^d, y, y^s, y^d, z, z^s, z^d,, and there will be 2^9 amount of possible corner and interior solutions.

In order to narrow down the list of the candidates, Yang and Ng [41] used the Kuhn-Tucker conditions to establish the following lemma.

Lemma 1: Each individual sells at most one good, does not buy and sell the same good, nor buys and self-provides the same good at the same time.

We define a *configuration* as a combination of zero and positive variables which are compatible with Lemma 1. There are 14 configurations from which the individuals can choose. A combination of all individual's configurations constitutes a *market structure*, or *structure* for short. There will be totally 7 market structures compatible with Lemma 1.

2.2 Configurations and Economic Structures

Let's firstly examine all possible structures that might occur in equilibrium.

I. Autarky Structures: Structure A and Structure B

(1) Structure A (Autarky without Intermediate Good z) consists of all individuals choosing configuration A (self-sufficiency), where an individual produces all the two final goods for self-consumption and without any intermediate good z.

(2) Structure B (Autarky with Intermediate Good z) consists of all individuals choosing configuration B (self-sufficiency), where an individual produces all the two final goods for self-consumption and with intermediate good z for producing good x.

II. Structures with Partial Division of Labour: P_A , P_B and P_C

(1) Structure P_A is a partial division of labour structure which contains configurations (xy/z) and (zy/x).

(2) Structure P_B is a partial division of labour structure which contains configurations (xz/y) and (y/x).

(3) Structure P_C is a partial division of labour structure which contains configurations (x/y) and (y/x).

III. Complete Division of Labour: Structure CC_A and Structure CC_B

(1) Structure CC_A is the complete division of labour with industrial cluster which contains configurations (x/yz), (z/xy) and (y/x).

(2) Structure CC_B is the complete division of labour without industrial cluster which contains configurations (x/yz), (z/xy) and (y/x). Note that the definitions and contents of their configurations are as same as Structure CC_A, yet it does not apply the industrial cluster patter in the manufacture of good x. The rough explanation for this difference is based on the trade-off between different fixed learning and entry costs, the institutional efficiency and mutual-trust coefficients of different economic and technology systems, the transaction costs and the level of coordination and management costs of industrial cluster. The solid and explicit analysis will be addressed below.

According to Sun, Yang and Zhou [37, 40], and Yao and Li [42], a general equilibrium is defined as a set of relative prices of goods and all individuals' labour allocations and trade plans, such that, (1) Each individual maximizes her utility, i.e., the consumption bundle generated by her labour allocation and trade plan maximizes her utility function for given prices; (2) All markets clear. More specific, Yang [40] has addressed the following theorem:

Theorem 1: For an economy with m goods and a continuum of ex ante identical consumer-producers with rational and convex preferences, and production functions displaying economies of specialization, and individual specific limited labour , the Walrasian general equilibrium exists and it is the Pareto optimum corner equilibrium.

Since the optimum decision is always a corner solution and the interior solution is never optimal according to Lemma 1, we cannot use standard marginal analysis to solve for a general equilibrium. We adopt a three-step approach to solve the general equilibrium. The first step is to narrow down the set of candidates for the optimum decision and to identify configurations that have to be considered. We can identify structures from compatible combinations of configurations, which we have done above. In the second step, each individual's utility maximization decision is solved for a given structure. The utility equalization condition between individuals choosing different configurations and the market clearing conditions are used to solve for the relative price of traded goods and numbers (measure) of individuals choosing different configurations. The relative price and numbers, and associated resource allocation are referred to as corner equilibrium for this structure. General equilibrium occurs in a structure where, given corner equilibrium relative prices in the structure, no individuals have an incentive to deviate from their chosen configurations in this structure. In the third step, we can substitute the corner equilibrium relative prices into the utility function for each constituent configuration in the given structure to compare the utility between this configuration and any alternative configurations. This comparison is called a total cost-benefit analysis. The total cost-benefit analysis yields the conditions under which the utility in each constituent configuration of this structure is not smaller than any alternative configuration. With the existence theorem of general equilibrium proved by Sun, Yang and Zhou [37], we can completely partition the parameter space into

subspaces, within each of which the corner equilibrium in a structure is a general equilibrium. As parameter values shift between the subspaces, the general equilibrium will discontinuously jump between structures. The discontinuous jumps of structure and all endogenous variables are called infra-marginal comparative statics of general equilibrium, and the three steps constitute an Infra-marginal analysis.

Following this procedure, we can solve for corner equilibria in all structures. The solutions of corner equilibria in 7 structures, the relative prices and relative number of different specialists are summarized in Table 1.

3. General Equilibrium and Its infra-marginal Comparative Statics

Through infra-marginal analysis. it will partition the parameter space into subspaces within each of which a particular structure occurs in equilibrium. With the Theorem 1, we can then compare corner equilibrium per capita real incomes across all structures, and the comparison partitions the seven-dimension $(K, t, \alpha, b, F, e, \theta)$ parameter space into several subspaces, within each of which one corner equilibrium is the general equilibrium. As parameter values shift between different subspaces, the general equilibrium discontinuously jumps between corner equilibria. This is referred to as infra-marginal comparative statics of general equilibrium.

In order to obtain analytical solution of the infra-marginal comparative statics for some specific ranges of parameter values, we conduct a close examination of per capita real incomes in different structures, which is given in Table 2.

Following Yang [40], it can be shown that a general equilibrium in this model is Pareto optimal. This first welfare theorem in this model with inter-individual networking decisions and endogenous network size of division of labour implies that the market function is to coordinate inter-individual networking decisions and to fully utilize network effects of division of labour on aggregate productivity, network of transactions, and level off specialization and roundabout production.

In this model, the institutional efficiency and mutual-trust related parameters (K, α, β), all play crucial roles in determining the per capita real income and the properties of the intermediate goods and industrial cluster under the division of labour structure, and that is $\frac{du}{dK} > 0$, $\frac{du}{d\alpha} > 0$ and $\frac{du}{d\beta} > 0$. Industrial cluster and roundabout production both are related to the vertical division of labour between high-end and low-end producers in a long production chain, while the comparison between their institutional efficiency and mutual-trust will be vital for the final decision in network structure of division of labour. Based on the above model, we can see that an economy with a higher institutional efficiency and mutual-trust enables each individual to specialize in a narrow range of production and to enjoy economies of specialization. The benefits gained from increasing returns to specialization and the division of labour will outweigh the transaction costs of markets. Industrial cluster in a competitive market is an effective way to promote division of labour and productivity progress if the institutional efficiency and mutual-trust of economic and technology systems are more competitive. We can summarize the above analysis into Proposition 1.

Proposition 1:

i) Absolute level of trading efficiency of goods determines the level of division of labour. As transaction efficiency is improved, the equilibrium level of division of labour increases, from autarky to complete division of labour; ii) Relative level of trading efficiency determines if the intermediate goods are self-supplied or through market transaction; iii) If the general effect of roundabout production is higher, then the roundabout production patter will be adopted; iv) The smaller fixed learning cost of intermediate good b, will increase the functions of the intermediate good, the level of production roundabout, the level of division of labour; v) If the efficiency coefficient of industrial cluster overwhelms the general effect of roundabout production, the structure with industrial cluster will prevail and thereby promote the division of labour and productivity progress based on inter-individual networking decisions, and it has no adverse effects on welfare and does not generate distortions in a competitive market.

Proposition 1 explicitly suggests a highly efficient transaction institution will sufficiently outweigh the transaction costs and provide each individual an incentive to specialize and to trade with each other by forming a network of division of labour.

Since there are more sophisticated interrelated effects among industrial cluster, network of division of labour and production supply chain, thereby we need further expend our discussion on these interrelationships in the rest of this section.

Scenario 1. Fixed learning and entry costs of intermediate good z is smaller than final good x, that is $b < F$

From above analysis, we can easily derive that $\frac{du}{dF} < 0$ and $\frac{du}{db} < 0$ when they are under the structures of autarky and partial division of labour, which indicates the fixed learning and entry costs have negative effect for the development of network of division of labour and the level of specialization and roundabout production. However, when we derive them under the structures of complete division of labour, some interesting results emerging, $\frac{du_{CCA}}{dF} > 0$, $\frac{du_{CCA}}{db} < 0$ and $\frac{du_{CCB}}{dF} > 0$, $\frac{du_{CCB}}{db} < 0$, which implies that under the complete division of labour, the higher fixed learning and entry cost of final good will has positive effect in increasing the productivity as well as the per capita real income, while the one for intermediate good still has negative effect on productivity. In other words, if the entry barrier for final good x in term of fixed learning and entry costs goes up, which may cause by the technology barrier, patent, special know-how, R&D and innovation cost and systems, etc., it will generate higher producer and profit for the producers of final good x.

Besides, it has been addressed by many literature [22] that low-end and high-end sectors in one production supply chain usually have different fixed learning and entry costs, and high-end sectors have higher one with regard to their R&D inputs and varied costs for products development and quality control, etc.. If the degree and effect of industrial cluster is stronger, i.e. the efficiency coefficient of industrial cluster β is larger, even with $b < F$ we still can have $u_{CCA} > u_{CCB}$, which means the industrial cluster is still prevailing as the optimal decision for the firm. Hence, in the term of production supply chain, the high-end firm, although they have larger fixed learning and entry costs, still can maintain their position in a competitive market if their efficiency coefficient of industrial cluster is higher, which is determined by the trade-off between:1) the level of coordination cost, management cost and endogenous transaction costs; 2) the institutional efficiency and mutual-trust coefficient to describe external economic and technology systems for specialization and industrial agglomeration, and that can be indicated by $\frac{du_{CCA}}{de} > 0$ and $\frac{du_{CCA}}{d\theta} < 0$. Therefore, to be the high-end or low-end of the production chain is not the personal choice anymore, it is substantially up to the institutional efficiency and mutual-trust of economic and technology related systems, such as property protection systems for intellectual property and private property, the technology spill-overs effect mechanism, and information exchange and communication mechanism, etc., as well as the efficiency for coordinating and managing the industrial cluster.

Since this model does not confine itself to one country only, it refers to one economy, and has no limit on the territory of One country. According to Porter [29], a cluster of independent and informally linked companies and institutions represents a robust organizational form that offers advantages in efficiency, effectiveness, and flexibility. Porter [27] addresses the local concentration processes that accelerate under the effect of globalisation. The competitive advantages of companies and industrial sectors participating in global competition are geographically concentrated, primarily due to agglomeration effects. He also mentions that it is not individual market players but rather regional clusters that participate in global competition. However, based on this model, under the new era of globalization and regionalization, we can also expend this economy among different countries with different production chains. From our analysis, the competition among different countries for high-end and low-end producers of one production chain is mainly based on the competition of the institutional efficiency and mutual-trust among their economic and technology systems. The function of the institutional setting and efficiency of the economic and technology

systems and the trading efficiency are crucially vital to determine the level of cluster, the network of division of labour, level of specialization and agglomeration, and consequent level of productivity and real income, rather than Porter's "geographical proximity" or geographic concentration [27], which can be approved by the results from Table 2, and also by the inequalities: $\frac{d(\frac{u_{CCA}}{u_{CCB}})}{dt} > 0$ when $\alpha \leq \beta$, and $\frac{d(\frac{u_{CCA}}{u_{CCB}})}{dt} < 0$ when $\alpha > \beta$. For particular, these inequalities and Table 2 indicate that even the geographic distance is larger, if the efficiency coefficient of industrial cluster β overwhelms the negative effect of geographic distance and the effect of roundabout production, industrial cluster is still the optimal decision and an effective way to promote division of labour and productivity progress. In other words, if the institutional arrangements and settings are not efficient enough, even the geographic distance is sufficiently short, people will still choice the regular trading and roundabout production, instead of industrial cluster. Hence, this model proves and implies that the industrial cluster can be organized geographically or/and non-geographically.

Scenario 2. If high-end production is more profitable, then why the low-end firms or intermediate goods suppliers cannot move to high-end of the production supply chain?

Taking structure CC_A and CC_B into consideration, we can first derive the following relationships:

$$\frac{d(\frac{M_x}{M_z})_{CCA}}{dF} < 0 \text{ and } \frac{d(\frac{M_x}{M_z})_{CCB}}{dF} < 0, \quad \frac{d(\frac{M_x}{M_z})_{CCA}}{db} < 0 \text{ and } \frac{d(\frac{M_x}{M_z})_{CCB}}{db} < 0.$$

The first group of inequalities implies if the high-end firm having a higher fixed learning and entry costs or entry barrier, the relative number of high-end firms will decrease which means when the entry barrier of high-end firms going up, it will be more difficult to become a high-end firm, and its relative number will go down. The second group of inequalities simply indicate that if the fixed learning and entry costs of intermediate goods going up, then the traction volume of them will decrease, and the incentives for purchasing intermediate goods from market will shrink. Consequently, the relative number of high-end firms which depending on them will also go down.

Scenario 3. The relative number of specialists with respect to the institutional efficiency and mutual-trust under complete division of labour

Regarding structures CC_A and CC_B, we can first derive the following relationships:

$$\frac{d(\frac{M_x}{M_z})_{CCB}}{d\alpha} > 0 \text{ and } \frac{d(\frac{M_x}{M_z})_{CCA}}{d\beta} > 0.$$

These two inequalities indicate that to become the high-end producer is depending on its institutional efficiency and mutual-trust of economic and technology systems. The higher institutional efficiency and mutual-trust will generate more high-end firms in a production chain. Therefore, the institutional efficiency and mutual-trust is most crucial factor in determining the competition among different countries for the high-end and low-end production.

Scenario 4. The Hub of Network of Division of Labour

Considering structures CC_A and CC_B, we can derive the following inequalities:

$$\frac{d(\frac{M_z}{M_x})_{CCA}}{dF} > 0 \text{ and } \frac{d(\frac{M_z}{M_x})_{CCB}}{dF} > 0,$$

which means when the fixed learning and entry costs of high-end firms are higher, then the relative number of intermediate goods and parts suppliers will increase. Since the entry barrier for the production of intermediate goods and parts are relatively lower, it will be more easily to enter this area, and the competition and high substitution and replacement effect among them are more severe. The intermediate goods and parts suppliers are forced to closely follow and surround the final good producer to survive. In other words, the high-end firms can control the final goods market through their high fixed learning and entry costs, such as the brand image, special know-how, patent, and market network, R&D and innovation capability, and etc., and they will be more likely to be the hub

of the network of division of labour and also can control the intermediate goods and parts suppliers through OEM (Original Equipment Manufacturing), subcontracting and other manners. On the contrary, the low-end firms have to encounter the serious substitution and replacement effect and competition among them, and also the challenges from the newcomers which consecutively entering these markets.

The above analysis of different scenario can generate the following proposition 2.

Proposition 2:

i) Under the structures of autarky and partial division of labour, which indicates the fixed learning and entry costs have negative effect for the development of network of division of labour and the level of specialization and roundabout production; ii) Under the complete division of labour, the higher fixed learning and entry cost of final good will has positive effect in increasing the productivity as well as the per capita real income, while the one for intermediate good still has negative effect on productivity; iii) If the high-end firm having a higher fixed learning and entry costs, the relative number of high-end firms will decrease which means when the fixed learning and entry costs of high-end firms going up, it will be more difficult to become a high-end firm; vi) The competition among different countries for high-end and low-end producers of one production chain is mainly based on the competition of the institutional efficiency and mutual-trust among their economic and technology systems; v) The improvement in institutional efficiency and mutual-trust leads to an expansion in the network of division of labour and an increase in the relative number of specialists in high-end production to that in a low-end production; vi) The high-end firms can control the final goods market through their high fixed learning and entry costs, and are more likely to be the hub of the network of division of labour; vii) Comparing with geographic distance, the institutional arrangement and setting are more vital for the emergency and evolution of industrial cluster. Industrial cluster can be organized geographically or/and non-geographically.

The above Proposition 2 indicates that as the institutional efficiency and mutual-trust develops, the function of intermediate goods will improve, the network of division of labour will expend and the economies of specialization and agglomeration will increase. Our analysis is consisting with some of the observations, such as Storper [36]. Besides, Porter [25] also mentions that the increased innovation by firms generates new niches and needs within and outside the cluster, leading to the emergence of new firms and thus the expansion of the cluster and the economy as a whole. The expansion and growth of the cluster can lead to a more cohesive set of activities by the firms and become manifest as integration. Expansion and growth may also be a foundation for moving upward on the global supply chain. Increased integration in the global market brings new pressures to local production systems in developing and developed countries. Mixed with market pressures are a number of governance-related issues that determine whether and how a local production system (cluster or industrial district) remains in or moves up a global supply chain. Their arguments can be explicitly demonstrated by this model, while there are further insights from the propositions which are not clearly addressed before, such as, under the complete division of labour, the higher fixed learning and entry cost of high-end producer will has positive effect in increasing the productivity and expend the network; if the high-end firm having a higher fixed learning and entry costs, it will be more difficult to become a high-end firm; it will not be the individual decision anymore to become high-end or low-end producer, rather it will substantially depend on the competition over institutional efficiency and mutual-trust of economic and technology systems among different regions or countries; the improvement in institutional efficiency and mutual-trust leads to an expansion in the network of division of labour and bring more producers into high-end production; the high-end firms have been chance to control the market through their high fixed learning and entry costs, and are more likely to be the hub of the network of division of labour. Comparing with geographic distance, the institutional arrangement and setting are more vital for the emergency and

evolution of industrial cluster, and industrial cluster can be organized geographically or/and non-geographically.

Our forgoing propositions also indicate that, a variety of economic structures may emerge in concurrence with economic development. They also support Adam Smith's [35] argument that the division of labour leads to the invention and the utilization of roundabout productive machines. Furthermore, they illustrate Young's proposition [43] that the division of labour for an economy is characterized by three components: the level of individual's specialization, its diversity of process, the new utilization of a good, its roundabout production, and the emergence of the vertical division of labour. This model also opposites the traditional argument that the "geographical proximity" [29] is more crucial to determine industrial cluster and economic growth or economic development, and we indicate the institutional setting of a particular economy are more valid for the emergency and evolution of industrial cluster and network of division of labour.

4. Concluding Remarks

This paper develops a Walrasian general equilibrium model based on inter-individual networking decisions to investigate the role of industrial cluster and network of division of labour in a competitive market. In this model there is no monopoly power, substitution among different specialists are allowed, therefore to be cluster hub does not need to be as a large corporation, which has been occurred and observed in recent decades [6, 10].

The function of the institutional setting and efficiency of the economic and technology systems, and the trading efficiency, are crucially vital to determine the level of cluster, the network of division of labour, level of specialization and agglomeration, and consequent level of productivity and real income, rather than Porter's "geographical proximity" or geographic concentration [27]. Industrial cluster in a competitive market is an effective way to promote division of labour and productivity progress if the institutional efficiency and mutual-trust of economic and technology systems are more competitive, and it has no adverse effects on welfare and does not generate distortions in a competitive market. Hence, a competitive market will fully explore total positive network effects of division of labour on aggregate productivity.

Industrial cluster in a competitive market is efficient and it ensures the network effects of division of labour can be fully exploited when the institutional efficiency and mutual-trust of industrial cluster overwhelms the general effect of roundabout production, and industrial cluster can promote aggregate productivity by enlarging the network effects of the division of labour against transaction costs. Hence, our attention should be placed on the improvement of institutional efficiency and mutual-trust of economic and technology systems, promotion of innovation and R&D, and maintain the institutional setting for free entry and learning process. Some promising extension of this model are to allow more layers of roundabout production, to count more variety over the conditions of trading efficiency and geographic distance, and to expend to the dynamic process for the interrelationship among industrial cluster, industrial network and institutional settings.

Especially after the 2020 pandemic, the world will be expected markedly different with the system of global supply chain. The institutional efficiency and mutual-trust will become more vital and crucial to determine the global production network, particularly for the high-end production pattern.

5. Acknowledgements

The author appreciates helpful comments from Paul Milgrom, Eric Maskin, Aris Spanos, George Prendergast, Nancy Fox, Hiroshi Ohta, and Warwick McKibbin. Earlier versions of this paper have been presented at the seminars held at Nihon University, Taiwan Industrial Technology Research Institute (ITRI), St. Joseph's University, Aoyama Gakuin University, and Monash University, and I am grateful to participants for valuable comments and discussion. I am responsible for any remaining error.

References

[1] Amin, A. and Thrift, N., 1994, Living in the global, in Amin, A. and Thrift, N. (eds), Institutions and Regional Development in Europe, Oxford: Oxford University Press, 1–22.

[2] Asheim, Bjorn T., Cooke, Philip (1999), 'Local Learning and Interactive Innovation Networks in a Global Economy', in Malecki, Edward J. Oinas, Paivi (eds), *Making connections: Technological learning and regional economic change*, 1999, Aldershot, U.K.. 145-178

[3] Audretsch, David B. and M. P. Feldman, 1999, Innovation in Cities: Science-Based Diversity, Specialization and Localized Competition, European Economic Review, 43(2), 409-429.

[4] Brusco, Sebastiano, 1982, The Emilian Model: Productive Decentralisation and Social Integration, Cambridge Journal of Economics, 6(2), 167–184.

[5] Burt, Ronald S., 1992, Structural Holes: The Social Structure of Competition, Cambridge, MA: Harvard University Press.

[6] Chandler, Alfred D., 1990, Scale and Scope: The Dynamics of Industrial Capitalism, Cambridge, MA: Harvard University Press, 1990.

[7] Coleman, James S., 1990, Foundations of Social Theory, Cambridge, MA: Harvard University Press.

[8] Cooke, Philip, 2002, Knowledge Economies: Clusters, Learning and Cooperative Advantage. London: Routledge.

[9] Eisingerich, Andreas B., Bell, Simon J. and Tracey, Paul., 2010, How Can Clusters Sustain Performance? The Role of Network Strength, Network Openness, and Environmental Uncertainty, Research Policy, 39(2), 239-253.

[10] Florida, Richard and Michael Kenny, 1990, The Breakthrough Illusion: Corporate America's Failure to Move from Innovation to Mass Production, New York: Basic Books.

[11] Fudenberg, Drew and Tirole, Jean, 2000, Pricing a Network Good to Deter Entry, Journal of Industrial Economics 48(4), 373-390.

[12] Grimes, Warren S., 1996, When do Franchisors have Market Power? Antitrust Remedies for Franchisor Opportunism, Antitrust Law Journal 65(1), 105-155.

[13] Harrison, Bennett, Kelley, Maryellen R., and Gant, Jon, 1996, Innovative Firm Behaviour and Local Milieu: Exploring the Intersection of Agglomeration, Firm Effects, and Technological Change, Economic Geography, 72(3), 233-258.

[14] Kinsella, T. K., 1989, Regional economic development organizations and their inter-organizational networks: towards a broadened view of development, Economic Development Review, 7(1), 14–19.

[15] Lazonick, William, 1991, Business Organisation and the Myth of the Market Economy, Cambridge: Cambridge University Press.

[16] Li, Ke, Chu, Chihning, Huang, Derfang, Chang, Chauchyun, and Li, Songlin,2010, Industrial Cluster, Network and Production Value Chain: A New Framework for Industrial Development Based on Specialization and Division of Labour, Pacific Economic Review, 15(5), 596-619.

[17] Marshall, Alfred, Principles of Economics (8th Edition), London: Macmillan, [1890] 1959.

[18] Marshall Alfred, Industry and Trade (3rd Edition), London: Macmillan, [1919] 1920.

[19] Nelson, Richard R. and Sampat, Bhaven N., 2001, Making Sense of Institutions as a Factor Shaping Economic Performance, Journal of Economic Behaviour and Organization 44, (1), 31-54.

[20] Nelson, Richard R. and Winter, Sidney G., 1982, An Evolutionary Theory of Economic Change, Cambridge, MA: Harvard University Press.

[21] Parrilli, Mario Davide and Sacchetti, Silvia, 2008, Linking Learning with Governance in Networks and Clusters: Key Issues for Analysis and Policy, Entrepreneurship and Regional Development, 20(4), 387-408.

[22] Parto, Saeed, 2008, Innovation and Economic Activity: An Institutional Analysis of the Role of Clusters in Industrializing Economies, Journal of Economic Issues, 42(4), 1005-1030..

[23] Perroux, Francois, 1950, Economic Space: Theory and Applications, Quarterly Journal of Economics 64(1): 89--104.

[24] Piore, Michael J. and Sabel, Charles F., 1984, The Second industrial Divide, New York: Basic Books.
[25] Porter, Michael E., 1990, The Competitive Advantage of Nations, New York: Basic Books.
[26] Porter, Michael E., 1994, The Role of Location in Competition, Journal of the Economics of Business, 1(1),35-39.
[27] Porter, Michael E., 1996, Competitive Advantage, Agglomeration Economies, and Regional Policy, International Regional Science Review, 19(1-2), 85–94.
[28] Porter, Michael E., 1997, New Strategies for Inner-City Economic Development, Economic Development Quarterly 1(11), 11-27.
[29] Porter, Michael E., 1998, Clusters and the New Economics of Competition, Harvard Business Review, 76(6), 77-90.
[30] Porter, Michael E., 2000a, Location, Competition, and Economic Development: Local Clusters in a Global Economy, Economic Development Quarterly, 14(1), 15-34.
[31] Porter, Michael E., 2000b, Locations, Clusters, and Company Strategy, in The Oxford Handbook of Economic Geography, edited by Gordon L. Clark, Maryann P. Eeldman, and Meric S.Gertler, Oxford: Oxford University Press, 253-274.
[32] Porter, Michael E., 2003, The Economic Performance of Regions, Regional Studies, 37(6-7), 549-678.
[33] Porter, Michael E., 2007, Clusters and the New Economics of Competition, Economic Integration and Spatial Location of Firms and Industries, 2, 51-64.
[34] Schmitz, Hubert and Khalid Nadvi., 1999, Clustering and Industrialization: Introduction, World Development 27(9), 1503-1514.
[35] Smith, Adam, 1776, An Inquiry into the Nature and Causes of the Wealth of Nations, reprint and edited by E. Cannan, Chicago: University of Chicago Press, 1976.
[36] Storper, Michael, 1995, The Resurgence of Regional Economies Ten Years Later: The Region as a Nexus of Untraded Interdependencies, European Urban and Regional Studies 2(3), 161-221.
[37] Sun, Guangzhen, Yang, Xiaokai and Zhou, Lin, 2004, General Equilibria in Large Economies with Endogenous Structure of Division of Labor, Journal of Economic Behavior and Organization, 55(2), 237-256.
[38] Tirole, Jean, 1989, The Theory of Industrial Organization (Cambridge: The MIT Press).
[39] Varamaki, Elina and Vesalainen, Jukka, 2003, Modelling Different Types of Multilateral Co-operation between SMEs, Entrepreneurship and Regional Development, 15(1), 27-47.
[40] Yang, Xiaokai, 2001, Economics: New Classical versus Neoclassical Frameworks (Cambridge, MA: Blackwell).
[41] Yang, Xiaokai. and Ng, Yew-Kwang, 1993, Specialization and Economic Organization: A New Classical Microeconomic Framework (Amsterdam: North-Holland).
[42] Yao, Shuntian and Li, Ke, 2008, Economic Networking and Stability, Pacific Economic Review, 13(5), 632-640.
[43] Young, Allyn, 1928, Increasing Returns and Economic Progress, The Economic Journal, 38, 527-542.

Table 1. Relative Prices, Per-Capita Real Income and Relative Number of Specialists in Different Structures

Structure	Relative Prices	Per-Capita Real Income	Relative Number of Specialists
A	N/A	$\frac{(1-b-F)^2}{4}$	N/A
B	N/A	$\alpha^{\alpha}\cdot\left(\frac{1-2b-F}{2+\alpha}\right)^{\alpha+2}$	N/A
P_A	$\frac{p_x}{p_z}$ $= \frac{(1-2b)^2}{4^{1-\alpha}\cdot\alpha^{\alpha}\cdot[(1-t)\cdot K]^{2\alpha-1}\cdot(1}$	$\frac{(1-2b)^{2\alpha}\cdot\alpha^{\alpha}\cdot[(1-t)\cdot K]^{2\alpha}\cdot(1-\alpha)^{2-2\alpha}\cdot(1-b-F)}{4^{\alpha}}$	$\frac{M_x}{M_z}$ $= \frac{(1-2b)^{3-2\alpha}\cdot(2-\alpha)^{\frac{1}{1-\alpha}}}{2^{3-2\alpha}\cdot\alpha^{\frac{1+\alpha-\alpha^2}{1-\alpha}}\cdot[(1-t)\cdot K]^{\frac{4\alpha-2\alpha^2-1}{1-\alpha}}\cdot(1-b-}$
P_B	$\frac{p_x}{p_y}=\frac{(1-b)\cdot(1+\alpha)^{1+\alpha}}{\alpha^{\alpha}\cdot(1-b-F)^{1+\alpha}}$	$\frac{(1-b)\cdot\alpha^{\alpha}\cdot[(1-t)\cdot K]\cdot(1-b-}{4\cdot(1+\alpha)^{1+\alpha}}$	$\frac{M_x}{M_y}=1$
P_C	$\frac{p_x}{p_y}=\frac{1-b}{1-F}$	$\frac{(1-b)\cdot(1-F)\cdot[(1-t)\cdot K]}{4}$	$\frac{M_x}{M_y}=1$

CC_A	$\frac{p_y}{p_z} = [(1-t)\cdot K]^{\frac{1}{2}}, \quad \frac{p_x}{p_z} = P1$	u_{CCA}	$\frac{M_x}{M_z} = M1 \ , \ \frac{M_y}{M_z} = M2$
CC_B	$\frac{p_y}{p_z} = \left[(1-t)\cdot K\right]^{\frac{1}{2}} \frac{p_x}{p_z} = \frac{(1-F)\cdot(\alpha^{\frac{\alpha}{1-\alpha}} - \alpha^{\frac{1}{1-\alpha}})^{1-\alpha}}{(1-b)^{1-\alpha}\cdot[(1-t)\cdot K]^{\frac{1-\alpha}{2}}}$	$\frac{(1-b)^{3-\alpha}\cdot[(1-t)\cdot K]^{\frac{4-\alpha}{2}}}{4\cdot(1-F)\cdot(\alpha^{\frac{\alpha}{1-\alpha}} - \alpha^{\frac{1}{1-\alpha}})^{1-\alpha}}$	$\frac{M_x}{M_z} = \frac{(1-b)^2\cdot[(1-t)\cdot K]^{\frac{1}{2}}}{\alpha^{\frac{1}{1-\alpha}}\cdot(1-F)^{\frac{2}{1-\alpha}}\cdot(\alpha^{\frac{\alpha}{1-\alpha}} - \alpha^{\frac{1}{1-\alpha}})} \quad \frac{M_y}{M_z} = \frac{(1-b)^{2(1-\alpha)}\cdot[(1-t)\cdot K]^{\frac{3-2\alpha}{2}}\cdot(\alpha^{\frac{\alpha}{1-\alpha}} + \alpha^{\frac{1}{1-\alpha}})}{\alpha^{\frac{1}{1-\alpha}}\cdot(1-F)^2\cdot(\alpha^{\frac{\alpha}{1-\alpha}} - \alpha^{\frac{1}{1-\alpha}})^{2(1-\alpha)}}$

Here, $P1 = \frac{(1-F)\cdot[(\alpha+e-\theta)^{\frac{\alpha+e-\theta}{1-\alpha-e+\theta}} - (\alpha+e-\theta)^{\frac{1}{1-\alpha-e+\theta}}]^{1-\alpha-e+\theta}}{(1-b)^{1-\alpha-e+\theta}\cdot[(1-t)\cdot K]^{\frac{1-\alpha-e+\theta}{2}}}$, $u_{CCA} = \frac{(1-b)^{3-\alpha-e+\theta}\cdot[(1-t)\cdot K]^{\frac{4-\alpha-e+\theta}{2}}}{4\cdot(1-F)\cdot[(\alpha+e-\theta)^{\frac{\alpha+e-\theta}{1-\alpha-e+\theta}} - (\alpha+e-\theta)^{\frac{1}{1-\alpha-e+\theta}}]^{1-\alpha-e+\theta}}$,

$M1 = \frac{(1-b)^2\cdot[(1-t)\cdot K]^{\frac{1}{2}}}{(\alpha+e-\theta)^{\frac{1}{1-\alpha-e+\theta}}\cdot(1-F)^{\frac{2}{1-\alpha-e+\theta}}\cdot(\alpha^{\frac{\alpha+e-\theta}{1-\alpha-e+\theta}} - \alpha^{\frac{1}{1-\alpha-e+\theta}})}$, and $M2 = \frac{(1-b)^{2(1-\alpha-e+\theta)}\cdot[(1-t)\cdot K]^{\frac{3-2\alpha-2e+2\vartheta}{2}}\cdot[(\alpha+e-\theta)^{\frac{\alpha+e-\theta}{1-\alpha-e+\theta}} + (\alpha+e-\theta)^{\frac{1}{1-\alpha-e+\theta}}]}{(\alpha+e-\theta)^{\frac{1}{1-\alpha-e+\theta}}\cdot(1-F)^2\cdot[(\alpha+e-\theta)^{\frac{\alpha}{1-\alpha-e+\theta}} - (\alpha+e-\theta)^{\frac{1}{1-\alpha-e+\theta}}]^{2(1-\alpha-e+\theta)}}$.

Table 2. General Equilibrium and Its infra-marginal Comparative Statics

Trading efficiency of good k	$K \to 0$			K are medium					K are large			
the efficiency coefficient of roundabout production α	α is small	α is large		K is relatively smaller given the value of α, β, F, t and b		K is relatively larger given the value of α, β, F, t and b			β is relatively smaller given the value of α; and the values of F and b are fixed		β is relatively larger given the value of α; and the values of F and b are fixed	
the fixed learning and entry cost F and b		b is relatively larger given the value of F	b is relatively smaller given the value of F	b is relatively larger given the value of F	b is relatively smaller given the value of F	b is relatively larger given the value of F		b is relatively smaller given the value of F				
the efficiency coefficient of industrial cluster β												
the coefficient of geographic distance t						t is relatively smaller	t is relatively larger		t is relatively smaller	t is relatively larger	t is relatively smaller	t is relatively larger
Equilibrium structure	A	A	B	P_C	P_B	P_A	P_B	P_A	CC_A	CC_B	CC_B	CC_A

Proceedings of the Tenth International
Conference on Information (Information'2021)
ISBN 4-901329-11-8

Reduction of Pressing Force and Friction Force in Miro Ultrasonic Knurling Technology Creating High Precision Texture

Shigeru Aoki*, Yasunori Sakai**, Tomohisa Tanaka***

*Tokyo Metropolitan College of Industrial Technology, Department of Mechanical Engineering, 140-0011 Tokyo, Japan, E-mail:aoki@g.metro-cit.ac.jp

**Shibaura Institute of Technology, College of System Engineering and Science, 337-8570 Saitama, Japan

***Tokyo Institute of Technology, School of Engineering, 152-8552 Tokyo, Japan

Abstract

Sliding surface in mechanical system is required to move smoothly and stop at target position. Sliding surface can move and stop by applying adequate friction force. Friction force is controlled by developing technology creating small texture on the surface with a few to a few hundred micrometer intervals. On the other hand, ultrasonic vibration is used in many manufacturing fields. In this paper, the effect of ultrasonic vibration is examined by the fundamental experiment. In the experiment making a groove on the surface with an indenter using a 2 dimensional table, pressing force and friction force are measured. These forces are reduced using ultrasonic vibration.

Keywords: Knurling, Ultrasonic vibration, Texture, Pressing force, Friction force

1. Introduction

Friction on the sliding surface of the machine is controlled by creating very small texture with a few to a few hundred micrometer intervals. By applying this technology to sliding surface of large industrial machines such as airplanes generators and machine tools and getting low friction surface, machine efficiency increases drastically. To realize low friction surface, a processing technology creating small wear resistant texture with high precision and high-efficiency is required. However, a practical processing technology creating small texture is not completed in conventional technology. On the other hand, ultrasonic vibration is applied to many processing technologies [1]. It is well known that residual stress in welded joint is reduced and surface roughness is improved in drilling of composite material. Then, the purpose of this study is to develop processing technology creating very small texture on large sliding surface by applying ultrasonic vibration to knurling and resolving problems of the conventional technology. In this paper, a fundamental experiment making groove using an indenter is conducted and the pressing force and the friction force are measured. As a result, both forces are reduced using ultrasonic vibration.

2. Processing Experiment Using Ultrasonic Vibration

Horn is designed and made to transmit vibration of the Langevin-type transducer to surface of workpiece efficiently. The frequency response function is measured using acceleration sensor changing frequency of input to transducer. 31.5 kHz is the peak frequency of the frequency response function [2].

Using the horn, an experiment is made creating groove on the surface of the workpiece by an indenter using ultrasonic vibration. Figure 1 shows the experimental setup. The specimen is fixed by bolts on 2-axis feed table. Tip shape of the indenter is cone. The indenter is pressed in vertical direction and the workpiece is fed in lateral direction. The indenter is fixed at the tip of horn and ultrasonic vibration is applied in vertical direction during processing. A three dimensional dynamometer is set under workpiece and the pressing force and the friction force are measured for various target depth of groove. Material of workpiece is aluminium (A2017).

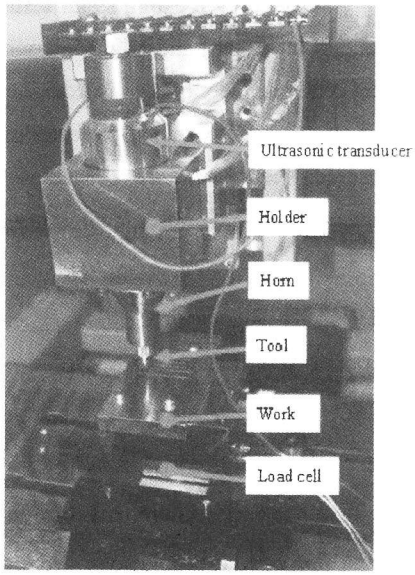

Fig.1 Experimental setup

Figure 2(a) and (b) show the pressing force and the friction force in which target depth is set as 30mm and 50mm, respectively. Red line is the pressing force and blue line is the friction force. The workpiece is fed in lateral direction after tip of the indenter reaches the target depth. The workpiece is processed without ultrasonic vibration. Ultrasonic vibration is applied after 30s. From both figures, the pressing force and the friction

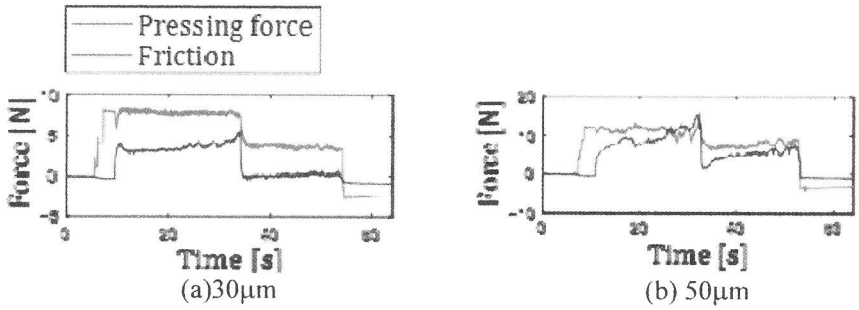

(a)30μm (b) 50μm

Fig.2 Pressing force and friction force

force are reduced when ultrasonic vibration is applied. Then, ultrasonic vibration is effective to reduce both forces.

3. Pressing Force and Friction Force

The target depth other than shown in Fig.2 is set and the average value of the pressing force and the friction force is obtained. Figure 3(a) and (b) show the results. Blue line shows force without ultrasonic vibration and red line shows force with ultrasonic vibration. The pressing force and the friction force are reduced using ultrasonic vibration during processing.

Next, ratio of the pressing force and the friction force on workpiece with ultrasonic vibration to that without ultrasonic vibration is examined. Figure 4(a) and (b) show ratio of the pressing force and ratio of the friction force, respectively. Ratio of both forces increases with the increase of target depth. For the large target depth, ratio the pressing force tends to be constant.

Third, in order to examine reduced force, difference between the pressing force and the friction force without ultrasonic vibration and those with ultrasonic vibration is shown in Fig.5(a) and (b). For pressing force, reduced force is approximately proportional to target depth.

4. Conclusions

The technology using ultrasonic vibration on knurling is examined for creating small texture on a large sliding surface to control friction force. For the fundamental experiment, groove is made using an indenter and the pressing force and the friction force are measured for various target depth. Obtained results are summarized as follows.

(1) The pressing force and the friction force are reduced using ultrasonic vibration.

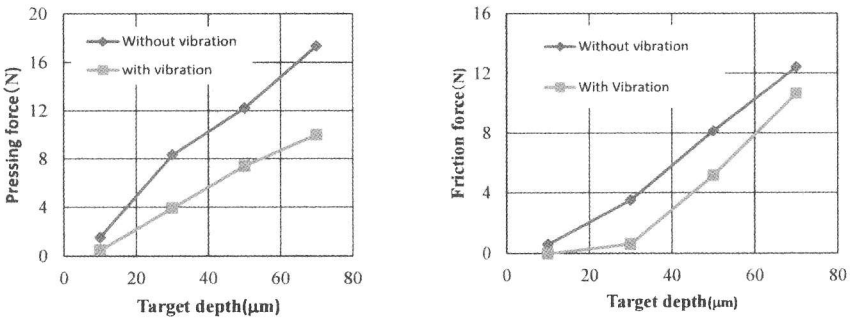

(a) Pressing force (b) Friction force

Fig.3 Pressing force and friction force

(2) Ratio of the pressing force and the friction force using ultrasonic vibration to those without ultrasonic vibration increases with the increase of target depth. For a large target depth, ratio of the pressing force tends to be constant,

(3) Difference between the pressing force without ultrasonic and that using ultrasonic vibration is approximately proportional to target depth.

4. Acknowledgements

The study on this paper is supported by Grants-in-Aid for Scientific Research No.18K03890.

References

[1] V. K. Astashev, V. I. Babitsky, Ultrasonic Processes and Machines, Springer-Verlag, Berlin Heidelberg, 2010.

[2] S. Aoki, Y. Saki, T. Tanaka, A Fundamental Experiment for Micro Ultrasonic Knurling Technology Creating High Precision Texture on Sliding Surface, Information, 23-3(2020), 205-212.

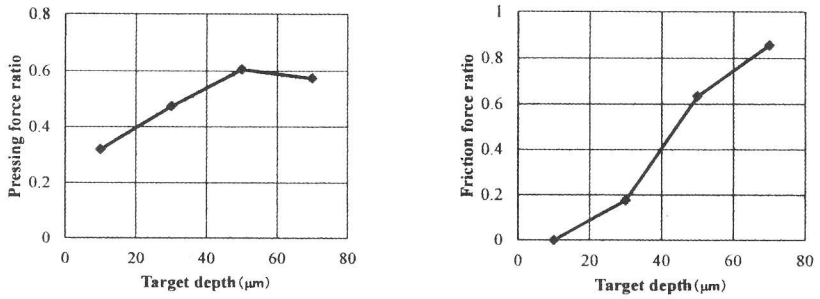

(a) Pressing force (b) Friction force

Fig.4 Ratio of pressing force and friction force for the case with vibration to those with vibration

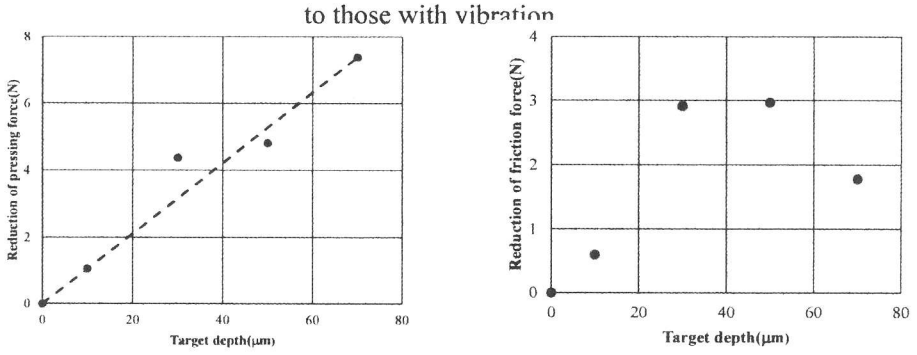

(a) Pressing force (b) Friction force

Fig.5 Reduction of pressing force and friction force

Proceedings of the Tenth International
Conference on Information (Information'2021)
ISBN 4-901329-11-8

The Prediction of PM2.5 Concentration Using an Improved Backpropagation

Siqi Han and Lei Li
Graduate School of Science and Engineering, Hosei University, Koganei, Tokyo 184-8584, Japan
E-mail: siqi.han.7n@stu.hosei.ac.jp, lilei@hosei.ac.jp

Abstract

As "smog" has becoming a topical issue in both domestic and international, people realized that even the blindly development of industry has brought a temporary progress of standard of living, but there are heavy coasts to pay. One of the most painful is the air pollution. Air pollution indexes, such as PM2.5, have gradually entered the public eye, and become an important reference for weather forecasts and people's travel. This paper is based on standard BP neural network, through the improved AM-BP, GA-BP, PCA-GA-BP to predict the concentration of PM2.5. The model is programmed and simulated with MATLAB, and the feasibility of the model is proved by experiments.

Keywords: PM2.5, BP neural network, additional momentum method (AM), genetic algorithm (GA), principal component analysis (PCA)

1. Introduction

PM2.5 is a particulate matter with a particle size of 2.5 μm (1/1000 of 2.5 mm) or less. It is easy for harmful substances such as microorganisms to adhere. PM2.5 research is a high-profile issue because it has a great impact on the air environment and human health. The traditional regression statistical model and numerical prediction model are the methods used for predicting the air quality in most cities domestic and abroad, but these methods cannot meet the management and utilization of massive data, and the accuracy is low. For complex nonlinear systems, BP artificial neural network can perform better function approximation and obtain higher fitting accuracy and prediction accuracy.

However, in practical application, BP neural network also has many defects. In the process of error reduction, it is easy to fall into the local minimum value, and the convergence speed of learning algorithm is slow. This article is based on the standard BP neural network, through the improved AM-BP, GA-BP, PCA-GA-BP to predict the concentration of PM2.5 and draw meaningful conclusions.

2. Artificial Neural Network

2.1 Back Propagation Neural Network

Suppose "M" represents the number of the input signals in the input layer, "I" represents the number of the nodes in the hidden layer and "P" represents the number of the nodes in the output layer. The input of the input layer is represented by X_M, the weight between the input layer and the hidden layer is represented by W_{MI}, and the weight between the hidden layer and the output layer is represented by W_{IP}. Y_P represents the output of the output layer. In the sample learning process, the input / output of each layer is calculated by the following equation.

$$U_I=\sum_{M=1}^{M_{MAX}} W_{MI}X_M \quad (1) \qquad V_I=\mathrm{f}(U_I) \quad (2)$$

$$U_P=\sum_{I=1}^{I_{MAX}} W_{IP}V_I \quad (3) \qquad Y_P= V_P=\psi(U_P) \quad (4)$$

Then, the learning error of the Pth neuron in the output layer becomes Eq. (5).

$$E_P(\mathrm{N})=D_P(\mathrm{N})-Y_P(\mathrm{N}) \quad (5)$$

The error energy of each neuron is $\frac{1}{2}E_{KP}^2(\mathrm{N})$. Add the error energies of the neurons in the output layer to obtain Eq. (6).

$$\mathrm{E(N)}=12\Sigma EKP2PMAXP=1 \quad (6)$$

2.2 Additional Momentum Back Propagation Neural Network

The so-called additional momentum method is to add part of the last weight adjustment quantity and regard it as the weight adjustment quantity of this learning, which is also the difference between AM-BP algorithm and BP algorithm. The formula for weight adjustment is as follows:

$$\Delta\mathrm{W(N+1)} = MC[\mathrm{W(N)-W(N-1)}]-\eta\partial E(N)\partial W(N) \quad (7)$$

In the above formula, MC represents the added momentum coefficient, and N is the number of training. From equation (7), when M_C=0, the weight adjustment of this learning is determined according to the gradient descent method. When the training weight of the network is close to the local minimum of the error surface, the local gradient value becomes very small. Adding momentum term can avoid the possibility of falling into a local minimum.

3. Genetic Algorithm

3.1Implementation of Genetic Algorithm

(1) Encoding. Before solving the problem, the genetic algorithm first represents the data in the solution space as the genotype string structure data in the genetic space. Different points in these string structure data are composed of different combinations of string structure data.

(2) Initialize the population, determine the population size, the maximum iteration ordinal number and other parameters, and use the random method to generate a feature string with a certain length as the initial population

(3) Fitness value evaluation. For different issues, the fitness function is selected in different ways.

According to specific issues, the fitness function is used to calculate the fitness values of all individuals in the group.

(4) Selection operation. Using roulette method for selection operation, keeping the best individual to the next generation, forming a new group.

(5) Crossover operation. Exchanging individual chromosomes to produce new individuals.

(6) Mutation operation. Using mutation operator to change the chromosome in the individual to produce a new individual.

(7) Judging the termination condition. And outputting the individual with the maximum fitness value obtained in the evolution process as the optimal solution.

3.2 Genetic Algorithm- Back Propagation Neural Network

Genetic algorithm optimization BP neural network is divided into three parts: determination of BP neural network structure, genetic algorithm optimization and BP neural network prediction. The number of input and output parameters of the fitting function determines the structure of the BP neural network, and then determines the length of the individual genetic algorithm. Genetic algorithm is used to optimize the weights and thresholds of BP neural network. Each individual in the population contains all the weights and thresholds of a network. The individual calculates the fitness value of the individual through fitness function, and the genetic algorithm finds the individual corresponding to the optimal fitness value through selection, crossover, and mutation. BP neural network prediction using genetic algorithm to get the optimal individual to the network initial weight and threshold value assignment, the network predicts function output after training.

3.3 Principal Component Analysis - Genetic Algorithm- Back Propagation Neural Network

PCA is a special multivariate statistical method that transforms multiple index problems into fewer indexes one, which is, the process of using dimensionality reduction to transform multiple variables in a high-dimensional space into a few main variables. However, these small amounts of data can still retain the information in the original data well and can reflect the main content of the original variables. each principal component is not transformed randomly but is a linear combination of the original variables.

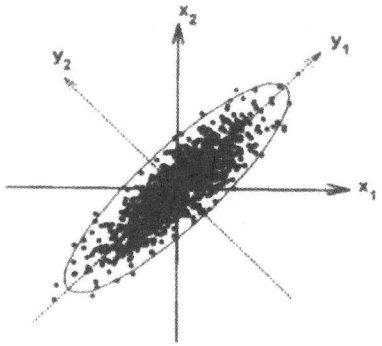

Figure1: Schematic diagram of the geometric meaning of PCA

Suppose in two-dimensional plane X=(x_1, x_2)'extract sample of capacity n, the scatter plot of the observed values of this sample is shown in Figure 1. According to Figure 1, The sample points are approximately scattered in an ellipse, with similar dispersion along the x_1 axis and x_2 axis, and x_1 and $x_2$show a clear linear correlation. From the knowledge of mathematical statistics, the degree of dispersion can be measured by the variance of the variable, and the magnitude of the variance reflects the amount of information contained in the variable. From the knowledge of mathematical statistics, the degree of dispersion can be measured by the variance of the variable, and the magnitude of the variance reflects the amount of information contained in the variable. Rotate the coordinates in Figure 1 counterclockwise by an angle of α, so that the x_1 axis rotates to the long axis direction of the ellipse y_1, and the $x_2$axis rotates to the short axis direction of the ellipse y_2, which becomes a new coordinate system. According to the rotation of coordinates, formula (8) is obtained.

$$\begin{cases} y_1 = x_1 cos\alpha + x_2 sin\alpha \\ y_2 = x_2 cos\alpha - x_1 sin\alpha \end{cases} \tag{8}$$

y_1 and y_2 are newly obtained variables. It can be clearly seen that these n sample observations are almost irrelevant in the new coordinate system. And the new obtained variable is a linear combination of $x_1$andx_2, Figure 2 shows that the dispersion of n sample observations along the axis $y_1$is the largest, that is, the variance of y_1 is much larger than that of y_2, which means that most of the information in the original data is contained by the $y_1$axis, while the variance of the y_2 axis is relatively much smaller. At this point, the loss of variable y_2 only causes a relatively small loss of information. Here, y_1 and y_2 are the linear combinations of the original variables x_1 and x_2.

4. Prediction of PM2.5

4.1The experimental data

Experimental data are the daily mean concentration of PM2.5 and other weather conditions in Beijing, China from January 1, 2011 to September 30, 2018. PM10, SO2, CO, NO2, O3,

maximum and minimum temperatures affect the PM2.5 concentration on the day.

Table 1: Represents part of the experimental data

Date	Maximum Temperature	Minimum Temperature	AQI	PM10	SO2	CO	NO2	O3	PM2.5
2011/1/1	9	-4	81	111	28	1.5	62	52	45
2011/1/2	9	-2	145	168	69	3.4	93	14	111
2011/1/3	4	-5	74	98	29	1.3	52	56	47
2011/1/4	6	-3	149	147	40	2.8	75	14	114
2011/1/5	1	-4	119	117	38	2.3	67	44	91

4.2 Experimental results and analysis

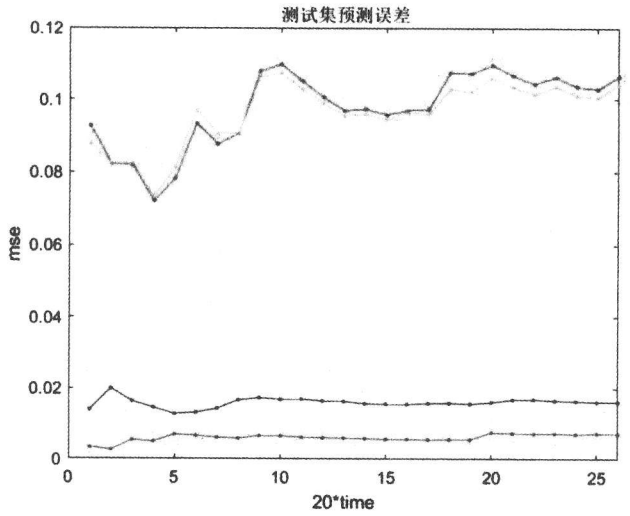

—BP, —AM-BP, —GA-BP, —PCA-GA-BP

Figure 2: Error curves of 4 prediction methods

Table 2: Comparison of results of 4 prediction methods

Test indicators	MSE	Time/s
BP	0.0977	171
AM-BP	0.0962	126
GA-BP	0.0160	106
PCA-GA-BP	0.0061	81

It can be seen from Figure 2 and Table 2 that compared to the BP model, the AM BP model has relatively small fluctuations and has relatively small prediction errors. The fitting degree of

BP algorithm is poor, and the AM-BP algorithm has greatly improved its prediction accuracy and running time. The experiment proves the optimization ability of genetic algorithm in complex nonlinear system. The algorithm that combines the genetic algorithm and the BP neural network improves the optimization ability of the BP neural network, prevents the BP neural network from falling into a local minimum during the training process, and accelerates the convergence speed. PCA can effectively reduce the input dimension of the BP neural network, remove unnecessary input variables, and finally accelerate the convergence speed of the BP neural network.

References

[1] 吴凌云, BP 神经网络学习算法的改进及其应用[J], 信息技术, 2003, 27(7): 42-44.

[2] 张怡文, 敖希琴, 时培俊, 郭傲东, 费久龙, 陈家丽, 基于 Pearson 相关指标的BP神经网络PM 2.5预测模型[J], 青岛大学学报(自然科学版), 2017年02期.

[3] 张德丰, MATLAB 神经网络编程, [M] .北京: 化学工业出版社, (2011).

[4] 周 品, MATLAB 神经网络设计与应用, [M] . 北京: 清华大学出版社, (2013).

[5] 韩力群, 人工神经网络理论、设计及应用, [M] . 北京: 化学工业出版社, (2004).

[6] 谢文兰, 对提高BP 神经网络泛化能力的分析和总结, 广东科技, (7) : 72-73.

[7] http://www.weather.com.cn/

[8]https://www.cnblogs.com/wangduo/p/6773601.html?utm_source=itdadao&utm_medium=referral

Proceedings of the Tenth International
Conference on Information (Information'2021)
ISBN 4-901329-11-8

Influence of Arbors on Indoor Natural Ventilation in Lower Floors of Buildings by Numerical Simulation

Liao Mingcheng*, Sung Wenpei**, Ho Chienwei***

*National Chin-Yi University of Technology, Department of Landscape Architecture, 41170 Taichung, Taiwan (R.O.C.), E-mail: liaomc@ncut.edu.tw

**National Chin-Yi University of Technology, Department of Landscape Architecture, 41170 Taichung, Taiwan (R.O.C.), E-mail: wps@ncut.edu.tw (Corresponding author)

***National Chin-Yi University of Technology, Department of Landscape Architecture, 41170 Taichung, Taiwan (R.O.C.), E-mail: x96za16@gmail.com

Abstract

In spatial landscape planning, arbors beautify the environment, increase the green coverage rate, and enhance environmental comfort, but their influences on surrounding wind fields and indoor ventilation in neighboring buildings are not widely discussed. Hence, with computational fluid dynamics (CFD) numerical simulation as the research method and the student dormitory of the National Chin-Yi University of Technology in Taichung City, Taiwan as the sample, this study explores the influences of arbor planning in the open space outside a building on the natural ventilation of the indoor space of lower floors. This study compares the influences of various variables on indoor air exchange rates, including form of plot plan, planting distance, porosity of arbors, and height of arbors. The goal is to increase the green coverage rate and introduce natural ventilation so as to provide indoor ventilation and maintain good indoor thermal comfort. This can help comply with the characteristics of a subtropical monsoon climate in a place where the site is located, thus providing reference for future plot plans and the design of the arbors around buildings.

Keywords: Urban heat island, Indoor natural ventilation, Arbors pattern, Air exchange rate, Computational fluid dynamics (CFD)

1. Introduction

According to related research of urban micro-climates, as one of the most effective ways to improve the outdoor climate and environment, planting arbors to increase the green coverage rate helps to reduce the influence of urban heat islands [1-4]. In spatial landscape planning, arbors beautify the environment, increase the green coverage rate, and enhance environmental comfort [5], but their influences on surrounding wind fields and indoor ventilation in neighboring buildings (in particular, the lower floors of buildings) are not widely discussed. Therefore, in order to introduce natural ventilation, the arbor planning of neighboring buildings must be taken into consideration. With computational fluid dynamics (CFD) numerical

simulation as the research method and the student dormitory of the National Chin-Yi University of Technology in Taichung City, Taiwan as the sample, this study explores the influences of arbor planning in the open space outside a building on the natural ventilation of the indoor space of lower floors. Results offer a reference for future arbor design around buildings.

2. Method

2.1 Research area

The research area is located in Taichung City, central Taiwan, which mainly has a subtropical monsoon climate. The sample building is a newly-built student dormitory with 2 floors underground and 7 floors above the ground, and it is a reinforced concrete structure. B1 and B2 are parking lots, the ground floor is a hall with a height of 5m, and the 2nd to 7th floors are dorm rooms with a height of 3.6m. The building is southeast-northwest-oriented, and the north and west sides are residential areas with a height of about 3-5 stories. The south side is a parking lot with an asphalt pavement, while the east side is green space of the campus.

2.2 Assessment basis

The air exchange rate is the number of times that the amount of air equivalent to the internal volume is exchanged per unit time, as shown in Eq. 1. The higher the rate is, the higher is indoor air change frequency and the easier the air can circulate. The air exchange rate varies with the types and purposes of buildings. The standard hourly air exchange rates of places are shown in Table 1 [6].

$$n = \frac{Q}{V} \qquad (1)$$

where, n is the air exchange rate (times/hr), Q is the air exchange (m^3/hr), and V is the interior volume (m^3).

2.3 Numerical simulation

2.3.1 Simulation software

This study adopts WindPerfect DX 2018, which is developed by E-Sim, a Japanese company. As 3-dimentional thermal fluid analysis software based on the theory of fluid mechanics, it can analyze the influences on wind fields between buildings and surrounding

environments. It is computer-aided software widely used for the analysis of wind environment on an urban street scale [7-8].

2.3.2 Climate conditions

The outdoor temperature is set at the average temperature of 28.0°C in summer in Taichung City, and the annual wind speed of 1.6 m/sec is taken as the benchmark for discussion according to the annual statistical data from the Taichung meteorological station of the Central Weather Bureau [9].

Table 1. Standard hourly air exchange rates of places [6]

Category	Place	Air exchange rate (times/hr)	Category	Place	Air exchange rate (times/hr)
Home	Kitchen	15	Medical institution	Waiting room	10
	Bedroom	6		Treatment room	6
	Living room	6		Ward	6
	Toilet	10		Operating room	15
Office	Meeting room	12	School	Classroom	6
	Workplace	6		Stadium	8
Restaurant	Banquet hall	10	Factory	Workroom	6
	Kitchen	20		Transformer room	20
	Eating area	6		Painting room	20

3. Results and discussion

Based on the simulation results, the flow rate and ventilation are calculated to obtain the air exchange rate. Figures 1-4 below compare the influences of various variables on indoor air exchange rates. Figure 5 shows the simulation results of flow fields in various forms of plot plans.

In terms of the form of plot plan, the indoor air exchange rate of double-row staggered arbors is the highest, while that of double-row arbors is the lowest. Comparing the number of arbors, double-row arbors are the most common, having a high green coverage rate and greatly influencing the indoor air flow introduction. The influence of planting distance is the greatest on the first floor. As the air exchange rate is proportional to the planting distance, planting distance has no significant influence on the air exchange rates on the second and third floors. The influence of arbor porosity is the greatest on the first floor. The air exchange rate is roughly proportional to this porosity, and such porosity has no significant influence on the air exchange

rates on the second and third floors. The height of arbors has no significant influence on the air exchange rate on the first floor, but greatly influences air exchange rates on the second and third floors.

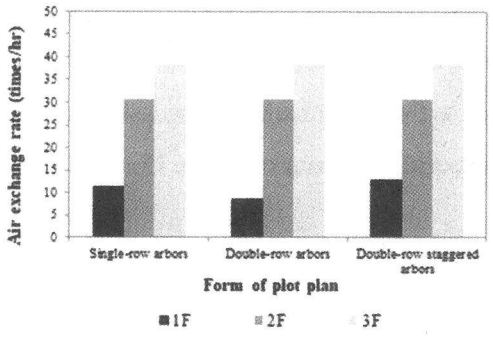

Fig. 1. Influences of forms of plot plans on indoor air exchange rates

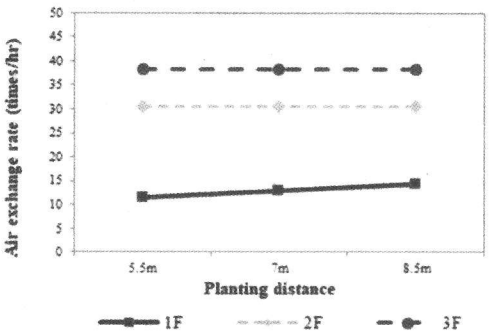

Fig. 2. Influences of planting distances on indoor air exchange rates

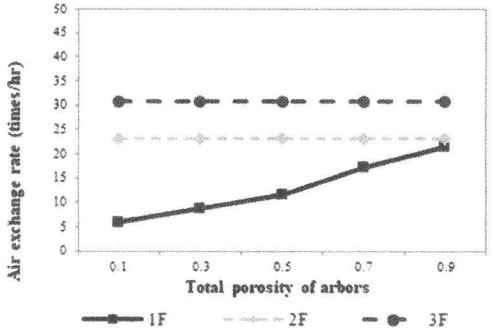

Fig. 3. Influences of porosity of arbors on indoor air exchange rates

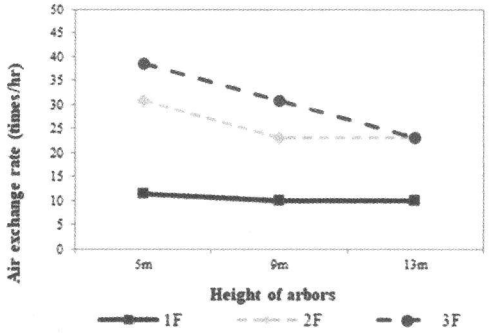

Fig. 4. Influences of heights of arbors on indoor air exchange rates

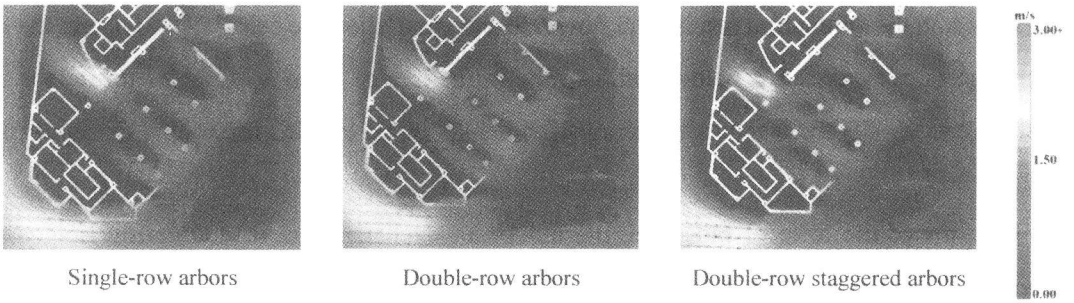

Fig. 5. Simulation results of flow fields in various forms of arbor plots

4. Conclusions

As one of the most effective ways to improve the outdoor climate and environment, planting arbors to increase the green coverage rate helps to reduce the influence of urban heat islands. From the perspective of urban greening, this research focuses on less discussed areas - namely, the influences of arbors on ambient wind fields and indoor air ventilation in neighboring

buildings. Taking a student dormitory in Taichung, central Taiwan as the sample building and Computational fluid dynamics (CFD) numerical simulation as the research method, this study compares the influences of various variables on indoor air exchange rates, including form of plot plan, planting distance, porosity of arbors, and height of arbors. The goal is to increase the green coverage rate and introduce natural ventilation so as to provide indoor ventilation and maintain good indoor thermal comfort. This can help comply with the characteristics of a subtropical monsoon climate in a place where the site is located, thus providing reference for future plot plans and the design of the arbors around buildings.

5. Acknowledgement

The authors would like to acknowledge the support of Taiwan Ministry of Science and Technology through grant No. MOST 106-2221-E-167-006 and MOST 109-2221-E-167-020 -.

References

[1] Coccolo S, Pearlmutter D, Kaempf J, Scartezzini J-L. Thermal Comfort Maps to estimate the impact of urban greening on the outdoor human comfort. *Urban Forestry & Urban Greening*. 2018;35:91-105.

[2] Fahmy M, Sharples S, Yahiya M. LAI based trees selection for mid latitude urban developments: A microclimatic study in Cairo, Egypt. *Building and Environment*. 2010;45(2):345-57.

[3] Lobaccaro G, Acero JA. Comparative analysis of green actions to improve outdoor thermal comfort inside typical urban street canyons. *Urban Climate*. 2015;14:251-67.

[4] Yang Y, Zhou D, Wang Y, Ma D, Chen W, Xu D, et al. Economical and outdoor thermal comfort analysis of greening in multistory residential areas in Xi'an. *Sustainable Cities and Society*. 2019;51:101730.

[5] Jamei E, Rajagopalan P, Seyedmahmoudian M, Jamei Y. Review on the impact of urban geometry and pedestrian level greening on outdoor thermal comfort. *Renewable and Sustainable Energy Reviews*. 2016;54:1002-17.

[6] ABRI. *Green Building Evaluation Manual - Basic Version*. New Taipei City: Architecture and Building Research Institute (ABRI), Ministry of the Interior, ROC (Taiwan); 2019.

[7] Hsieh C-M, Huang H-C. Mitigating urban heat islands: A method to identify potential wind corridor for cooling and ventilation. Computers, *Environment and Urban Systems*.

2016;57:130-43.

[8] Hsieh C-M, Jan F-C, Zhang L. A simplified assessment of how tree allocation, wind environment, and shading affect human comfort. *Urban Forestry & Urban Greening.* 2016;18:126-37.

[9] CWB. Monthly mean wind velocity (10 minutes), 2020, Available from: https://www.cwb.gov.tw/V8/E/C/Statistics/monthlymean.html.

Proceedings of the Tenth International
Conference on Information (Information'2021)
ISBN 4-901329-11-8

Acceleration and Displacement Response Characteristics of System with Friction Subjected to Random Vibration (Effect of Damping Ratio and Natural Period)

Shigeru Aoki*, Katsumi Kurita**

* *Tokyo Metropolitan College of Industrial Technology, Department of Mechanical Engineering, 140-0011 Tokyo, Japan, E-mail:aoki@g.metro-cit.ac.jp*

** *Tokyo Metropolitan College of Industrial Technology, Department of Mechanical Engineering, 140-0011 Tokyo, Japan, E-mail:Katsumi@metro-cit.ac.jp*

Abstract

Various types of devices have been developed to reduce seismic response of the mechanical systems. Base isolation system is one of them. The authors have developed a base isolation system with friction for relatively small mechanical system. In ordinary case, response of mechanical system decreases with the increase of friction coefficient. However, in the experiment to examine the effectiveness of base isolation system, it is found that acceleration response takes minimum value at some friction coefficient. In this paper, experimental results are examined using the equivalent linearization method. It is demonstrated that acceleration response takes minimum value at some friction coefficient in some conditions. The effect of the damping ratio and the natural period is examined.

Keywords: Random vibration, Nonlinear vibration, Vibration isolation system, Friction coefficient, Equivalent linearization method, Seismic excitation, Damping ratio, Natural period

1. Introduction

In order to reduce seismic response of the mechanical system, various types of devices have been developed. In such devices, friction characteristic is used in some devices and base isolation systems with friction are practically used [1].

The authors have developed a base isolation system for prevention from overturning of relatively small structures and shown the effectiveness of system by experiment and numerical analysis. In ordinary case, response of system decreases with the increase of friction coefficient. However, during experiment to examine the effectiveness of the base isolation system, it is observed that acceleration response takes minimum value at some friction coefficient in some conditions.

In this paper, this fact is examined for the mechanical system subjected to random vibration using the equivalent linearization method. As input, stationary white noise is used. The effect of the damping ratio and the natural period is examined.

2. Analytical model and equation of motion

The mechanical system including base isolation system with friction is modeled as a single-degree-of-freedom-system as shown in Fig.1. In this figure, m_m is mass of the mechanical system, c_m is damping coefficient, k_m is spring constant, F is friction characteristic, x_m is absolute displacement of the mechanical system, y_t is absolute displacement of the ground. Friction force is assumed to be applied between the mechanical system and the ground.

The equation of motion with respect to relative displacement of the mechanical system to the ground $z_m=x_m-y_t$ is given as

$$\ddot{z}_m + 2\zeta_m\omega_m\dot{z}_m + {\omega_m}^2 z_m + f = -\ddot{y}_t \tag{1}$$

where $\zeta_m = c_m/\left(2\sqrt{m_m k_m}\right)$ and $\omega_m = \sqrt{k_m/m_m}$ are the damping ratio and the natural circular frequency of the mechanical system, respectively. f is F/m. As friction characteristic, Coulomb friction shown in Fig.2 is introduced. f is given as the following equation.

$$f = \mu g\dot{z}_m/\lceil\dot{z}_m\rceil \tag{2}$$

where μ is friction coefficient and g is acceleration of gravity. Equation (1) is equivalently linearized as

$$\ddot{z}_m + \left(2\zeta_m\omega_m + c_{eq}\right)\dot{z}_m + {\omega_m}^2 z_m = -\ddot{y}_t \tag{3}$$

where c_{eq} is equivalent damping coefficient.

3. Equivalent damping coefficient

Equivalent damping coefficient c_{eq} for stationary excitation is obtained using relative velocity response as follows. c_{eq} is determined as square of difference between Eq.(1) and

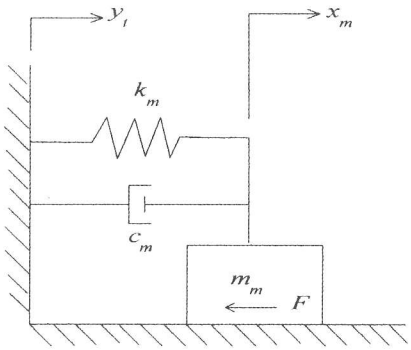

Fig.1 Analytical model of mechanical system

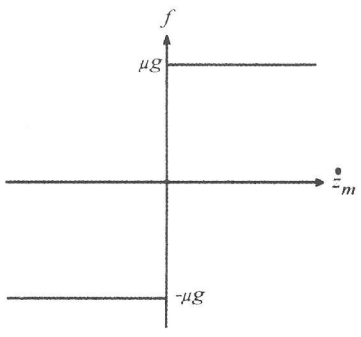

Fig.2 Coulomb friction

Eq.(3) is minimized as

$$\frac{\partial}{\partial c_{eq}} E\left[\left(\mu g \mathrm{sgn}(\dot{z}_m) - c_{eq}\dot{z}_m\right)^2\right] = 0 \tag{4}$$

From Eq.(4), c_{eq} is given as

$$c_{eq} = \frac{\mu g E[\dot{z}_m \mathrm{sgn}(\dot{z}_m)]}{E[\dot{z}_m{}^2]} \tag{5}$$

It is assumed that probability distribution function of $\dot{z}_m$ is the normal distribution with zero mean as

$$f(\dot{z}_m) = \frac{1}{\sqrt{2\pi}\sigma_{\dot{z}_m}} \exp\left(-\frac{\dot{z}_m{}^2}{2\sigma_{\dot{z}_m}{}^2}\right) \tag{6}$$

where $\sigma_{\dot{z}_m}$ is the standard deviation of relative velocity response. Using Eq.(6), c_{eq} is given from Eq.(5) as

$$c_{eq} = \sqrt{\frac{2}{\pi}} \frac{\mu g}{\sigma_{\dot{z}_m}} \tag{7}$$

4. Analysis for stationary white noise excitation

For stationary white noise excitation with intensity S_0, $\sigma_{\dot{z}_m}$ is obtained as

$$\sigma_{\dot{z}_m} = \sqrt{\frac{\pi}{2\zeta_m \omega_m + c_{eq}} S_0} \tag{8}$$

Substituting Eq.(7) into Eq.(8), quadratic equation of $\sigma_{\dot{z}_m}$ is obtained as

$$2\zeta_m \omega_m \sigma_{\dot{z}_m}{}^2 + \sqrt{\frac{2}{\pi}}\, \mu g \sigma_{\dot{z}_m} - \pi S_0 = 0 \tag{9}$$

The standard deviation of relative displacement response is obtained as

$$\sigma_{z_m} = \sqrt{\frac{\pi}{(2\zeta_m \omega_m + c_{eq})\omega_n{}^2} S_0} \tag{10}$$

The standard deviation of absolute acceleration response is obtained as

$$\sigma_{\ddot{x}_m} = \sqrt{\left(2\zeta_m \omega_m + c_{eq}\right)^2 \sigma_{\dot{z}_m}{}^2 + \omega_m{}^4 \sigma_{z_m}{}^2} \tag{11}$$

5. Results of analysis

In Fig.3(a) and (b), the standard deviation of acceleration and displacement response of the system, respectively, are shown. In these figures, ζ=0.01 and $T_n(2\pi/\omega_n)$=2.0s. It is found that the standard deviation of acceleration of the mechanical system takes minimum value at some friction coefficient. Friction coefficient which takes minimum value decreases with the decrease of excitation. On the other hand, standard deviation of displacement decreases with

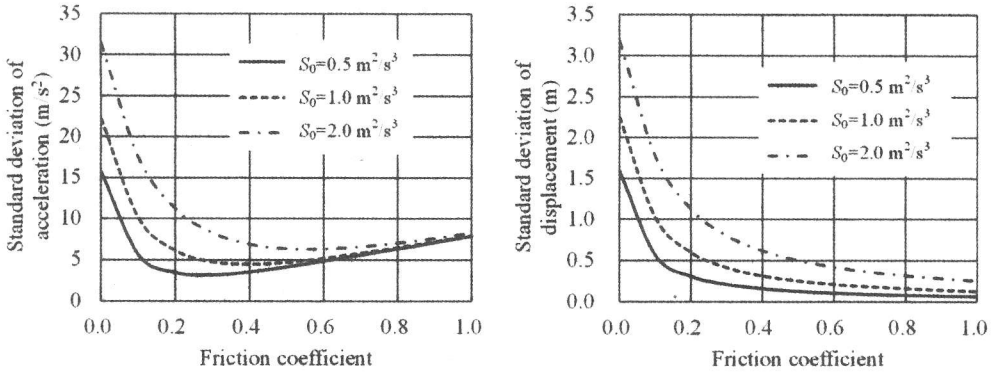

(a) Acceleration (b) Displacement

Fig.3 Standard deviation (ζ_m=0.01, T_m=2.0s)

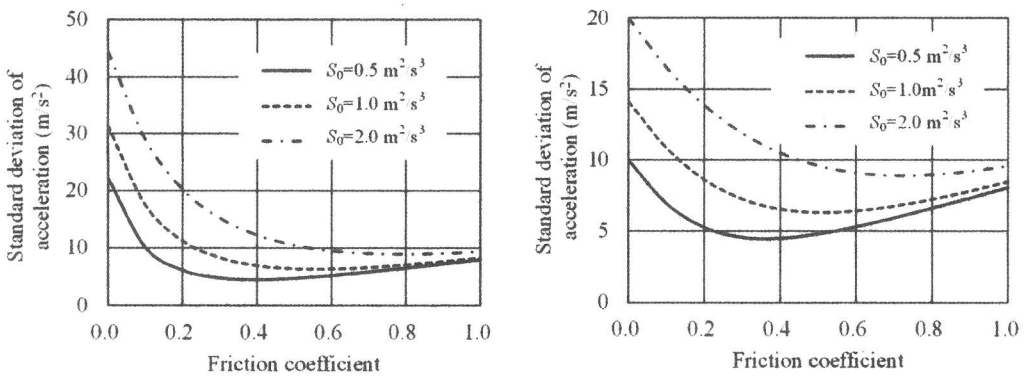

(a) ζ_m=0.01, T_m=1.0s (b) ζ_m=0.05, T_m=1.0s

Fig.4 Standard deviation of acceleration (ζ_m=0.01, T_m=2.0s)

the increase of the friction coefficient. In Fig.4(a) and (b) show the standard deviation of acceleration for ζ_m=0.01, T_m=1.0s and ζ_m=0.05, T_m=1.0s, respectively. The friction coefficient which takes minimum value increases as the natural period is shorter. The standard deviation decreases with the increase of the damping ratio.

6. Conclusions

Analytical method for calculation of the standard deviation of response of the mechanical system with friction is proposed. The standard deviation of acceleration takes minimum value at some friction coefficient. The effect of the damping ration and the natural period on this characteristic is shown.

References

[1] Calvia,P.M., Calvi,G.M., Historical development of friction-based seismic isolation systems, Soil Dynamics and Earthquake Engineering, 106, (2018), 14-30.

Proceedings of the Tenth International
Conference on Information (Information'2021)
ISBN 4-901329-11-8

An Approach for Deformed Image Detection with Template Matching

Hong Shen

Faculty of Science and Technology, Tohoku Bunka Gakuen University
Kunimi 6-45-1, Aoba-ku, Sendai, Miyagi 981-8551, Japan

Abstract

Template matching is a technique in digital image processing for detecting a specified part in an image which matches a template image. It can be used to assist in recognizing road signs so as to navigate a robotic car. However, it cannot work well when the reference image is deformed. In this paper, we present a way to detect a specified template image from a deformed reference image by utilizing template matching. Experimental results are reported and the future work is discussed.

Keywords: image processing, template matching, deformed image

1. Introduction

In recent years, various techniques for self-driving of robotic cars are developed rapidly. It is important for a robotic car to correctly recognize road signs from reference images viewed from the car. Template matching is a technique in digital image processing for detecting a specified part from a reference image which matches a template image. It can be used to recognize road signs to navigate a robotic car. The images of various road signs are kept as template images. The method of template matching works well only when a template image completely matches some part of a reference image. However, a road sign is always viewed with some rotation angle from the camera equipped on the car when a robotic car runs on a road, hence the reference image obtained from the camera is always deformed. It causes the road sign cannot be detected correctly from the deformed image.

In our research, we try to deform the road sign as a template image to match the deformed original image. Experiments are performed to match the reference image which is viewed with some rotation angle, not right in front of the robotic car, and the experimental results are reported.

2. Template Matching

Template matching[1][2][3][4] is a technique in digital image processing for detecting a specified part of a reference image which matches a template image. It can find a desired template in the large reference image by sliding the template window in a pixel-by-pixel basis,

computing the degree of similarity between the reference image and the template image.

Figure 1 shows the main part of the template matching program. The variable n1 stands for the reference image, and variables x and y are the coordinates of the pixel in the image. The variable n2 stands for the template image, and variables s and t are the coordinates of the pixel in the template image.

```
mindif = width[n2]*height[n2];
  for(y=0;y<height[n1]-height[n2];y++){
     if (y % 10 == 0) printf("line%d¥n",y);
     for(x=0;x<width[n1]-width[n2];x++){
         sum=0;
         for(t=0;t<height[n2];t++)
             for(s=0;s<width[n2];s++)
                sum += abs( image[n1][x+s][y+t] -
                            image[n2][s][t] );
         if ( sum < mindif )
             for(t=0;t<height[n2];t++)
                for(s=0;s<width[n2];s++)
                    image[n3][x+s][y+t] =
              255 - image[n1][x+s][y+t];
```

Figure 1. Part of the template matching program

Here, we have an execution example shown in figure 2. Figure 2-1 shows the reference image, and figure 2-2 shows the template image. The image shown in figure 2-1 is searched and the degree of similarity between figures 2-1 and 2-2 is computed. The matching results are given in figure 2-3, in which the detected template is expressed black and white reversed.

画像処理・認識は知能情報
処理の一種と考えること
ができる.

Figure 2-1. Reference image

処

Figure 2-2. Template image

画像処理・認識は知能情報
処理の一種と考えること
ができる.

Figure 2-3. Matching results

3. Deformed Image Detection

Template matching works well when the reference image is viewed just in the right front of the robotic car. However, the reference image is usually viewed with a rotation angle in almost all cases, and it will be viewed as a deformed image. When a rotation angle exists between the template and the reference image, the conventional template matching algorithm described above cannot detect the template image correctly. The conventional way of solving this problem is to rotate the reference image to detect the template image when a rotation exists between the template and the reference image. It is computationally expensive, and is not practical for real-time processing.

In our research, we deform the template image in various deformable angles in order to match the reference image, and kept them in the library. Since the template image would be a small part of the reference image, the computation time can be expected to be reduced.

Figure 3 shows the experimental results. Figure 3-1 shows the reference image, in which the road sign is views as an elliptical shape. The image of the road sign which is used as the template image is shown in Figure 3-2, which is rotated till matching the reference image. Figure 3-3 shows the detected road sign from the reference image.

Figure 3-1 Reference image

Figure 3-2 Road sign used as the template image

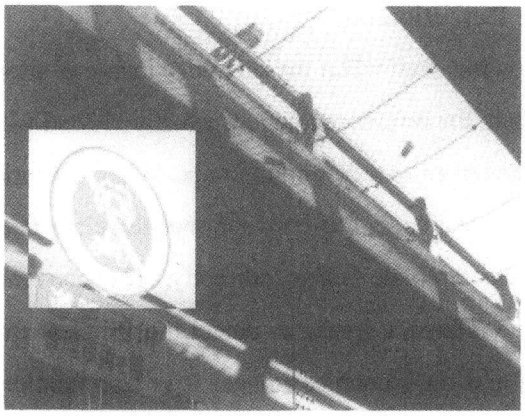

Figure 3-3 Detected template image

4. Conclusions

In this paper, we have presented a way to detect the template image from a deformed reference image by deform the template image to accelerate the computing processing. The experimental result is reported.

The research is in progress. There are many interesting topics to be pursued around this research. We need more experimental results. This will be addressed in our future work.

References

[1] Template Matching Techniques in Computer Vision, R. Brunelli, Theory and Practice, Wiley, 2009.

[2] Grayscale Template-Matching Invariant to Rotation, Scale, Translation, Brightness and Contrast, H. Y. Kim and S. A. Araújo, IEEE Pacific-Rim Symposium on Image and Video Technology, Lecture Notes in Computer Science, vol. 4872, pp. 100-113, 2007

[3] FAsT-Match: Fast Affine Template Matching, Korman S., Reichman D., Tsur G. and Avidan S., CVPR2013.

[4] The Template Update Problem., Matthews, I., Ishikawa, T., Baker, S., IEEE Transaction Pattern Analysis and Machine Intelligence 26(6), 810–815 (2004)

Proceedings of the Tenth International
Conference on Information (Information'2021)
ISBN 4-901329-11-8

Restitution Coefficient at Collision between a Bottom of Small Structure and a Plate by Rocking Vibration

Katsumi Kurita*, Shigeru Aoki**

*Tokyo Metropolitan College of Industrial Technology, Department of Mechanical Engineering, 1-10-40 Higashi-Oi, Shinagawa, Tokyo, Japan, E-mail:katsumi@metro-cit.ac.jp

**Tokyo Metropolitan College of Industrial Technology, Department of Mechanical Engineering, 1-10-40 Higashi-Oi, Shinagawa, Tokyo, Japan, E-mail:aoki@g.metro-cit.ac.jp

Abstract

It is important for overturning prevention by seismic ground motion of small structures installed inside buildings to understand characteristics of restitution coefficient at collision. In this study, characteristics of restitution coefficient at collision were investigated based on vibration experiments. In case of the restitution coefficient fixed value, it was difficult to fit the rocking vibration waveforms between observed and numerical analysis. However, in case of the restitution coefficient that is introduced nonlinear effects, they were good agree between them.

Keywords: Rocking vibration, Restitution coefficient, Small structure, Free vibration

1. Introduction

It is important topics for seismic disaster prevention to prevent overturning of small structures inside buildings by seismic ground motion. Therefore, it needs to understand the overturning process of small structures on seismic ground motion. According to Miyata *et al.* (2018), they indicated that a small structure on the table shook by sine or seismic ground motion have generated rocking vibration, have overturned in non-steady state [1]. It indicates the importance to understand characteristics of rocking vibration. Since the bottom of small structure collides with the table repeatedly in rocking vibration, the restitution coefficient at collision is one of important factor.

In this study, characteristics of the restitution coefficient at collision in rocking vibration is investigated by vibration experiment and numerical analysis.

2. Motion equation of free rocking vibration

A model for the experiment of free rocking vibration is shown in Fig. 1. Providing an initial angle for it, the free rocking vibration is generated. The equation of motion is as followings,

$$I_0\ddot{\theta} + mgR_2 \sin(\phi - |\theta|)\mathrm{sgn}(\theta) = 0 \qquad (1)$$

where I_0 is inertial moment, θ is rotation angle, g is gravity acceleration. And the sng means a function of signal. A relation of angular velocity variation at collision between the bottom of specimen and the table is

$$\dot{\theta}(t^+) = e\dot{\theta}(t^-) \tag{2}$$

An example of results is shown in Fig. 2. In case of restitution coefficient e=1.00, that is perfectly elastic collision, the amplitude and period on rocking vibration indicate the fixed values, and period T=0.42 s. In case of e=0.95 and 0.85, the waveforms of rocking vibration indicate damped vibration motion. The damping ratio ζ in these cases are ζ=0.04 and 0.11, respectively. And the periods indicate progressively shorter from T=0.36 s to 0.14 s in case of e=0.95, and T=0.28 s to 0.12 s in case of e=0.85.

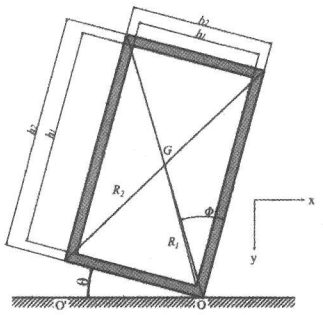

Fig. 1 Model for experiment and numerical analysis.

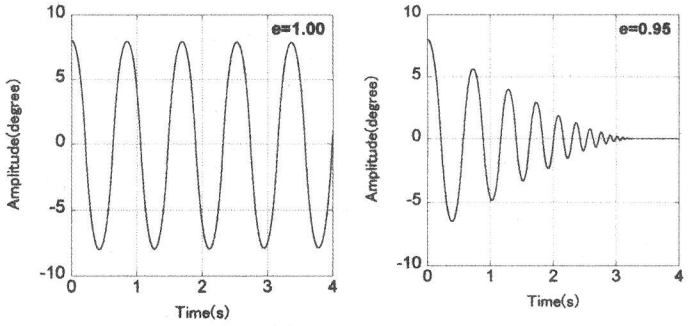

Fig. 2 Results of free rocking vibration waveform by numerical analysis.

3. Experiment of free rocking vibration

An overview of free rocking vibration experiment using the specimen is shown in Fig. 3, and results are in Fig. 4. In case of the table made by aluminum, the period and damping decreased from T=0.49s to 0.10s, and from ζ =0.07 to 0.03, respectively. On the other hand, in case by cork seat, they are from T=0.73s to 0.10s, and from ζ =0.06 to 0.03, respectively.

Comparison results between the observed waveform and the fitting by forward modeling are shown in Fig. 4. The wave shapes of first part between them are good agreement. However, it is difficult to explain waveforms between them with phase differences at later part, assuming the restitution coefficient is fixed value.

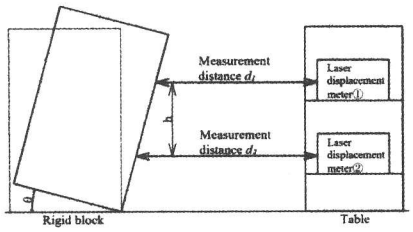

Fig. 3 Outline of measuring system.

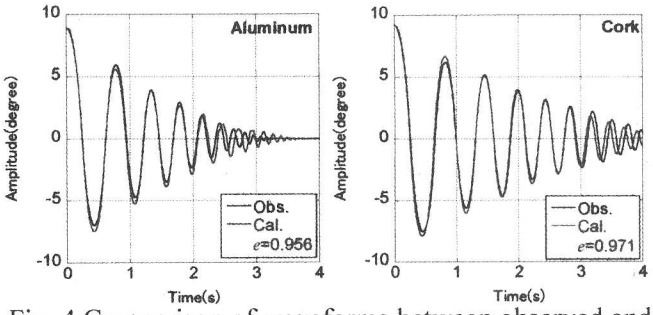

Fig. 4 Comparison of waveforms between observed and numerical analysis.

4. Numerical analysis with non-linear effects

Next, we used a model of quadrilateral hysteresis loop characteristic by Masewa and Watanabe (1975) [2] shown in Fig.5 and do the numerical analysis. Assuming the model of quadrilateral hysteresis loop character shown in Fig. 5, the restitution coefficient is expressed in the following equation,

$$e = v_2 / v_1 = 1.00, v \le \bar{v} \qquad (3\text{-a})$$

$$e = v_2 / v_1 = \sqrt{K_2 / K_3 + (1 - K_2 / K_1)(K_1 / K_3)(\bar{v} / v_1)^2}, v_1 > \bar{v} \qquad (3\text{-b})$$

where $f(x, \dot{x})$ indicates the reaction force, K_1, K_2, K_3 are a slope of reaction force characteristic against displacement. And v_1, v_2 are velocity before and after the collision, respectively. $\bar{v}$ is a velocity of boundary between the perfectly elastic collision and the elastic collision, expressed in the following equation,

$$\bar{v} = \delta_0 \sqrt{K_1 / m} \qquad (4)$$

where δ_0 indicates a deformation of elastic limit, δ_0=0.27 mm is used in this study. From a relation between the restitution coefficient and the collision velocity shown in Fig. 6, the restitution coefficient is depending on collision velocity.

Based on results by experiment of free rocking vibration, optimized parameters K_1, K_2, and K_3 by forward modeling were estimated, and investigated. Comparison results between the experiment and numerical analysis in case of the aluminum and the cork shown in Fig, 7, it is improved to introduce the mode, good agreement between them.

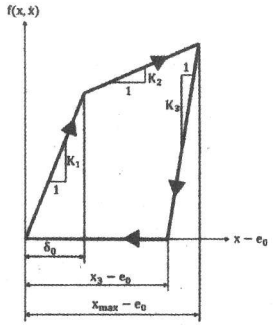

Fig.5 Quadrilateral hysteresis loop characteristic

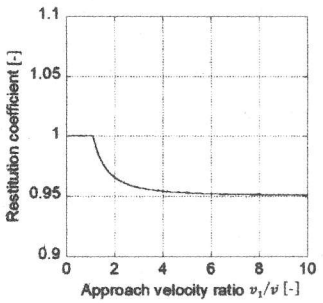

Fig.6 Relationship between restitution coefficient and approach velocity ratio (K_1=3.05, K_2=2.71, K_3=3.00)

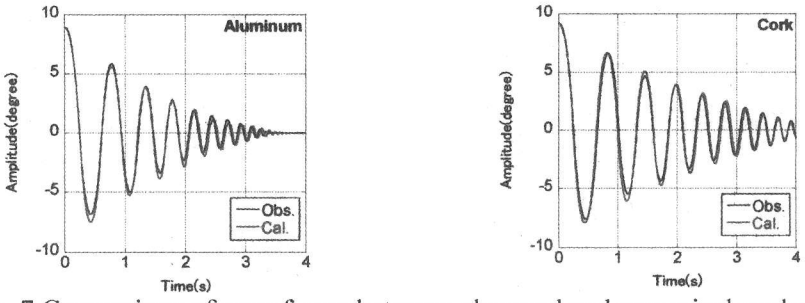

Fig. 7 Comparison of waveforms between observed and numerical analysis using nonlinear model.

5. Conclusions

In this study, characteristics of restitution coefficient at collision of the table on rocking vibration was investigated by excitation experiment and its numerical analysis.

It is possible to explain the waveforms between experiment and numerical analysis with the model proposed by Maesawa and Watanabe. It means the restitution coefficient at collision indicates non-linearity.

References

[1] Miyata, M., Kurita, K. and Aoki, S., Study on rocking vibration characteristics by free and forced vibration for structures, Dynamics & Design Conference 2018 (2018), 219 (in Japanese).

[2] Maezawa, S. and Watanabe, T., Analysis on steady state response of system with hysteresis loop characteristics (2nd report, for system with restitution force having quadrilateral hysteresis loop characteristics), Transactions of the Japan Society of Mechanical Engineers, Vol.41, No.352 (1975), pp.3458–3469 (in Japanese).

Proceedings of the Tenth International
Conference on Information (Information'2021)

ISBN 4-901329-11-8

Reduction Method of Residual Stress for Welding in Stainless Steel by Ultrasonic Vibration

Akira Nakazato*, Kurita Katsumi**, Shigeru Aoki**, Shigeomi Koshimizu***, Tsuyoshi Matsuyama ***

* *Advanced Course, Tokyo Metropolitan College of Industrial Technology, 1-10-40 Higashi-oi Shinagawa-ku, Tokyo 140-0011, Japan*

** *Tokyo Metropolitan College of Industrial Technology, 1-10-40 Higashi-oi Shinagawa-ku, Tokyo 140-0011, Japan*

*** *Advanced, Institute of Industrial Technology, 1-10-40 Higashi-oi Shinagawa-ku, Tokyo 140-0011, Japan*

Abstract

Welding is a joining method used for many structures. However, residual stress is generated near the bead. We have proposed a method of reducing residual stress using ultrasonic vibration during welding in rolled steel for general structures. On the other hand, it is used the stainless steel for important structures. In this research, the effectiveness of the method of reducing residual stress using ultrasonic vibration during welding was examined by built-up welding using the stainless steel.

Keywords: Built up welding, Stainless Steel, Ultrasonic Vibration, Residual Stress, Acceleration

1. Introduction

Welding is a joining method used for many structures, and to melt the material applying heat locally. Since the tensile residual stress is generated in the process of cooling and hardening, and make less the fatigue limit of base material. Therefore, a method of welding tensile residual stresses without a special device is developing using ultrasonic vibration load. According to previous studies [1][2], they indicated that it was an effective method to reduce the welding residual stress using ultrasonic vibration load in case of built-up welding with metal block of rolled steel for general structure SS400 and of butt welding with thin metal sheets.

Since the melting point of stainless steel used for important structures such as a nuclear reactor is higher temperature than that of rolled steel for general structure, it expects that the welding residual stress of stainless steel is higher than that of rolled steel for general structure. The residual stress is one of the reasons that is caused stress corrosion cracking. Therefore, it is important to develop a method of welding reducing residual stress in stainless steel.

In this study, the effectiveness of welding residual stress reduction method using ultrasonic vibration load is investigated for austenitic stainless steel SUS304.

2. Experimental Methods

2.1. Welding

Figure 1 shows a drawing of specimen in this experiment. The material is a block of stainless steel SUS304. Before welding, the surface of specimen is polished and annealed. And, the oxide layer on the surface of specimen is removed with hydrochloric acid and CPL solution.

A thyristor-controlled CO2/MAG automatic welding machine was used to do a 150-mm-long weld on the center of specimen. A mixture gas of argon and carbon dioxide was used as a shielding gas to prevent welding defects such as blow holes. The welding conditions are shown in Table 1.

Comparing the reduction of welding residual stress, the specimens with vibration lord at the frequency of 36 kHz, of 58 kHz and without load were prepared, where the acceleration amplitude is 2000 m/s^2, was measured by acceleration pickup at the point shown Fig. 1. Since chromium carbides were deposited near the bead after welding, the surface was again removed with hydrochloric acid and CPL solution.

2.2. Fabrication of Weld Test Specimens

Welding residual stresses in the bead direction at 15 points every ±10 mm from the center of the bead were measured as shown in Figure 3. X-ray residual stress measurement device was used for the measurement of welding residual stress. To limit an area of irradiation by X-ray, it was covered by black vinyl tape with a frame with 20 mm × 20 mm.

Table.1. Welding conditions

Wire diameter [mm]	1.2
Welding current [A]	180
Welding voltage [V]	21
Welding speed [A]	2.0
Shield gas	Ar + CO_2

Table.2. Stress measurement conditions

Parsing method	ISO-inclination method
Measurement mode	fixed method
Divergence slit [deg]	1
Light receiving slit [deg]	1
Counting time [s]	10
Step	0.15°
Measurement range	143.00°~152.90°
2θ	149.05°
Bulb	Cr
X-ray	CrK-β

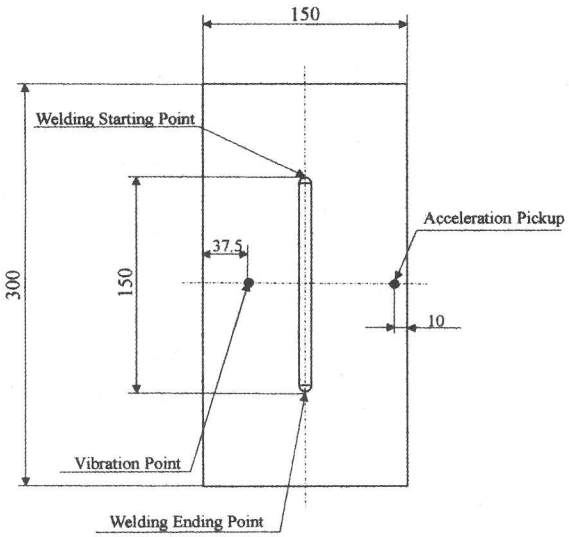

Fig.1. Welding situation of test plate

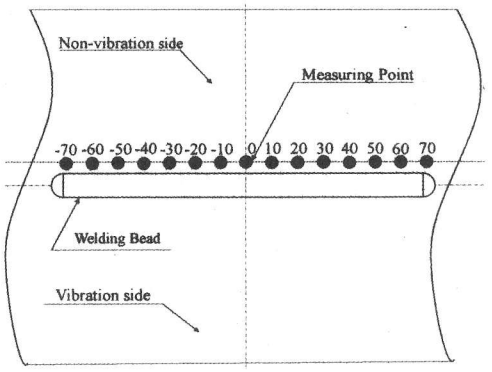

Fig. 2 Location of welding residual stress measurement point

3. Experimental results

2.2. Fabrication of Weld Test Specimens

Figure 3 shows the results of residual stress measurement by built up welding loaded with the ultrasonic vibration at the frequency of 36 kHz, 58 kHz, and without loaded. The tensile residual stress is generated overall in bead direction, and increase toward to the end of welding. Comparing results of welding residual stress between with and without ultrasonic vibration load, it was reduced with ultrasonic vibration load. However, the reduction rate between the ultrasonic vibration load at the frequency of 36 kHz and of 58 kHz, it was almost same, was maximum most 100 MPa. It suggests that the difference in frequency had little effect on the amount of residual stress reduction.

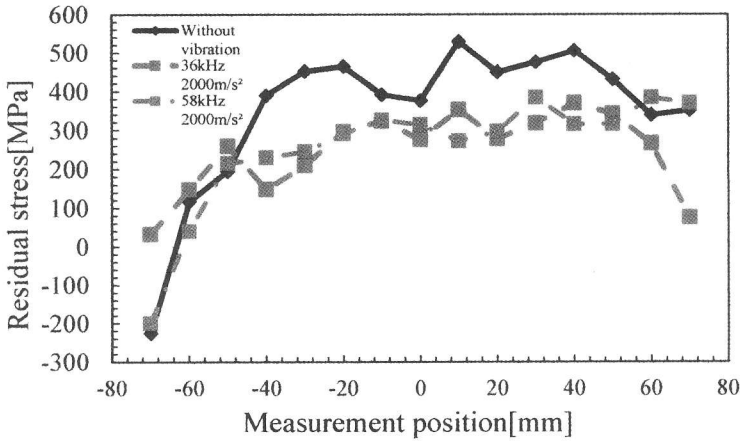

Fig. 3. Residual stress on the bead direction

4. Conclusions

Built up welding was performed on the block of austenitic stainless steel SUS304 loaded by ultrasonic vibration, and the effectiveness of welding residual stress reduction method using ultrasonic vibration was investigated. As a result, the method of welding loaded the ultrasonic vibration at the frequency of 36 kHz and of 58 kHz can reduce welding residual stresses for austenitic stainless steel SUS304. The effects of difference of ultrasonic frequency on welding residual reduction is small.

They indicate that the method of reducing welding residual stress by using ultrasonic vibration is effective for austenitic stainless steel SUS304.

References

[1] Shigeru Aoki, Tadashi Nishimura, Tetsumaro Hiroi, Seiji Hirai and Kunihiko Mineki, Reduction in Residual Stress of Welded joint Using Local Plasticity Caused by Ultrasonic Vibration (Welding of wheels), *Journal of Japan Society for Technology of Plasticity*, 48-554, p.53-56, 2007.

[2] Shigeru Aoki, Tadashi Nishimura, Tetsumaro Hiroi, and Seiji Hirai, Reduction of Residual Stress for Welding Joint Using Ultrasonic Vibration Load, *Transactions of the Japan society of Mechanical Engineers. C*, 77, 657, p.1613-1618, 2001.

Proceedings of the Tenth International
Conference on Information (Information'2021)

ISBN 4-901329-11-8

Behavior of Exhibits Fixed with Nylon Gut by Seismic Motion

Yu Tamura*, Katsumi Kurita**, Shigeru Aoki**

** Advanced Course, Tokyo Metropolitan College of Industrial Technology, 1-10-40 Higashi-oi Shinagawa-ku, Tokyo 140-0011, Japan*

***Tokyo Metropolitan College of Industrial Technology, Department of Mechanical Engineering, 1-10-40 Higashi-Oi, Shinagawa, Tokyo, Japan*

Abstract

It is important for seismic disaster prevention of exhibits in the museum to understand behavior them by seismic motion. In this study, Behavior of exhibits in the museum fixed by nylon guts have performed by vibration test. And conditions to prevent overturning of exhibits fixed by nylon guts were investigated. The exhibit fixed by nylon guts have generated rocking vibration and sliding motion by seismic motion. It expects that the sliding motion at the bottom of exhibit caused overturning. It is effective for overturning prevention to increase friction coefficients between the bottom of exhibits and the display table.

Keywords: Exhibits in the museum, Nylon gut, Vibration test, Friction coefficient

1. Introduction

In order to prevent earthquake disaster, the exhibits in the museum are taken measures to prevent overturing. For example, there is a way of lowering the center of gravity on the exhibits, of fixed by bolts and of put the exhibits on the felt seats [1]. In particular, a nylon gut, which is used for accessories and fishing line, is the most effective way for exhibits fixing on site [2]. Since it is low costs, many museums use it to fix exhibits. However, the exhibits fixed with nylon guts were overturned by seismic motion on the 2011 off the pacific coast of Tohoku earthquake [3]. Therefore, it is important to understand behavior of the exhibits fixed with guts during an earthquake. In this study, the behavior of exhibits fixed with gut by seismic motion are investigated by vibration test.

2. Behavior of an exhibit model by vibration test

Figure 1 shows the model of exhibit made by acrylic used in vibration test. The size and mass are 70×70×455 mm and 1.83 kg, respectively. The overturning acceleration of the model is about 150 Gal.

An overview of the vibration test device is shown in Fig. 2. The model was placed in the center of a stand, and fixed with nylon guts. The 1995 Southern Hyogo Prefecture Earthquake at JMA Kobe (Kobe wave), the 2004 Niigata-ken Chuetsu earthquake at K-NET NIG019 (Niigata wave) and the 2016 Kumamoto earthquake at KiK-net KMMH16 (Kumamoto wave) were used as input waves for the test.

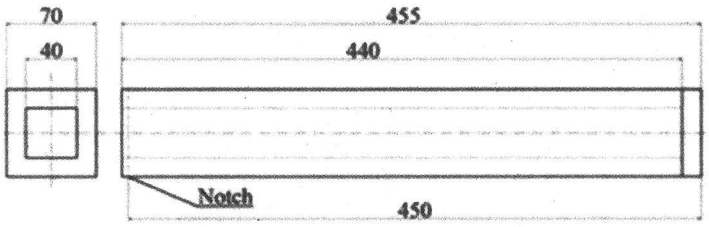

Fig.1 Exhibit model

The input waveform (Niigata wave), and the response waveform at the top of model fixed by nylon guts with tension of 14.7 N are shown in Fig. 3. The response waveform indicates large amplitude from 10 sec against the input, and an asymmetric shape at around 15 sec. These are due to generate rocking vibration of the model and sliding motion of it at the bottom of model after experiment shown in Fig. 4. Therefore, it is expected that a reason of overturned on the exhibits fixed with nylon guts is sliding motion of the model at bottom by seismic motion.

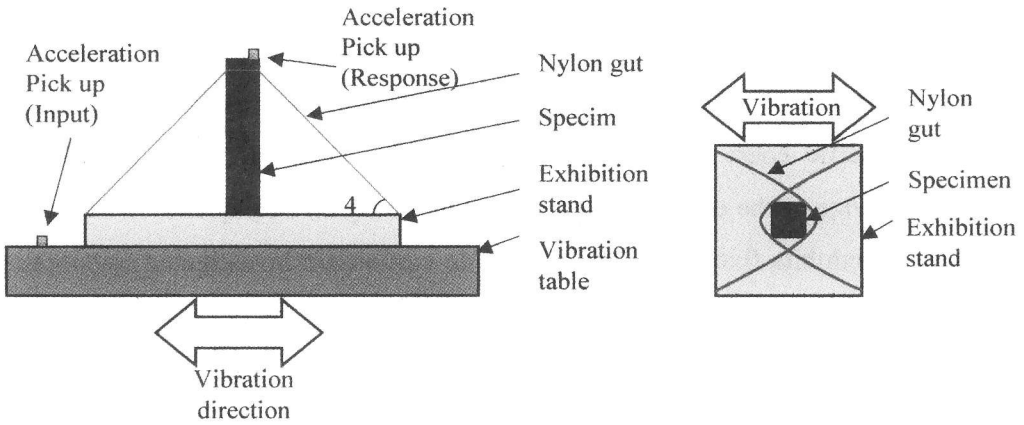

(a) Side view of experimental device (b)Top view of experimental device

Fig.2 Experimental device

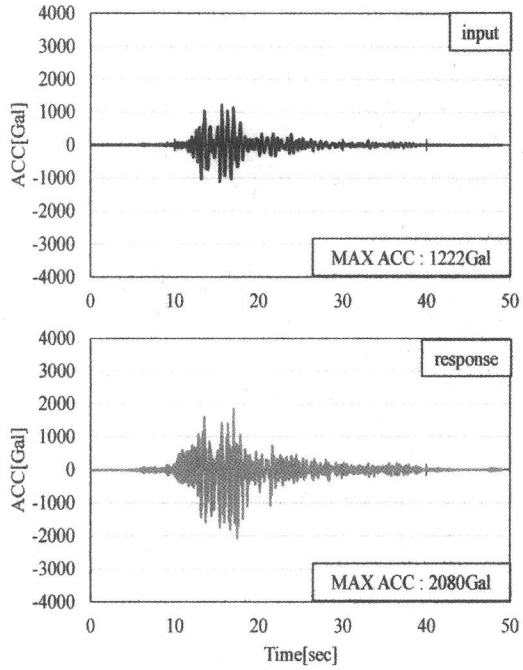

Fig. 3 Input and response acceleration waveforms using Niigata wave

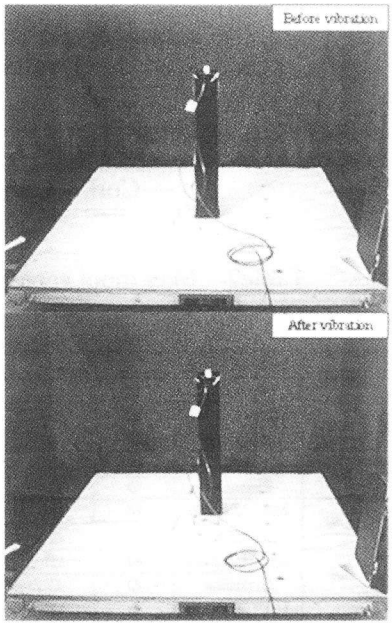

Fig. 4 Behavior of exhibits using Niigata wave

3. Effects of friction coefficient at the bottom of exhibits on behavior

In this section, effects of friction coefficient at the bottom of exhibits on behavior of the exhibits is investigated by vibration test. The conditions of vibration test and static friction coefficient are shown in Table 2. And the tension of nylon guts was set at 2.45 N and 4.9 N.

The maximum input acceleration and status of exhibits behavior under a condition of tension force of nylon guts with 4.9 N using Niigata and Kobe waves are shown in Table 2. Where a symbol ○ means stable condition, △ is sliding motion, □ is rocking vibration, △□ is sliding + vibration and × is overturn. In case of Niigata wave, the behavior of model with a condition of low friction case (A-W) indicates sliding motion. Increasing a value of friction coefficient, the model did not generate sliding motion. The maximum input amplitude without sliding motion in Niigata wave is 336 Gal in case of A-W, 884 Gal in case of A-C, and in case of C-C. In case of Kobe wave, in case of A-W it is 421 Gal. and in case of A-C and C-C it did not generate sliding motion. It is possible to suppress sliding motion by increasing the static friction coefficient.

Table1 Friction coefficients

Conditions	Friction coefficient [-]
Acrylic – Wood (A-W)	0.26
Acrylic – Cork (A-C)	0.45
Cork – Cork (C-C)	0.61

Table2 Max input acceleration amplitude and status (tension: 4.9[N])

4.9[N]			Amplitude level[%]									
			10	20	30	40	50	60	70	80	90	100
Niigata	A-W	MAX ACC[Gal]	115	234	336	473	598	723	852	965	1078	1199
		Evaluation	○	○	○	△	△	△□	△□	△□	△□	×
	A-C	MAX ACC[Gal]	113	229	349	469	588	720	844	962	1075	1191
		Evaluation	○	○	□	□	□	□	□	△□	△□	△□
	C-C	MAX ACC[Gal]	113	232	352	472	600	723	847	968	1091	1200
		Evaluation	○	○	○	□	□	□	□	□	△□	△□
Kobe	A-W	MAX ACC[Gal]	64	125	186	250	334	421	510	611	705	783
		Evaluation	○	○	○	○	□	□	△□	□	△□	△□
	A-C	MAX ACC[Gal]	62	121	182	250	331	417	507	607	704	780
		Evaluation	○	○	○	○	□	□	□	□	□	□
	C-C	MAX ACC[Gal]	61	121	184	252	333	417	507	611	705	783
		Evaluation	○	○	○	○	□	□	□	□	□	□

5. Conclusions

In this study, the behavior of exhibits fixed with gut by seismic motion were investigated by vibration test. The results are as follows,

1. Exhibits fixed with nylon guts are generated rocking vibration and sliding motion by seismic motion. Overturning of exhibits was caused by sliding motion at the bottom of model.
2. Increasing the coefficient of static friction between the bottom of the model and the display stand, it is possible to prevent the exhibits from sliding motion.

References

[1] Tatsuo Ohomachi, Masashi Takase, Takumi Toshinawa, Current seismic countermeasures for displaying artwork and evaluation of the performance of trial seismic-free displays, *Proceedings of the Civil Engineering Society*, No. 507, (1995), 191-199.

[2] Japan Association of Museums (ed.). *Revised Guide Book for Handling Museum Materials: A Guide for Packing and Transporting Cultural Properties and Works of Art*, Gyosei, (2016), p. 230.

[3] Noriyuki Tomita, *Verification of Earthquake Resistance Measures for Art Works Underway: 'Seismic Isolation Table' Does Not Topple Over, 'Tegus' Partly Damaged*, Nihon Keizai Shimbun, (2011-6-17), Evening Edition, p. 16.

Proceedings of the Tenth International
Conference on Information (Information'2021)

ISBN 4-901329-11-8

ISODS: An ISODATA-Based Initial Centroid Algorithm

Noah Gardner[1], Sahar Yarmohammadtoosky[2],
Anthony Phan[3], and Chih-Cheng Hung[4]

Kennesaw State University, Marietta, GA, USA[1,3,4]

Iran University of Science and Technology, Tehran, Iran[2]

[1]ngardn10@students.kennesaw.edu, [2]yarmohamadishr@gmail.com,
[3]aphan5@students.kennesaw.edu, [4]chung1@kennesaw.edu

Abstract

Iterative Self-Organizing Data Analysis Technique (ISODATA) is a clustering algorithm based on the K-Means algorithm that intends to find the correct number of clusters through merging and splitting. It is difficult to determine the correct number of clusters in many real-world applications, in particular, remote sensing image interpretation. Compared to K-Means, the ISODATA algorithm should be resilient to initial cluster centers. However, ISODATA is also sensitive to initial cluster centers which impacts the performance of the algorithm. This work proposes using the ISODATA approach of splitting clusters to select quality initial cluster centers, called Iterative Self-Organizing Data Split (ISODS). The proposed approach is evaluated on several benchmark UCI datasets as well as the Salinas-A hyperspectral image dataset. The results are evaluated using standard clustering evaluation measures. When ISODS is used together with ISODATA, the performance is improved and the generated clusters more closely resemble the expected number of clusters.
Keywords : Clustering, ISODATA, Initial Centroids, Remote Sensing

1 Introduction

Remote sensing technology is used when the data collection takes place at a remote distance from the subject matter, such as the study of daily weather and long-term climate change, land cover monitoring, ecosystem modeling of vegetation, and so on [1, 2]. Multispectral imaging technology is one of the instruments for remote sensing used since the late 1960s [3]. It has been applied to numerous electronic imaging applications, including food inspection, forensic science, medical surgery and diagnosis, and military applications [4, 5, 6]. Because of the difficulty of obtaining prior knowledge in remote sensing studies, unsupervised classification and cluster analysis have great importance compared to supervised classification [7].

Unsupervised learning is a machine learning technique used when the data has no pre-existing labels and looks for patterns in the dataset with minimum human supervision and without external guidance. In contrast to supervised

learning, where a training set of inputs and observations are given to the method, unsupervised learning uses only the inputs and should find an interesting pattern in the dataset. Cluster analysis is an example of unsupervised learning. In clustering analysis, unlabeled and unsorted data points are grouped and segmented according to similarities and differences to find structure in the inputs, group it into meaningful clusters, and understand the dataset better.

One of the most popular clustering algorithms is called ISODATA clustering, based on the K-means algorithm with some variations. The ISODATA method's preference in comparison with the K-means algorithm is that the ISODATA algorithm uses splitting and merging forms for clusters. The ISODATA method allows starting from arbitrary cluster centers and obtains better partitioning results than the K-Means algorithm, but it is not entirely resilient to initial cluster centers. In this paper, a novel method using the ISODATA approach of splitting clusters to select quality initial cluster centers is proposed.

The paper is organized as follows: Section 2 introduces K-Means and ISODATA clustering algorithms. The new proposed algorithm is explained in Section 3. We present the experimental results in Section 4. Finally, Section 5 contains concluding remarks.

2 Background

The K-Means algorithm is an unsupervised clustering algorithm and aims to partition N observations into K clusters [8]. Data points in the same cluster are very similar to each other and have less variation compared to data points assigned to other clusters. The user defines K, the number of expected clusters. Following is a description of the K-Means algorithm:

For selecting the initial cluster centers, there are two standard methods: Random Centers, and K-Means++ [9]. In Random Centers, K samples are randomly chosen from the dataset to serve as the initial cluster centers. In K-Means++, 1 sample is randomly chosen from the dataset to serve as the initial cluster center. Then, $K - 1$ samples are iteratively selected, where the probability of a sample being chosen as a cluster center is the distance of the sample from previously chosen centers [9]. The K-Means algorithm is susceptible to initial starting cluster centers, where different initial values can result in a different classification [10].

ISODATA is another frequently used clustering algorithm and is based on the K-Means algorithm [11]. Like K-Means, cluster centers are iteratively updated and reassigned to the samples in the dataset. However, ISODATA determines the number of clusters dynamically and allows for a different number of cluster centers. In contrast, the K-Means algorithm requires a fixed user-set parameter of the number of expected clusters. The advantage found within ISODATA allows for discovery of a different number of clusters, which is achieved through discarding clusters with a small number of member samples, and merging and splitting clusters that meet certain parameters.

There are some disadvantages to the ISODATA algorithm. First, it is sensitive to the specified parameters. These parameters should be fine-tuned for optimal performance based on the attributes of the dataset being tested. In addition, similar to K-Means, it is sensitive to initial cluster centers, although less so than K-Means due to the extra processes of discarding, splitting, and

merging. The initial centroids can affect both the quality of clusters produced and the number of iterations required to converge [10].

3 Proposed Method

The proposed clustering algorithm's objective is to improve the result we obtain from the clustering algorithms by targeting the initial cluster centers. Inspired by the ISODATA algorithm, Iterative Self-Organizing Data Split (ISODS) uses the splitting process from ISODATA to create the required initial cluster centers to use for a clustering algorithm. The algorithm is outlined below:

- **Step 1:** Choose one observation as a cluster center from the dataset.
- **Step 2:** Assign each element of the dataset to the cluster based on the minimum distance from the cluster center.
- **Step 3:** Re-calculate new cluster centers for each cluster by computing the mean of all patterns assigned to each cluster.
- **Step 4:** If the number of clusters is equal to K, then the process is terminated. If the number of clusters is greater than K, then the clusters with the fewest members is discarded, and the algorithm moves to **Step 2**.
- **Step 5:** Calculate the standard deviation of each cluster in each dimension. Then, split each cluster along the dimension with the greatest standard deviation and move to **Step 2**.

This method began as a modified ISODATA process. However, the modification was unique in that there is a clear distinction from the proposed change and the beginning of the original process. Although more complex than other methods of generating initial cluster centers, this approach guarantees separation between clusters. As a result, ISODS can be used to generate clusters for other clustering algorithms, such as K-Means.

4 Results

Due to the response of the ISODATA algorithm to the discarding, merging, and splitting parameters, these parameters should be carefully selected. Since the goal of this research is to explore the impact of initial cluster centers on ISODATA, we use a relatively simple approach for generating ISODATA parameters. Based on the available training data with included labels, each class is summarized with the mean and standard deviation of that class, as well as the number of members in each class. Typically, since we are working with unsupervised learning algorithms, class information may not be available.

For the first experimental results shown in Table 1, we explore applying ISODS to ISODATA and K-Means by using benchmark UCI *Iris,* and *Wine,* [12]. We also show results from applying Random Centers and K-Means++ Centers. We used 80% of the data for training and 20% of the data for testing to evaluate the models. Following standard practice, the models were trained

on the training data, then fit to the test data. For the ISODATA parameters, we used the approach of summarizing the class data based on the information in the training data. The output labels (cluster assignments) were compared to the ground truth labels contained in the test data using pair-counting measures.

To evaluate the cluster results, external cluster validation measures are used. We utilize pair-counting measures which rely on counting matching pairs between two sets of data to determine agreement and disagreement [13]. The pair-counting measures applied are *Rand index* (RI - agreement probability), *adjusted Rand index* (ARI), *Mirkin's index* (MI - disagreement probability), and *Hubert's index* (HI - (*P*(*agree*) - *P*(*disagree*))) [14, 15]. When comparing ground truth labels to cluster assignments, RI can serve as an estimation of the accuracy. ARI is similar to the RI, though it is corrected for chance and thus does not count randomly generated labels [16].

Table 1: UCI benchmark dataset results averaged over 1000 iterations of ISODATA comparing three different initial cluster center algorithms (*Init.*). Clusters shown due to averaging. ARI - adjusted Rand index; RI - Rand index; MI - Mirkin's index; HI - Hubert's index.

ISODATA						
Init.	Iter.	Clusters	ARI	RI	MI	HI
			Iris			
ISODS	13.46	2.599	**0.646**	0.826	0.173	0.653
KM++	15.43	2.544	0.628	0.816	0.184	0.631
Rand	11.90	2.41	0.607	0.802	0.198	0.604
			Wine			
ISODS	9.16	1.836	**0.313**	0.618	0.382	0.236
KM++	8.76	1.816	0.307	0.612	0.388	0.224
Rand	9.26	1.810	0.304	0.608	0.391	0.217
K-Means						
			Iris			
ISODS	2.29	3	**0.623**	0.833	0.167	0.667
KM++	4.149	3	0.584	0.811	0.189	0.621
Rand	29.402	3	0.569	0.797	0.203	0.593
			Wine			
ISODS	3.145	3	**0.882**	0.947	0.053	0.895
KM++	5.388	3	0.839	0.926	0.074	0.851
Rand	24.775	3	0.834	0.920	0.080	0.840

Then, we applied ISODATA using different initial cluster center approaches to the Salinas-A hyperspectral image dataset [17]. Salinas-A is a small subscene of the Salinas image. It has a size of 86 pixels by 83 pixels, each pixel contains 224 bands, and each pixel is assigned to 1 of 6 classes, disregarding the background. Due to the large number of dimensions in this dataset, prinicipal component analysis (PCA) is used to extract features [18]. In this experimental setup, we use 3 prinicipal components as the input to the model. We utilize the same 80/20 test-train split as the previous experiment and Z-Score Normalize the data. Additionally, the same ISODATA parameter selection approach is employed. We save the best performing model (based on test data performance) for each initial cluster center approach and fit each pixel to the original dataset

to obtain the pictures shown in Figure 1. Finally, the external cluster validation measures are shown in Table ??.

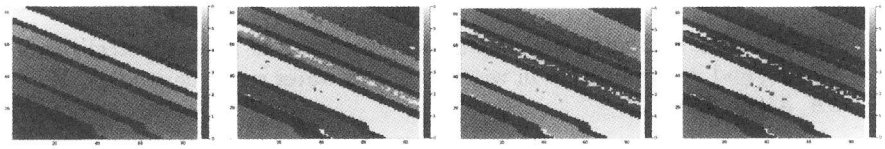

(a) (b) (c) (d)

Figure 1: Heatmap showing cluster assignments of each pixel using ISODATA with different initial cluster center methods. (a) Salinas-A Ground Truth; (b) Random Centers (ARI=0.798); (c) KM++ Centers (ARI=0.781); (d) ISODS Centers (ARI=0.758).

5 Conclusion

This study presents a method for generating initial cluster centers based on a splitting approach, Iterative Self-Organizing Data Split (ISODS). We tested ISODS on bechmark datasets as well as the Salinas-A hyperspectral image dataset. Both tests on average shows the performance of ISODS using external cluster validation measures, especially on the *adjusted Rand index* measure. Additonally, ISODS may decrease the number of iterations required for a clustering algorithm such as ISODATA or K-Means to converge. However, due to the complexity of the ISODS approach compared to other initial centroid algorithms, specifically calculating the means of the clusters, the context should be considered when applying this method. When used in conjunction with ISODATA, ISODS shows an average number of clusters generated closer to the expected output.

Acknowledgements

This research was supported by the College of Computing and Software Engineering at Kennesaw State University. We also want to thank our Laboratory for Machine Vision and Security Research for providing us resources and mentoring.

References

[1] John R. Jensen. *Introductory digital image processing: a remote sensing perspective.* Prentice-Hall, 1996.

[2] Srivatsa Mallapragada, Michael Wong, and Chih-Cheng Hung. Dimensionality reduction of hyperspectral images for classification. *9th International Conference on Information*, 2018.

[3] David Landgrebe. Information extraction principles and methods for multispectral and hyperspectral image data. *Information Processing For Remote Sensing*, page 3–37, 1999.

[4] M Govender, K Chetty, and H Bulcock. A review of hyperspectral remote sensing and its application in vegetation and water resource studies. *Water SA*, 33(2), 2009.

[5] Christian Fischer and Ioanna Kakoulli. Multispectral and hyperspectral imaging technologies in conservation: current research and potential applications. *Studies in Conservation*, 51(sup1):3–16, 2006.

[6] Oscar Carrasco, Richard B. Gomez, Arun Chainani, and William E. Roper. Hyperspectral imaging applied to medical diagnoses and food safety. *Geo-Spatial and Temporal Image and Data Exploitation III*, 2003.

[7] Arbab Abbas, N. Minallh, Nasir Ahmad, Sahibzada Abdur Rehman Abid, and Muhammad Khan. K-means and isodata clustering algorithms for landcover classification using remote sensing. 48:315–318, 04 2016.

[8] S. Lloyd. Least squares quantization in pcm. *IEEE Transactions on Information Theory*, 28(2):129–137, 1982.

[9] David Arthur and Sergei Vassilvitskii. K-means++: The advantages of careful seeding. volume 8, pages 1027–1035, 01 2007.

[10] Pasi Fränti and Sami Sieranoja. K-means properties on six clustering benchmark datasets. *Applied Intelligence*, 48(12):4743–4759, 2018.

[11] G. Ball and D. Hall. Isodata, a novel method of data analysis and pattern classification. 1965.

[12] Dheeru Dua and Casey Graff. UCI machine learning repository, 2017.

[13] Mohammad Rezaei and Pasi Fränti. Set matching measures for external cluster validity. *IEEE Transactions on Knowledge and Data Engineering*, 28(8):2173–2186, 2016.

[14] Lawrence Hubert and Phipps Arabie. Comparing partitions. *Journal of Classification*, 2(1):193–218, 1985.

[15] Marina Meilă. Comparing clusterings by the variation of information. *Learning Theory and Kernel Machines Lecture Notes in Computer Science*, page 173–187, 2003.

[16] William M. Rand. Objective criteria for the evaluation of clustering methods. *Journal of the American Statistical Association*, 66(336):846–850, 1971.

[17] Grupo de Inteligencia Computacional (GIC). Hyperspectral remote sensing scenes. Accessed: 2021-1-05.

[18] Craig Rodarmel and Jie Shan. Principal component analysis for hyperspectral image classification. *Surv Land inf Syst*, 62, 01 2002.

Proceedings of the Tenth International
Conference on Information (Information'2021)
ISBN 4-901329-11-8

SLN-D2CNN Model for Lymph Node Metastasis Diagnosis

Ruigang Ge *, Guoyue Chen **, Kazuki Saruta ***, Yuki Terata ****

* *Akita Prefectural University Graduate School of Systems Science and Technology, School of Media Signal Processing Lab, 015-0055 Yurihonjo, Japan, E-mail: d21S001@akita-pu.ac.jp*

** *Akita Prefectural University of Systems Science and Technology, School of Media Signal Processing Lab, 015-0055 Yurihonjo, Japan, E-mail: chen@akita-pu.ac.jp*

*** *Akita Prefectural University of Systems Science and Technology, School of Media Signal Processing Lab, 015-0055 Yurihonjo, Japan, E-mail: saruta@akita-pu.ac.jp*

**** *Akita Prefectural University of Systems Science and Technology, School of Media Signal Processing Lab, 015-0055 Yurihonjo, Japan, E-mail: terata@akita-pu.ac.jp*

Abstract

Sentinel lymph node biopsy (SLNB) is a common tool to identify breast cancer metastasis. Presently, SLNB detection of cancer migration mainly relies on naked eye observation based on pathologists' experience. It is time consuming and fatiguing to look at all the tissue samples under a microscope and to form a diagnosis based on cell morphology, which may result in missed diagnoses. This paper aims to improve this situation using convolutional neural network (CNN) models. This research adopts the fusion of 2 current mainstream CNN models (VGG16 and DensNet121) as the baseline of the model, and the back-end is equipped with a custom convolutional facilitated network learning and the accelerated training using migration learning to develop a proposed model for the purpose of multi-model integration. An experiment of the model against its baseline and each generic evaluation index of each model that makes up the baseline was completed with the quality cancer pathology dataset provided by the Kaggle event. The experimental results show that the AUC accuracy value of the proposal network model is as high as 0.986, which is more accurate for discriminating with images.
Keywords: Convolutional neural network, Whole slide imaging, Proposed model, Transfer learning, Baseline, Feature extraction.

1. Introduction

The prevalence of cancer in women has sparked strong social concern. According to the Global Burden of Disease study [1], the incidence of breast cancer tops the list, followed by lung cancer, cervical cancer, and endometrial cancer. It is well known that metastasis and the recurrence of breast cancer are important factors causing death of patients. In clinical medicine, SLNB technique based on sentinel lymph node (SLN) tissue section is considered as the "gold standard" for breast cancer metastasis diagnosis. Using Hematoxylin Eosin (H&E) staining in combination with the all-digital sectioning whole slide imaging (WSI) [2]

technique to accomplish computer-aided pathology diagnosis. In particular, the use of CNN models, which is good at image classification and recognition, has important scientific and application value for the discrimination whether a tissue is infected with breast cancer metastasis in WSI pathology images of SLNB. At present, most studies are generally based on single CNN or custom shallow CNN models, with problems such as less reliability, diverse feature extraction [3,5], low discriminative accuracy and poor generalization. Therefore, this research proposes a model that combines mainstream high-quality 2 CNN models (Vgg16 and Desnet121) as the baseline. The two models are fused and improved to form a combined model with multi-scale spatial feature extraction and extending feature span from natural images to medical images, i.e., the SLN-D2CNN model. We further improved the accuracy of breast cancer metastasis discrimination with this model. As for model training technique, we use migration learning as the fast training in the proposed model baseline to obtain the highest accuracy.

2. Composition of the model and experiment preparation

Due to the variety and morphology of breast cancers, different subclasses of breast cancers cause problems such as approximation of texture features and cell nucleus spatial structure features. Therefore, we adopt two mainstream deep CNN models that have not only achieved excellent results in the Large Scale Visual Recognition Challenge (ILSVRC) but also are widely used and effective in research in various fields today, drawing on existing competition models for large-scale natural image ImageNet training sets and related research in their fields. CNN models [4,5], i.e., VGG16 with multiple 3x3 convolutional stacks and Densnet121 with dense type connections, are used as the baseline of our proposed model, and the higher-order preliminary features extracted from each model of the baseline are obtained by a transfer learning method. Finally, the features obtained by the convolutional processing learning are output through the Global Average Pooling (GAP) layer and the fully connected (FC) layer with one neural unit of Sigmoid to discriminate the SLN-WSI pathology images

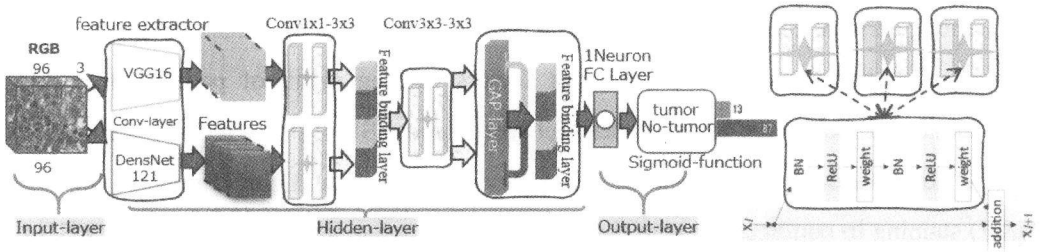

Figure 1. Structure of the proposed SLN-D2CNN

Figure 2. Construction between resnetv2 conv-layer

by the proposed model, and we name this proposed model as SLN-D2CNN (as shown in Figure 1). Where baseline subsequently customizes the composition inside the convolutional processing (shown in Figure 2), this combined composition is based on the best method derived from rensentv2 in ImageNet classification to obtain the best accuracy.

The experimental benchmark dataset in this manuscript is derived from Kaggle's PCam dataset [7], which is a collection of 400 H&E-stained high-resolution images sampled by a 40x objective, decomposed into 327,680 color images of 96×96 pixels in size with duplicate items removed, and affiliated with an improved version of a subset of the Camelyon16 dataset [8]. In the PCam dataset, each image has a binary label, i.e., images containing metastatic cancer cells are labeled as "1"; normal tissue images are labeled as "0", as shown in Figure3.

Therefore, we convert the clinical detection of SLN metastatic cancer cells into a positive "1" and negative "0" image binary classification task. In order to reduce model overfitting and enhance the generalizability of the model, the method in Table 1 is used in this research.

Table 1 Data enhancement and pre-processing

Methods Name	Method details
Image normalization processing	for each batch size of images, we used Z-score normalization done and image scaled to between 0 and 1.
Image flipping enhancement processing algorithm	for each image,we flip it randomly from two orthogonal directions(horizontal and vertitcal),thus there are four transforms for each image.
Image random rotation processing	for each image we can rotate 90°, 0° or -90°, after which we randomly rotate -15° to 15°.

In this study, 85% of the PCam is randomly selected as the training set and the remaining 15% as evaluation data for the performance of the model. In addition, the area under the ROC curve (AUC) and validation set of loss are used as evaluation metrics in this experiment and combined with the evaluation data. To verify the reliability of our model, we conducted controlled experiments of the proposal model SLN-D2CNN against its baseline model 2CNN and the single CNN model that composed each model of the baseline.

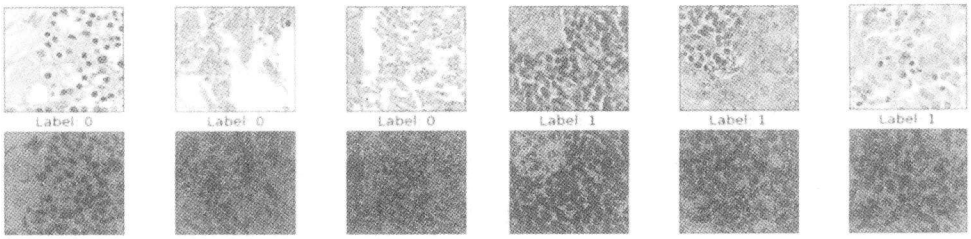

Figure 3 (The upper part shows the sample data with "0" or "1" labels in the PCam dataset, and the lower part shows the image normalization results of this manuscript)

3. Experimental results and conclusions

From Figure 4, it can be seen that the maximum determination accuracy of each CNN is Vgg16: 0.943, DensNet121: 0.963, baseline model 2CNN: 0.970, and the proposal model SLN-D2CNN has the highest value of 0.986. In addition, the validation results from Figure 5

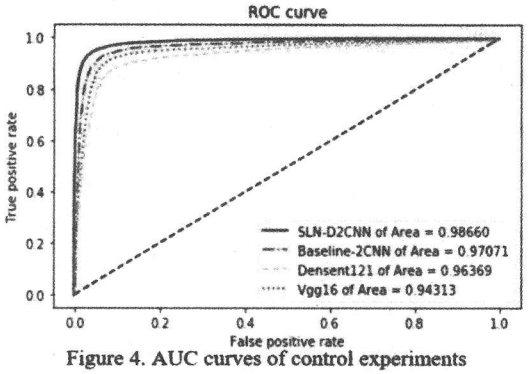

Figure 4. AUC curves of control experiments

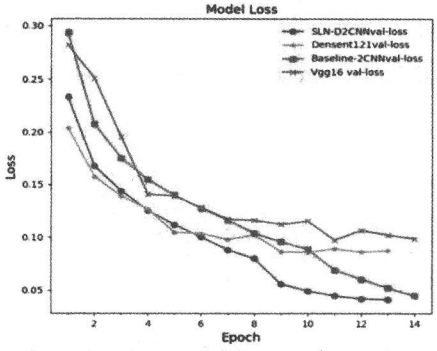

Figure 5. Loss curve of the control experiments

show that the SLN-D2CNN in the first 15Epoch in the validation set Loss also shows significantly lower results than each CNN learned at the same time as well as the baseline 2CNN. In this research, we propose the breast cancer migration discrimination proposed model SLN-D2CNN by fusion of 2 valid pre-trained deep CNNs as a baseline and subsequent learning by custom segmental convolution. With the PCam dataset we confirm that SLN-D2CNN outperforms the individual CNNs as well as the baseline model 2CNN in terms of AUC accuracy.

References

[1] Heer, et al. "Global burden and trends in premenopausal and postmenopausal breast cancer: a population-based study." *The Lancet Global Health 8.8* (2020), e1027-e1037.

[2] Barker, et al.Automated classification of brain tumor type in whole-slide digital pathology images using local representative tiles. *Medical Image Analysis*, 30 (2016),60-71.

[3] Motlagh, Mehdi Habibzadeh, et al. Breast cancer histopathological image classification. A deep learning approach. *BioRxiv*: 242818. (2018).

[4] Simonyan, Karen, and Andrew Zisserman. Very deep convolutional networks for large-scale image recognition. *arXiv preprint arXiv:*1409.1556, (2014).

[5] Huang G, Liu Z, et al.Densely connected convolutional networks. Proceedings of *the IEEE conference on computer vision and pattern recognition*, (2017), 4700-4708.

[6] He, Kaiming, et al. Identity Mappings in Deep Residual Networks. *European Conference on Computer Vision Springer, Cham*, (2016),630-645.

[7] The DataSet https://github.com/basveeling/pcam.

Welcome to INFORMATION'2021 Online Conference

BACKGROUND AND AIMS

The most distinctive feature in the development of modern sciences and technologies is that various sciences, which were classified so far according to their research objects and methodologies, penetrate and combine with each other gradually. Therefore, many new disciplines and technologies were born from boundary areas of those existing sciences. Today, from classical sciences to modern technologies, almost all sciences and technologies are depended on each other so closely that they cannot exist and grow independently and have to grow in harmony with each other. There is an abstract, general and cross-cutting concept that concerns all scientific methodologies and sciences, it is "Information".

The International Conference on Information is an interdisciplinary international conference series. It provides a forum for all scientists and technicians throughout the world to exchange scientific information such as original ideas, research methods and research results related to all scientific fields.

The first conference Information'2000 (Fukuoka, Japan), the second conference Information'2002 (Beijing, China), the third conference Information'2004 (Tokyo, Japan), the fourth conference Information'2006 (Cork, Ireland), the fifth conference Information'2009 (Kyoto, Japan), the sixth conference Information'2013 (Tokyo, Japan), the seventh conference Information'2015 (Taipei), the eighth conference Information'2017 (Tokyo, Japan) and the ninth conference Information'2018 (Tokyo, Japan) has been held grandly separately.

The Tenth Online conference, Information'2021, will be held in Hosei University, Tokyo, Japan on March 6 - 7, 2021. Information'2021 will include keynote addresses, invited speeches, special workshops, contributed presentations (Lectures or Posters). The conference proceeding will be published by International Information Institute (ISBN 4-901329) and available to delegates at the time of registration. And the papers presented in the conference will be selected as regular papers for publication in INFORMATION: An International Interdisciplinary Journal (ISSN 1343-4500) or other journals.

Proceedings of the Tenth International Conference on Information

Published by International Information Institute